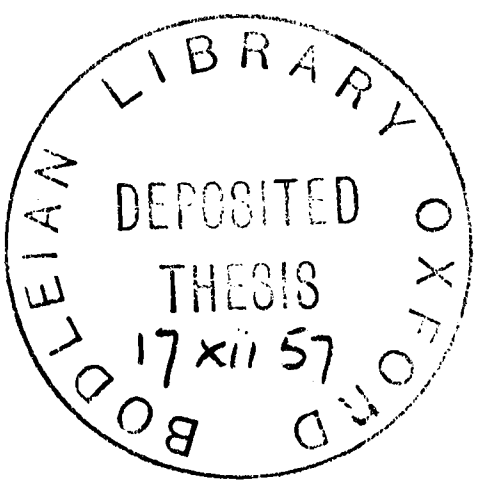
THE EFFECT OF TEMPERATURE ON THE STATIC AND DYNAMIC STRENGTH PROPERTIES OF METALS

- by -

C. J. Malden

A Thesis submitted for the Degree of

Doctor of Philosophy



Engineering Laboratory.

University of Oxford.

June, 1957.

ACKNOWLEDGEMENTS

The writer wishes to thank the following for their assistance in the course of this study.

Dr. J. D. Campbell whose support and guidance at all times was much appreciated.

Professor J. L. M. Morrison and Mr. A. N. Dickson of the Department of Mechanical Engineering, University of Bristol, who arranged for the vacuum annealing of the steel specimens.

Mr. A. H. Gearing and the other members of the workshop staff who were most helpful in the design and construction of equipment.

ABSTRACT.

A survey is presented of earlier investigations concerning the effect of temperature on the static and dynamic strength properties of iron and steel. Results are given of static and dynamic tests performed on a medium-carbon steel at temperatures ranging from +15°C to -183°C. Also investigated is the effect of various amounts of permanent dynamic strain on the subsequent static and dynamic properties of the steel. A correlation of the results of the above tests with the various mechanisms of deformation is permitted by photomicrographic examination of the tested specimens. Finally the results of the dynamic tests are compared with a delay-time theory.

In order to be able to measure the true specimen strains in the low temperature static tests, a low temperature strain gauge was developed. This gauge, which incorporates wire resistance strain gauges, was used to find static stress-strain curves at a number of temperatures. From the variation of static upper yield stress with test temperature an estimate of σ_0, the yield stress at absolute zero, is obtained. This value of σ_0 is used in comparing the results of the dynamic tests with a delay-time theory. It is also shown that as the test temperature is lowered the slip by which the ferrite deforms

in the static tests becomes finer.

The dynamic apparatus employed in this investigation was such that eccentricity of loading was reduced to a minimum. A falling weight was used to apply compressive stress waves of the order of 10^5 lb./in^2 and duration 110 microseconds to the test specimens. Wire resistance strain gauges were used to obtain stress time records at points on a weighbar and on an anvil bar, just above and just below the specimen faces. From these records a method of wave analysis gives stress against time and particle velocity against time curves for both faces of the specimen. Using these derived curves dynamic stress-strain curves are found at various impact velocities and test temperatures. These stress-strain curves indicate the large increase in strength of the steel under such loading conditions — the dynamic stress-strain curves being from 100 to 200% higher than the room temperature static stress-strain curve. A further comparison of the above curves shows that for identical velocities of impact, as the test temperature is lowered the time to yield, and upper and lower yield stresses increase, whereas the permanent deformation, the ratio of dynamic upper yield stress to static upper yield stress at the same temperature, and the maximum and average strain rates all decrease. It is also

found that in dynamic tests deformation occurs primarily by very fine slip. However, in some of the low temperature impacts twinning also occurs. Results indicate that the stress at which twins are initiated is approximately independent of temperature and strain rate. It is thought that for the medium carbon steel under test, this stress for twin formation is in the range 121,000 lb./in^2 to 128,000 lb./in^2.

The yield stress, delay-time results obtained in the dynamic tests are compared with Campbell's delay-time theory. This theory, which assumes that yield will occur when a critical number of source dislocations have been released from their atmospheres of carbon or nitrogen, is found to be in fair agreement with the experimental results. The greatest discrepancy between the theory and the results obtained occurs at the lower test temperatures. This is attributed mainly to twin formation.

It is found that the effect of deforming the steel dynamically is to render it softer for subsequent static deformation of the same type. In particular the static upper yield stress is reduced to a minimum after about 1 permanent dynamic strain. Also it is found that the effect of 'pulsing' steel, i.e. subjecting it to a rapidly applied stress of insufficient magnitude and duration to

cause yielding, is to reduce the upper yield stress obtained during static reloading. The effect of dynamic deformation at a low temperature on the subsequent static stress-strain curve is also considered. It is found that the static stress-strain curve obtained after an impact is little affected by lowering the test temperature, provided that the magnitude and duration of the impact stress are increased so as to obtain the same permanent strain.

It is also shown that 'pulsing' the steel lowers the dynamic upper yield stress obtained in a subsequent impact test. It is found that the effect of a given stress pulse is greater on the subsequent dynamic upper yield stress than it is on the subsequent static upper yield stress. Also, whereas after a small amount of permanent dynamic strain an upper yield point is still evident in a static retest, in a dynamic retest the yield point has almost been eliminated.

Finally, repeated impact tests appear to indicate that Campbell's criterion for yielding, i.e. that a critical number of dislocations must be released from their atmospheres, is approximately valid whether or not the dislocations are freed in one or several impacts, provided that no strain ageing occurs between tests.

TABLE OF CONTENTS

Page

PART I

1-1. INTRODUCTION 1

1-2. APPARATUS 16

(1) Dynamic 16

(i) Mechanical Impact Machine 16

(ii) Apparatus for obtaining low temperatures 19

(iii) Gauges 20

(iv) Electrical Auxiliaries 21

(v) Photographic 23

(2) Static 23

(i) General 23

(ii) Gauges 24

(a) Baty cylinder gauge 24

(b) Low temperature gauge 24

(iii) Electrical Auxiliaries 28

(iv) Apparatus for obtaining low temperatures 29

1-3. CALIBRATION 30

(1) Dynamic 30

(i) Calibration of the oscilloscope .. 30

(ii) Calibration of the gauges 31

(iii) Calibration of the amplifiers .. 34

(iv) Calibration of the thermocouples .. 37

(v) Temperature variation along the specimen 40

(vi) Temperature rise during impact .. 41

(2) Static 41

(i) Calibration of the gauges 41

(a) Baty cylinder gauge 41

(b) Low temperature gauge 42

1-4. A DELAY TIME THEORY 45

1-5. METHOD OF WAVE ANALYSIS 50

(i) General theory 50

(ii) The analysis of the stress-time and particle velocity-time curves .. 53

(a) Upper face 53

(b) Lower face 56

(iii) Dynamic stress-strain curves 57

(iv) Variation of yield stress with delay-time .. 58

1-6. TESTING TECHNIQUES 60

(1) Static 60

(ii) Dynamic 61

(iii) Micrographic examination of specimens 62

PART II

2-1. SPECIMENS 63

2-2. STATIC TESTS 64

(1) Experimental results 64

(i) Test results 64

(ii) Micrographic examination 66

(2) Discussion of results 72

2-3. DYNAMIC STRESS-STRAIN CURVES 77

(1) General 77

(2) Experimental results 78

(i) Room temperature results 78

(a) Dynamic stress-strain curves .. 78

(b) Micrographic examination 88

(ii) Results obtained at $-41^{\circ}C$ 88

(a) Dynamic stress-strain curves .. 88

(b) Micrographic examination 97

(iii) Results obtained at $-84^{\circ}C$ 97

(a) Dynamic stress-strain curves .. 97

(b) Micrographic examination 105

(iv) Results obtained at -121 °C 105

(a) Dynamic stress-strain curve .. 105

(b) Micrographic examination 108

(3) Discussion of results 112

2-4. STATIC PROPERTIES OF THE STEEL AFTER DYNAMIC COMPRESSION .. 118

(1) General 118

(2) Experimental results 118

(i) Effect of impacting at room temperature 118

(ii) Effect of impacting at low temperatures 124

(iii) Micrographic examination 128

(3) Discussion 133

2-5. DYNAMIC PROPERTIES OF THE STEEL AFTER DYNAMIC COMPRESSION .. 143

(1) General 143

(2) Experimental results 144

(3) Discussion 151

2-6. A COMPARISON OF THE DELAY-TIME RESULTS WITH A DELAY-TIME THEORY .. 158

(1) General 158

(2) Experimental results 159

(3) Discussion 168

7-7. SUMMARY 175

(1) Experimental results 175

(2) Discussion 177

8-. CONCLUSIONS 179

APPENDIX I

I An analysis of the low temperature strain gauge 182

II The rise in temperature of a specimen during dynamic deformation .. 188

REFERENCES 190

LIST OF FIGURES

Figure	Title	Page
1.	Mechanical Impact Machine	17
2.	Assembly of electrical auxiliaries	22
3.	Plunger loading device	25
4.	Low temperature strain gauge	26
5.	The strain gauge used in the low temperature static tests	27
6.	Electrical circuit used to measure static strains	26
7.	Elastic records obtained at +15°C and -41°C for an impact velocity of 238 in./sec.	32
8.	Variation of gauge factor with specimen temperature	35
9.	Amplifier frequency response	36
10.	Thermocouple calibration curves	39
11.	Variation of temperature along the specimen ..	35
12.	Calibration curve for low temperature strain gauge	43
13.	Lagrange diagram showing method of calculating α and β	54
14.	Static stress-strain curves obtained at a number of test temperatures	65
15.	Variation of upper yield stress with temperature	67
16.	Micrographs taken before and after static deformation at +15°C	7[illegible]
17.	Micrographs taken after static deformation at -183°C	71
18.	Records obtained at +15°C for an impact velocity of 430 in./sec.	79 80

19. Average elastic record, weighbar record and stress-time curve for the specimen upper face — impact velocity = 430 in./sec., temperature = +15°C .. 82

20. Derived stress and particle velocity curves for the specimen faces (430 in./sec. and +15°C) 83

21. Strain rate curve (+15°C and 430 in./sec.) .. 85

22. Dynamic stress-strain curves at +15°C 87

23. Micrographs taken before and after impact at 503 in./sec. and +15°C .. 89

24. Records obtained at -41°C and +15°C for an impact velocity of 470 in./sec. .. 91 92

25. Average elastic record, weighbar record and stress-time curve for the specimen upper face — impact velocity = 470 in./sec., temperature = -41°C .. 93

26. Derived stress and particle velocity curves for the specimen faces (470 in./sec. and -41°C) 94

27. Strain-rate curve (470 in./sec. and -41°C) .. 95

28. Dynamic stress-strain curves at -41°C 96

29. Records obtained at +15°C and -84°C for an impact velocity of 503 in./sec. 99 100

30. Average elastic record, weighbar record and stress-time curve for the specimen upper face — impact velocity = 503 in./sec., temperature = -84°C .. 101

31. Derived stress and particle velocity curves for the specimen faces (503 in./sec. and -84°C) 102

32. Strain-rate curve (503 in./sec. and -84°C) .. 103

33. Dynamic stress-strain curves at -84°C 104

34. Micrographs taken after impact at 503 in./sec. and -84°C 106

35. Records obtained at -121°C and +15°C for an impact velocity of 503 in./sec. 107

36. Average elastic record, weighbar record and stress-time curve for the specimen upper face — impact velocity = 503 in./sec., temperature = -121°C .. 109

37. Derived stress and particle velocity curves for the specimen faces (503 in./sec. and -121°C) 110

38. Dynamic stress-strain curve at -121°C 111

39. Records obtained at impact velocities of 308 in./sec. and 34[illegible] in./sec. 120, 121

40. Elastic and test stress-time curves obtained at various impact velocities 122, 123

41. Static stress-strain curves obtained after dynamic impact 125

42. Static stress-strain curves showing the softening effect of a previous dynamic test 127

43. Micrograph taken after 4% strain—1·2% dynamic plus 2·8% static 129

44. Micrographs obtained after impacts at 5[illegible] in./sec. and -84°C .. 131

45. Micrographs obtained after 8·2% strain — 4·2% dynamic at -84°C plus 4% static at +15°C 132

46. Elastic record, test record, and stress-time curve for the specimen upper face (impact velocity = 365 in./sec.) .. 134

47. Curves of $(\text{stress})^{13}$ against time for dynamic tests .. 136

48. Reduction of static upper yield stress caused by pulsing 139

49. Records obtained for an impact velocity of 430 in./sec. 145

50. Elastic and test stress-time curves obtained at various impact velocities 146 147

51. Derived stress-time curves for the specimen upper face .. 149

52. Derived stress-time curves for the specimen upper face .. 150

53. Curves of $(\text{stress})^{13}$ against time for various impact velocities .. 154

54. Test stress-time curves obtained by impacting a specimen twice at 301 in./sec. 147

55. Neighbar records at +15°C and -41°C 160

56. Yield stress against time to yield referred to constant strain rate tests .. 169

57. Yield stress against time to yield — results obtained by Krafft (27), Clark and Wood (22) in constant stress tests 173

58. Diagramatic representation of the low temperature strain gauge 187

TABLES

		Page
I	Dynamic stress and strain values (+15°C and 430 in./sec.)	86
II	A comparison of the dynamic stress-strain curves obtained at various temperatures and impact velocities	113
III	Yield stress, delay-time results at +15°C ..	137
IV	The effect of various stress pulses on the subsequent static upper yield stress ..	137
V	Yield stress, delay-time results at +15°C ..	162
VI	Yield stress, delay-time results at -41°C ..	164
VII	Yield stress, delay-time results at -84°C ..	165
VIII	Yield stress, delay-time results at -121°C ..	165

1-1. INTRODUCTION

In 1894 Sir James Dewar (1) presented to the Royal Institution a paper entitled "The scientific uses of liquid air". In this discourse he expressed the view that all common metals and alloys increase in 'tenacity' at low temperatures. Since this day a great deal of research has been undertaken to ascertain the effect of test temperature on the static and dynamic strength properties of metals.

This thesis presents investigations that have been undertaken on a medium carbon steel at temperatures ranging from room temperature to that of liquid oxygen. As temperatures below -50°C are not likely to be met with in practice, the practical value of such tests is limited; however, the results may have considerable theoretical significance.

The first main contribution in this field was made in 1905 by Hadfield (2) who investigated the static strength properties of iron and some iron alloys at liquid air temperatures. His research showed how accurate were the observations of Sir James Dewar in so far as the static stress-strain curves were considerably higher at the low temperature than at room temperature. Hadfield also observed that at constant rates of straining low temperatures decreased

the ductility of iron and most iron alloys. Later De Haas and Hadfield (3) extended the temperature range of the above tests down to that of liquid hydrogen (-253°C). They found little difference in tensile strengths from those observed earlier by Hadfield, and concluded that the tensile strengths of metals reach an approximate upper limit at -188°C. Contrary evidence to this concept of a peak tensile strength has been provided by other investigators. The majority of the results of Lindemann and Lindemann (4) indicated greater strength at -253°C than at -188°C. Similarly Fahrenhorst and Schmid (5) found that the resolved critical shearing stress of single crystals increased from -188°C to -253°C. In both these cases (4,5), however, the results showed considerable scatter. More in accordance with the observations of de Haas and Hadfield were the results of Eldin and Collins (6). They found that the yield stress of S.A.E. 1020 steel increased rapidly from room temperature to -212°C; however, from -212°C to -261°C brittle fracture occurred before the onset of yield. Their results also indicated that the stress at fracture had a maximum at -170°C.

The work of Eckdam and Mebs (7) is of importance, as from their tests on a number of metals they found approximate straight line relationships between the absolute temperature and the logarithm of the stresses at yield, ulti-

mate tensile, and fracture points respectively, such that the lower the temperature the higher the stresses. They also found that whereas at low temperatures the ductility of steel was decreased, that of copper was increased.

For crystals of armco iron Cottrell and Churchman (8) found jagged stress-strain curves at liquid oxygen temperatures. They attributed this unevenness to the formation of twins, for at higher test temperatures smooth stress-strain curves were obtained and deformation occurred primarily by normal slip. Similar 'saw-tooth' static stress-strain curves were obtained by Paxton and Churchman (9) at -196°C, however, at -70°C well marked upper yields followed by lower yield extensions up to 3% strain were observed.

The above researchers were primarily concerned with finding static properties at low temperatures, and all concluded that the static stress-strain curves of iron and iron alloys were raised by lowering the temperature of the test.

The way materials behave when they are rapidly deformed by any system of forces is of great importance in many branches of engineering. The force system may be continuously applied, as in sheet rolling and wire drawing processes, or may be suddenly applied and of short duration. This latter case includes explosions, hammer forgings, impact ex-

trusions or generally any shock loading of a structure. In order to realise the effect of a low temperature on the dynamic strength properties of steel a comprehensive knowledge of the dynamic behaviour of steel at room temperature is first required. A brief summary of some research on the effect of subjecting steel to varying rates of strain at room temperatures is now given.

In 1905 Hopkinson (10) subjected iron wire to tensile impact, and found that for a time of the order of 10^{-4} seconds, iron appeared to be able to withstand stresses considerably greater than the static yield stress without permanent deformation occurring. For a similar loading time Mason (11) observed that yield occurred at a stress approximately equal to 180% of the static yield stress of the steel under test.

Morrison (12) carried out a series of tests on two steels using two machines — one a rapid and one a slow strain-rate machine. His results which indicated that the shorter the time to yield the greater the yield stress, were compared by Campbell (13) with a delay time theory. For delay times less than about one second this theory, which predicted a straight line relationship between the logarithm of delay time and the logarithm of yield stress, approximately fitted Morrison's results. Campbell also obtained

good agreement between his theory and the results of Vreeland, Wood and Clark (14).

Ginns (15) investigated delay times of the order of 10^{-3} seconds. He found that for steel, the yield point was increased over 100% by impact loading. Also the ultimate tensile strength was increased but not to the same extent as was the yield stress. Ginns was also among the first to try to record dynamic stress-strain curves; he measured the stress with a type of resistance gauge and the strain by photo-electrical means.

From his bouncing ball experiments Taylor (16) found that the whole stress-strain curve followed by a specimen was raised above the static stress-strain curve and obtained a dynamic upper yield stress 2·6 times that found statically. A higher ratio of dynamic to static yield stress was found by Whiffen (17) who fired projectiles against a steel plate and thus obtained strain rates up to 12,200/sec. Using Taylor's (18) theoretical analysis of such impacts, based on velocity of impact and specimen dimensions before and after impact, Whiffen concluded that the dynamic yield stress was 3·23 times the static yield stress.

For a medium-carbon steel, and using a maximum strain rate of the order of 940/sec, Campbell and Duby (19) found that yield occurred at a stress approximately 2·5 times

the static yield stress, however, after yield the ratio of dynamic stress to static stress at a given strain became less as the strain increased. They also presented excellent room temperature dynamic stress-strain curves.

The above summary is of necessity both brief and incomplete, however, it does give some idea of the increase in the upper yield stress that can be obtained by increased rates of strain. Far less research has been undertaken to investigate the effect of low temperatures on the dynamic properties of steel.

One of the first investigations into the effect of temperature on the dynamic properties of steel was performed by Zener and Holloman (20) who used temperatures down to that of liquid nitrogen. They observed that at a constant strain rate the dynamic yield stress of a medium-carbon steel increased as the test temperature became lower, and empirically deduced that the stress required for a given plastic strain would be the same for two tests provided that the logarithm of the ratio of the strain rates divided by the difference between the reciprocals of the test temperatures remained constant.

Clark and Wood (21) using a rapid load machine described in an earlier paper (22), investigated the effect

of temperature upon the time delay for yielding in annealed mild steel. The temperature range used was -60°C to +121°C. On plotting yield stress against the logarithm of the delay time they found that, at a constant temperature and for delay times less than about one second, their results approximately fitted straight lines such that the shorter the delay time the greater the yield stress. Further work by the same authors (23), on low carbon and nitrogen content steel, over the same temperature range roughly verified their earlier delay time results.

Baron (24) carried out tensile tests on a number of metals and alloys at temperatures of 20°C, -78°C and -196°C using strain rates of 10^{-3}sec^{-1} and 10^{-2}sec^{-1}. He found, as had earlier investigators, that strain rate and temperature have a marked effect on iron and the softer ferritic steels. He also found that for delay times less than about one second the variation of upper yield stress with temperature and strain rate appeared to obey an activation energy relationship. Within this range of delay times he found that the activation energy for yielding varied with the stress in a manner predicted by Cottrell and Hilly (25).

Both static and dynamic tests, at temperatures down to -196°C, were performed by Krafft, Sullivan, and Tipper (26) on iron and a medium carbon steel. They found that

the dynamic upper yield stresses were all higher than the static by an amount that varied with temperature. At room temperatures the ratio of dynamic to static upper yield stresses was about 2·5 for both iron and steel. At lower temperatures as the yield by normal slip in static tests gave way to the formation of twins this ratio decreased. Using a modified form of this earlier apparatus Krafft (27) subjected mild steel to impacts at low temperatures. On plotting yield stress against the logarithm of delay time as other researchers had done (21,23) he found that at constant temperature his results fitted straight lines. For temperatures above -75°C these lines sloped as Wood and Clark's (21,23) had done, however, at -75°C and -183°C constant stress plateaux were observed. He attributed these to the formation of twins.

Metallographic examination has been of great importance in the study of the static and dynamic properties of metals. The main mechanism of deformation in iron and steel is slip. In static tests at room temperature the slip is coarse, whereas with dynamic deformation there is evidence that the slip is very fine. Campbell, Ruby, and Puttick (28) observed that in steel subjected to slow deformation, coarse slip in ferrite occurred in very narrow

regions on corrogated surfaces, this behaviour appeared to be related to the presence of an ageing precipitate. However, in rapidly strained steel, coarse slip was absent — the metal deforming by fine slip which occasionally formed deformation bands. Also the apparent grain boundary movement previously observed by Campbell and Duby (19) was found to be a localised shear imposed by the requirements of continuity. Only one specimen dynamically tested by these investigators (19,28) exhibited twins and this specimen had been specially treated. This was attributed either to the raising of the critical stress for slip by precipitation of cementite on dislocations, or the lowering of the critical stress for twinning by an increase in grain size. The existence of a grain size factor in twinning had been reported earlier by Clark and Craig (29).

That twinning is a predominant feature of deformation at high rates of strain and low temperatures has been observed by several investigators. Hadfield (2) observed that at liquid oxygen temperature iron tended to deform in static tests by the formation of twins as well as by coarse slip. As mentioned earlier other investigators (8,9) had attributed jagged static stress-strain curves to the sudden formation of twins. Cottrell and Churchman (8) found that after thoroughly decarbonising and denitriding iron deformation

occurred by coarse slip alone, whereas the untreated specimens exhibited twinning. Also they suggested that the stress needed to produce twinning as well as that needed to produce the yield phenomenon is increased by a strain ageing process.

Geil and Carwile (30) tested iron specimens slowly in tension at low temperatures. They found that the number of twins per unit area increased from upper yield to lower yield but did not increase from there on. However as the specimens were further strained the twins spread out. Bending of twins, due to the deformation of grains subsequent to the formation of twins was also noticed. They also found that some twins formed before yield, and they suggested that twinning may be a nucleation and growth process and not a simultaneous shear mechanism as sometimes proposed (24,25).

Baron (24) found twins in iron and steel at -196°C in static tests and at -78°C and below in dynamic tests. He suggested a critical resolved shear stress for twinning, and thought that this stress is not greatly affected by the temperature or the strain rate. He also suggested that the upper yield stress is reduced when twins are formed at a lower stress.

In 1954 Krafft, Sullivan and Tipper (26) suggested a critical stress range for the formation of twins, namely 30,000 to 40,000 lb./in^2 for iron and 85,000 to 95,000 lb./in^2.

for steel. They concluded that it was immaterial whether this stress was obtained by lowering the temperature or by increasing the strain rate. That twins could form at room temperature at high rates of strain has been shown by Carrington and Gayler (31). They examined specimens that had been fired against a steel plate (17) and suggested that the observed twins and compression bands had been formed before yield in order to relieve the high stresses.

As mentioned above, Krafft (27) found stress plateaux at -196°C and -75°C when he plotted the logarithm of delay time against yield stress. At -196°C the plateau was at 146,000 lb./in^2 whereas at -75°C the plateau stress was 119,000 lb./in^2. He suggested that these plateaux were caused by the result of initial deformation by twinning. Clark and Wood (21) also found a constant stress plateau at -196°C but at a stress of 126,000 lb./in^2.

The above review shows that although the existence of a critical resolved shear stress for twinning in metals, has been suspected, it has not been proved satisfactorily by experiment. Recent work (32) seems to have established it for cadmium, but no conclusive evidence has been found concerning steel.

Although many experimental investigations have been

made of the behaviour of steel under rapid loading, little has been revealed as to the properties of the steel after such treatment. Just how steel behaves, either statically on dynamically, after dynamic loading is not clear. There are two cases to consider, firstly static properties after dynamic loading, and secondly dynamic properties after dynamic loading.

The available information concerning the effect of such treatment on the static properties is very limited and somewhat contradictory. Warnock and Pope (33) found that deformation due to impact did not raise the static yield stress, whereas Harris and White (34) found that the microhardness of dynamically deformed steel was greater than if the same amount of deformation had been obtained statically. Experiments by Campbell and Ruby (19) showed that mild steel specimens strained about 4% in dynamic compression gave static stress-strain curves some 10% lower than those of specimens strained the same amount statically. Ruby (35) also found that the static upper yield stress of mild steel was considerably reduced after the material had been loaded by a stress pulse of insufficient magnitude and duration to cause yielding. This he attributed to the freeing of a number of dislocations insufficient to cause yield. When the specimen was reloaded statically the upper yield stress was

reduced, since less dislocations had to be freed to cause yield than in a non-pulsed specimen. Ruby also suggested that such a 'pulsing' technique, to remove the upper yield point of sheet steel, could possibly be used as a substitute for the sheetrolling process.

The dynamic properties of steel after dynamic loading have been investigated by several researchers. The majority of these have been concerned with finding the relationship between the yield stress and delay time by use of a repeated impact technique. Vreeland, Wood and Clark (36,14) concluded from such an investigation that provided the ageing period between pulses is shorter than a critical recovery time, the specimen yields when the cumulative time at a constant stress is approximately equal to the normal delay time at that stress. They also found that under conditions of rapid loading an anelastic microstrain of 30×10^{-6} precedes the yield strain, of which 50% is recovered immediately after pulsing. They attributed this microstrain to the release of dislocations from their atmospheres of carbon and nitrogen atoms. Once freed the dislocations moved through the crystals and were stopped by obstacles such as subgrain boundaries. The full microstrain, at a stress insufficient to cause yield, was said to be reached when at the source, the back stress due to piled up dislocations

balanced the applied stress. The existance of such an anelastic microstrain before yield had been observed earlier by Docherty (37). Experiments by Grant (27) using a steel tested by Johnson, Clark and Wood (37a) indicated, as had the results of the above investigators (36,14), that the cumulative time to yield at a constant stress agreed well with the time taken to yield in single impact at the same stress. There thus seems to be greater agreement among investigators as to the dynamic properties of steel after dynamic loading than as to the static properties after the same treatment.

The research presented in this thesis was undertaken in order to determine accurately the effect of low temperatures on the dynamic and static strength properties of a medium carbon steel. It was hoped to obtain both static and dynamic stress-strain curves over a range of temperatures and to compare Campbell's (13) delay time theory with the results obtained. Also it was intended to investigate the effect of prior dynamic compression on both the static and dynamic strength properties of the steel. Finally, metallographic examination of specimens before and after test was planned, as physical results appear to be so dependent upon the mechanism of deformation. Thus if twins

were formed in some of the tests it was hoped to determine whether or not they appeared at a critical stress and if so the value of the stress.

1-2. APPARATUS

(1) Dynamic

(i) Mechanical impact machine.

Figure 1 shows the impact machine used in this investigation. The dynamic load was applied by the falling weight which had sufficient inertia and stiffness to ensure that no appreciable loss of velocity occurred on impact.

Ideally the stress σ generated by an impact velocity V is given by

$$\sigma = \rho c V \qquad (1)$$

Because the weighbar consisted of three lengths, each of different diameter, the stress given by (1) was magnified before reaching the specimen. From the theory of wave propagation (38) in thin rods the stress transmitted into a section of area A_2 from a section of area A_1 is given by

$$\sigma_t = \sigma_1 \frac{2}{1 + \frac{A_2}{A_1}} \qquad (2)$$

where σ_t is the transmitted stress, and σ_1 the incident stress. Assuming ideal transmission at each change of section (equation 2), the stress applied to the specimen is 2·10 times as large as that generated at the impact end

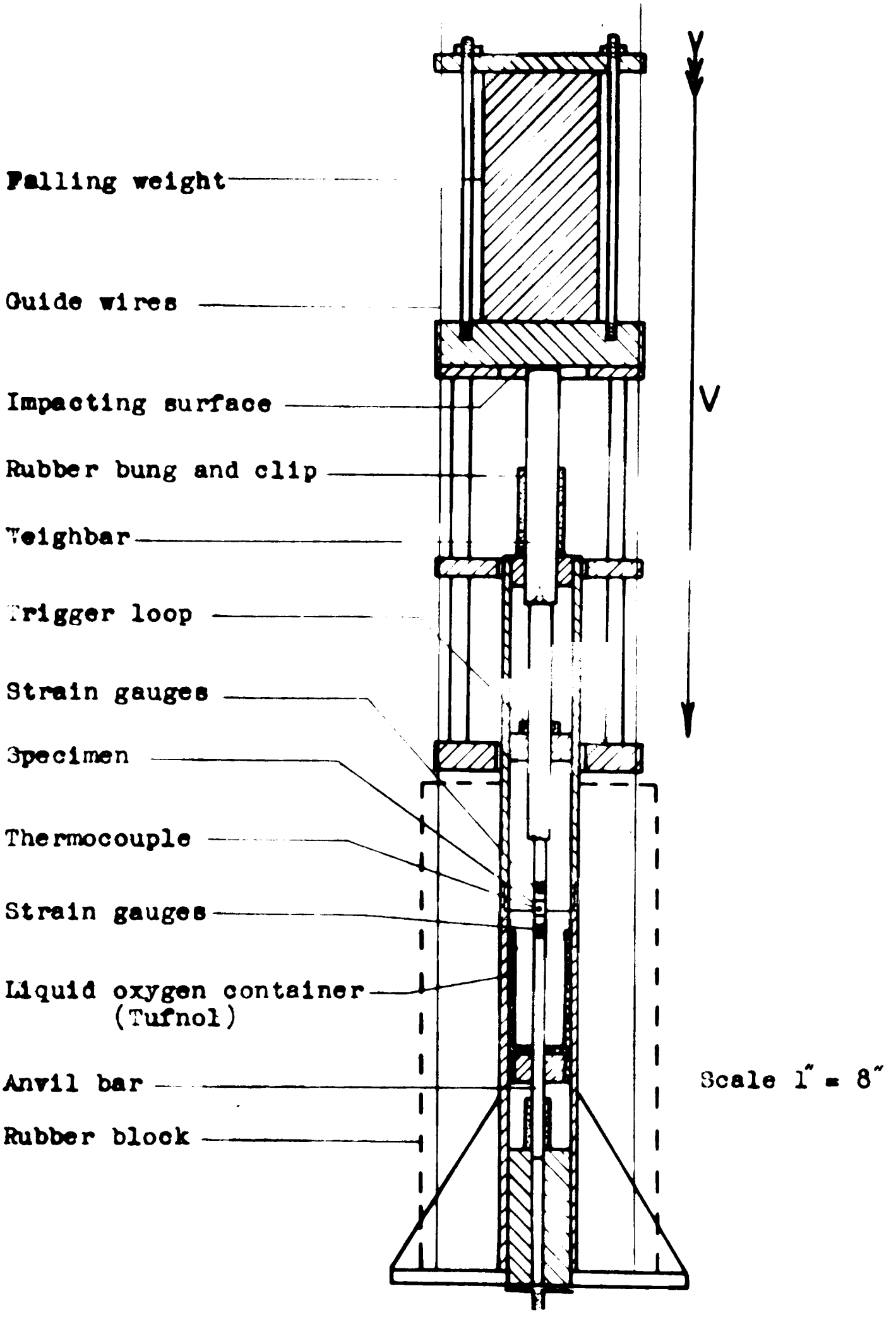


FIGURE 1. Mechanical Impact Machine.

by the falling weight (see section 1-5). Without this stress magnification yield would not have occurred in some of the low temperature tests.

The duration of the stress wave was dictated mainly by the distance of the specimen from the free end of the anvil bar, the impact being terminated soon after the reflected wave from the free end reached the specimen-anvil bar face. Also the lengths of the rods were such that the wave reflected from the change of section A, after travelling up to the impacting plate and back again, reached the specimen upper face after the unloading wave reflected from the free end of the anvil bar. Similarly the wave reflected from section B after travelling up to section A and back again, also arrived at the specimen upper face after the unloading wave.

The specimens, $\frac{1}{8}$ inch in diameter and $\frac{1}{2}$ an inch in length, were lapped in contact with the high strength weighbar and anvil bar. The weighbar and anvil bar were prevented from falling by clamped rubber discs. After impact these rubber discs arrested the bars and the weight was arrested by the rubber blocks.

The advantage of the machine was that eccentricity of loading was reduced to a minimum. This was effected not only by having the impact end of the weighbar machined to

a spherical shape of radius 8 inches, but also by the fact that bending waves in an elastic rod travel more slowly than plane waves (38), the velocity of the former decreasing with increasing wavelength.

(ii) Apparatus for obtaining the low temperatures.

To lower the specimen temperature the tufnol container shown in Figure 1 was partially filled with liquid oxygen. The specimen was kept at a constant temperature by maintaining a slow feed of liquid oxygen into the container from a constant head reservoir. To alter the temperature the rate of feed could be altered, or the position of the specimen relative to the liquid oxygen surface could be changed. A slot in the container maintained a constant level of liquid oxygen and hence ensured a constant specimen temperature at any container position.

The temperature did not have to be held constant for a long period although, as pointed out above, this could easily be done. The temperature only had to be maintained during calibration and up to the moment of impact, a period of a few minutes.

A copper-constantan thermocouple bound tightly to the specimen was used to measure the specimen temperature (see section 1-3 for calibration of the thermocouples).

(iii) Gauges

Two types of resistance strain gauges were used to record the stress waves in the weighbar and anvil bar.

Type 12A gauges (approximate resistance 120 ohms, gauge factor 2·10 length 0·60 inches), manufactured by E. Tinsley and Co., were first used. These gauges are advantageous for dynamic work since they have a minimum thickness of insulation between the gauge wire and the metal surface. Unfortunately, however it was found that fracture often occurred between the active part of the gauge and the termination strip. This can probably be attributed to the fact that 12A gauges are intended for static use involving large strains. To accommodate these large strains a loop of gauge wire was purposely left completely slack near the above mentioned joint. It was here that fracture occurred. Only a few tests were performed using 12A gauges before converting to Tinsley type 20B gauges (approximate resistance 125 ohms, gauge factor 1·94, length 0·25 inches). Although the thickness of the insulation between the gauge wire and the metal surface was greater than in the 12A gauge, the new gauges had their advantages. They were smaller than type 12A and the degree of fixity at the gauge element — termination strip was such that fracture seldom occurred here.

Three gauges in series were used on the weighbar and

three on the anvil bar. The 20P gauges were centered 0·375 inches from the specimen ends of these bars, whereas the corresponding distance with 12A gauges was 0·60 inches.

The gauges were fixed with Durofix cement, dried for 24 hours in air and for five hours in an oven at 70°C. Finally they were water-proofed with Di-jell.

(iv) Electrical auxiliaries.

The assembly of the electrical auxiliaries is shown in Figure 2. The gauges were included in one arm of a Wheatstone bridge circuit, thus allowing their resistance to be compared before and after impact. For calibration purposes closing switch S1 inserted large non-inductive resistances in parallel with the gauges thus simulating a known strain.

The output from the gauges was amplified by the Solartron amplifier and the extra push-pull stage, this amplified output was then applied to the Y plates of a high speed cathode ray oscilloscope (V.C.R.97). A single sweep generator provided the horizontal deflection of the spot, and this was switched to full brightness by a pulse applied to the grid of the tube. The beam was interrupted every two microseconds by means of a 500 Kc/s oscillation superimposed on the brightening pulse. Facilities for 10 microsecond

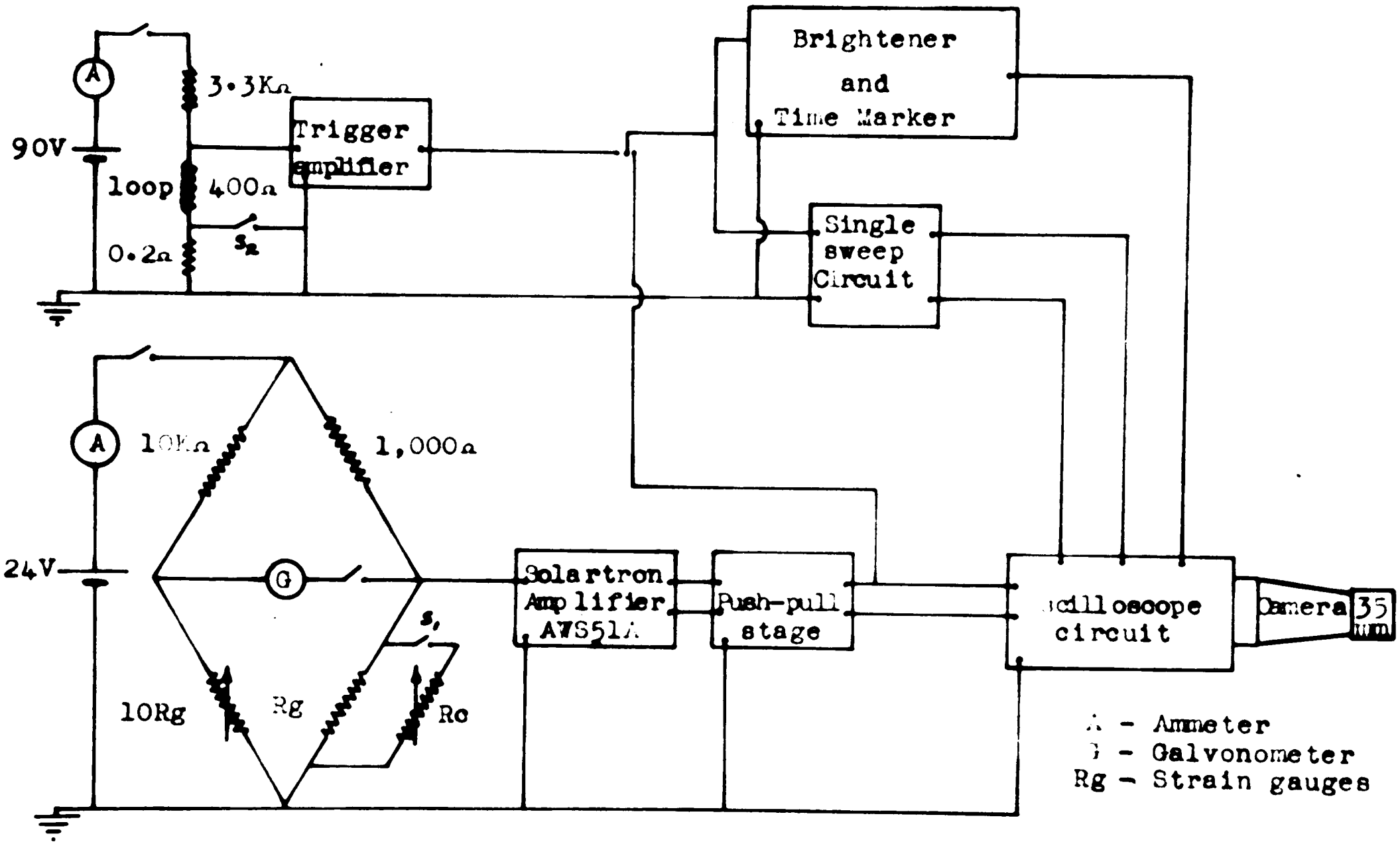


FIGURE 2 Assembly of electrical auxiliaries.

markings on the trace were also available but these were seldom used. A magnetostrictive pulse, obtained from a coil surrounding the weighbar, was used to trigger the sweep and brightener circuits.

To obtain a datum line on the oscilloscope the mercury switch S_2 short circuited a 0·2 ohm resistance in series with the trigger loop. The appearance of a datum line also ensured that the amplifier, brightener and sweep circuits were operating correctly.

(v) Photographic.

The camera used to record the calibration lines and subsequent pulse was a Cossor Model 427 oscillograph camera with a f/3·5 lens. The film used was Ilford recording film, type 5091 and was developed in Ilford Oscillograph developer I.33. The negatives obtained were inserted in an enlarger and the image traced on graph paper.

(2) Static

(1) General.

The static testing machine used was a 10 ton Denison machine. This machine had recently been tested by the makers who found it to be accurate to 1 . To minimise

eccentricity the load was applied through ball bearings and high tensile steel plungers as shown in Figure 3. The specimen was lapped in contact with the plunger faces and centered by means of a brass ring. The load was assumed to be axial as long as seizure of the plungers did not occur. This check could be made by revolving the block.

(11) Gauges.

(a) Baty cylinder gauge.

At room temperatures a Baty cylinder gauge reading to 10^{-4} inch was used to measure the strain. This gauge gave the deformation between the plunger faces i.e. one half of the actual specimen strain. As this gauge could not be used in low temperature tests a special gauge was designed for such use.

(b) Low temperature gauge.

This gauge is shown in Figures 4 and 5. Figure 5 shows the gauge and the high tensile steel plungers. The plungers fit in accurately turned recesses that have holes in the centre to permit the specimen to bear against the plunger faces. The specimen was first centered by means of a brass ring of internal diameter 0·500 inches and external diameter that of the hole in the top recess (·685 inches).

As the specimen was deformed the rings were squeezed

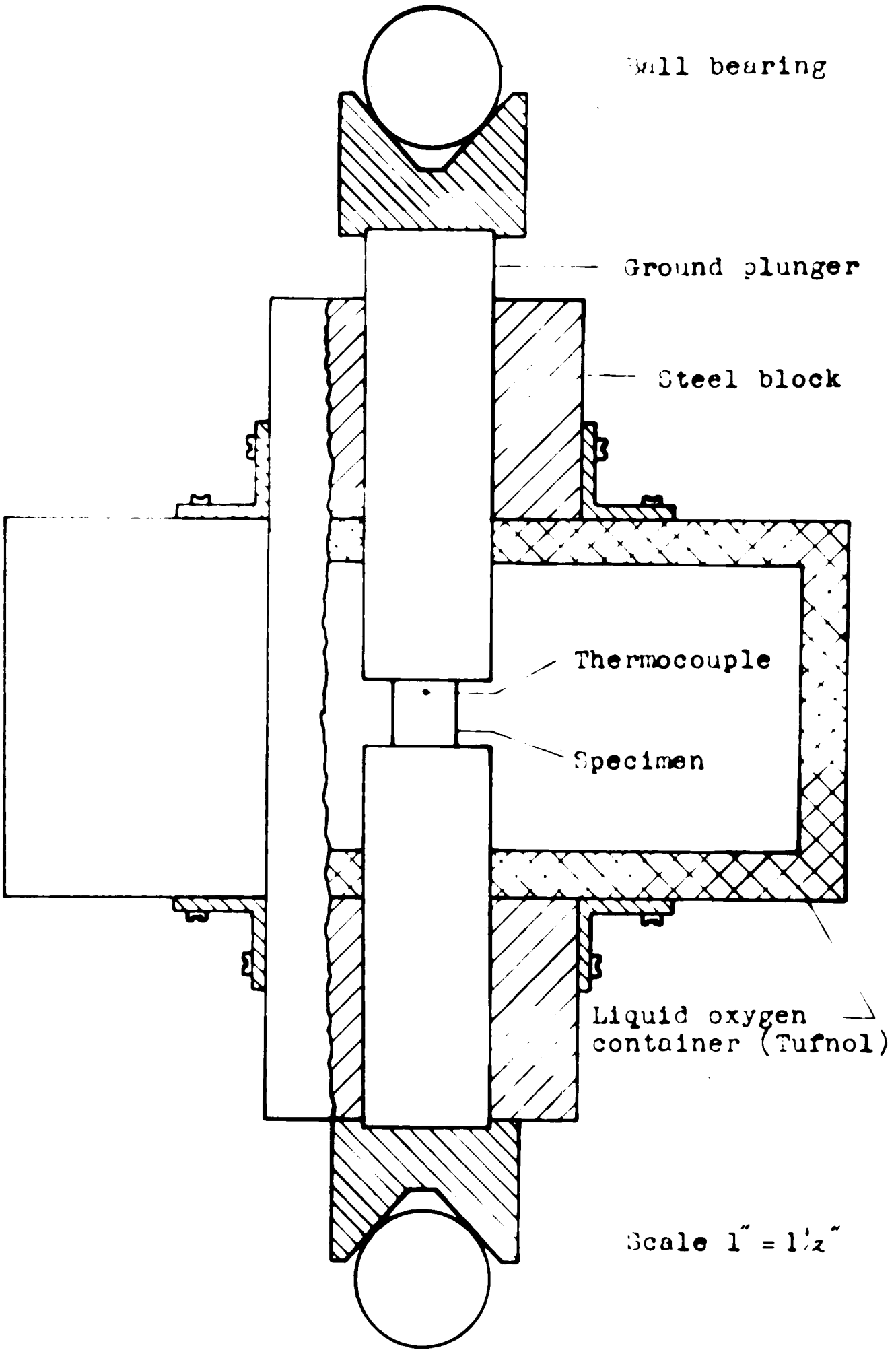


FIGURE 3 Plunger loading device.

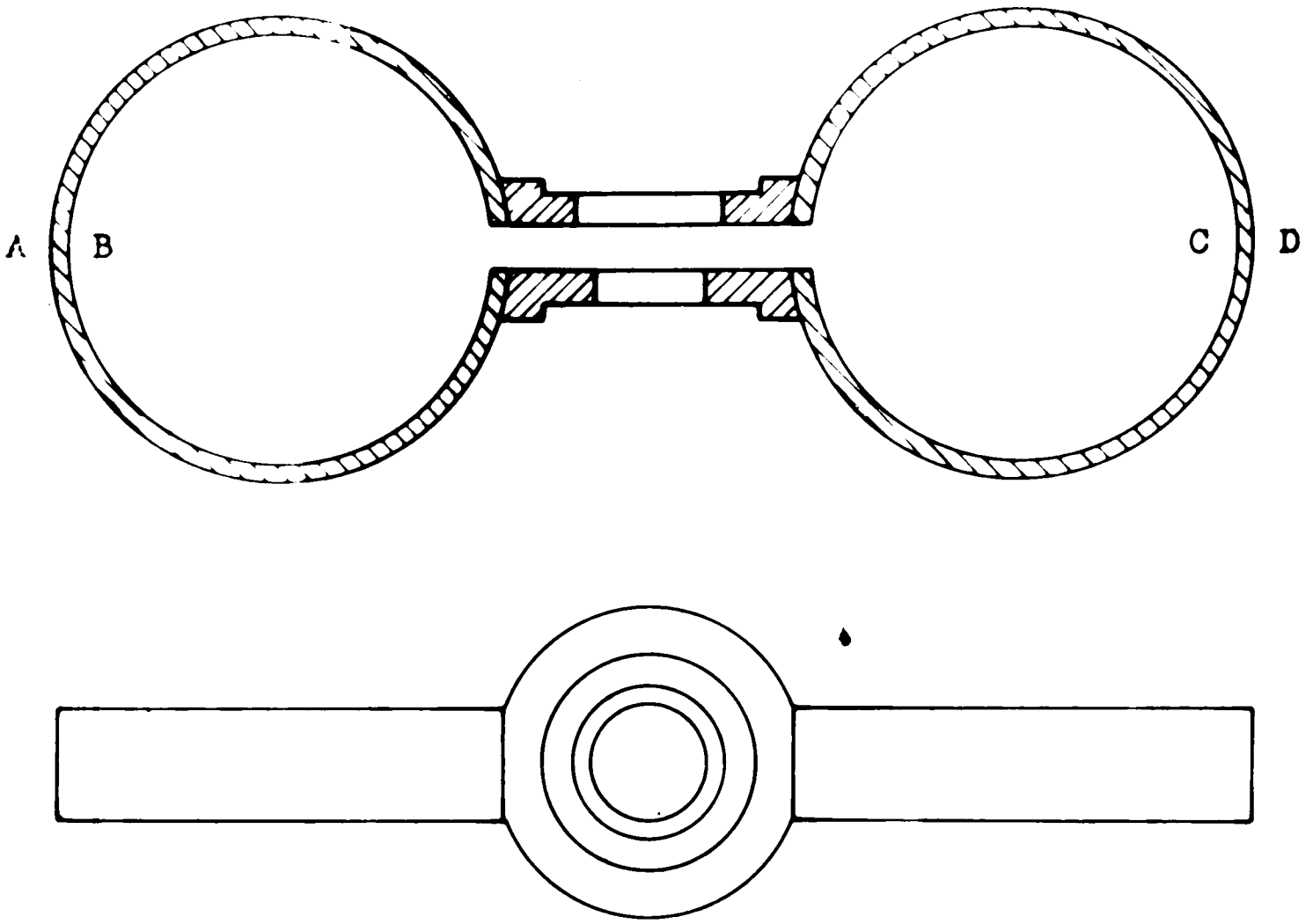


FIGURE 4 Low temperature strain gauge. (Scale 1" = 1")

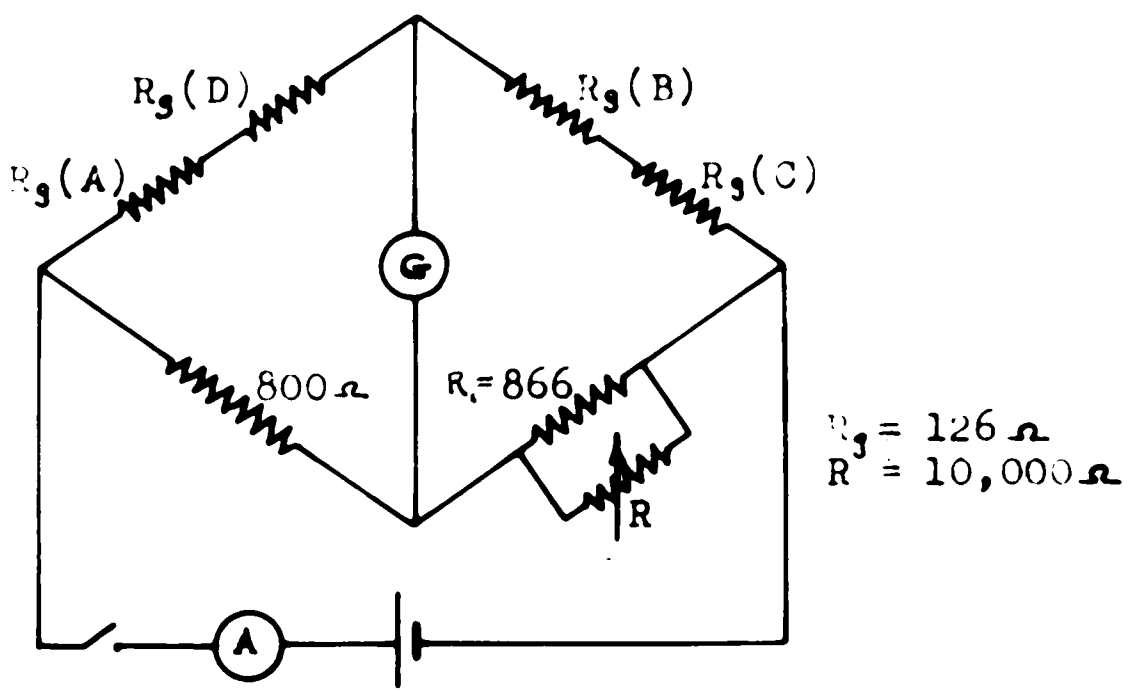


FIGURE 6 Electrical circuit used to measure static strains.

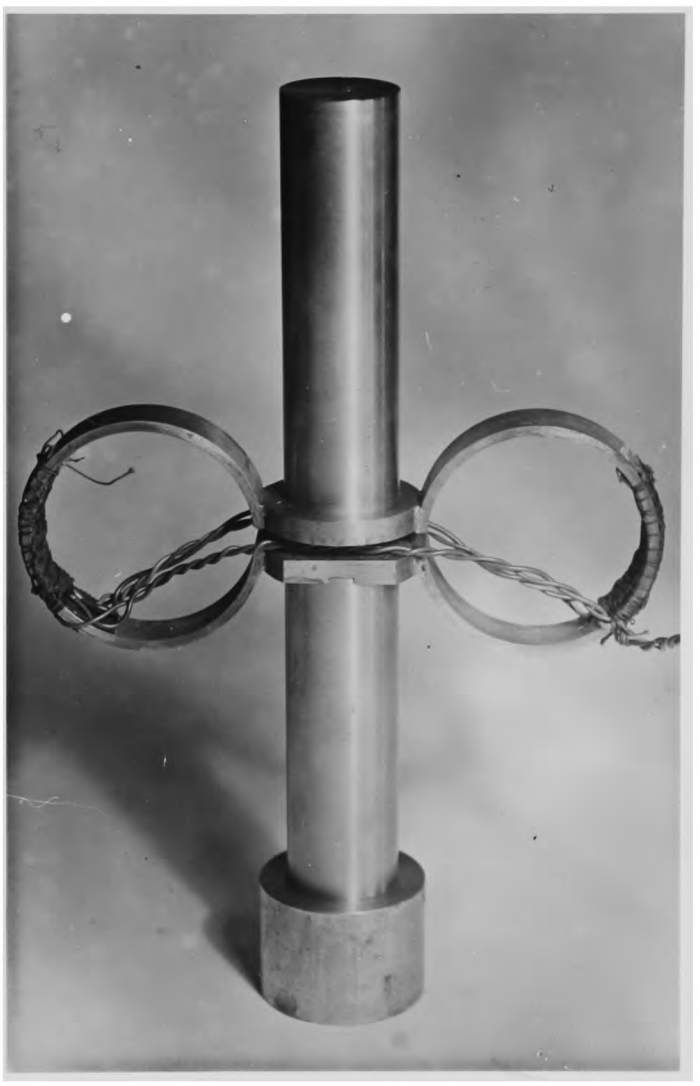


FIGURE 5 The strain gauge used in the low temperature static tests.

in, and at points A, B, C and D the strain was greatest. Type 20B resistance strain gauges measured the strain at these points and were placed in a Wheatstone bridge circuit so as to give maximum sensitivity for a given strain. From the known calibration of the gauge the specimen strain was easily found. (see section 1-3 for calibration)

(iii) Electrical auxiliaries.

The strain measuring circuit is shown in Figure 6. The gauges at A and C were in series in one arm of the bridge and the gauges at B and D, also in series, were in another arm. This arrangement gave maximum sensitivity and was temperature compensated, thus doing away with the need for any dummy gauges.

Appendix 1 shows that if s is the strain at points A, B, C and D, caused by a specimen strain Δ, then

$$\Delta = \frac{s}{\cdot 0075} \qquad (3)$$

This means that the strain at A, B, C and D was considerably less than that at the specimen; however, the electrical circuit was such that s was measured to 10^{-6} and hence Δ to approximately 10^{-4} i.e. of the same order as that given by the Baty cylinder gauge.

(iv) Apparatus for obtaining the low temperatures.

After the gauge had been positioned, the specimen centralised and the thermocouple bound around the specimen, the two tufnol boxes were bolted to the steel block, (Figure 3). This tufnol container was partially filled with liquid oxygen and the specimen temperature was kept constant by maintaining a slow feed of liquid oxygen into the box from a constant head reservoir. This method was found to work satisfactorily, for if the temperature did alter slightly during the test it could be brought back to its original value by altering the flow of liquid oxygen to the box. As in the dynamic low temperature tests, the temperature was measured by a copper-constantan thermocouple.

1-3. CALIBRATION

(1) Dynamic

(1) Calibration of the oscilloscope.

Immediately prior to impact a series of horizontal calibration traces were recorded on the oscilloscope. These traces were obtained by inserting a number of large non-inductive resistances in parallel with the gauges, thus simulating known strains.

As the change in resistance of the gauges (ΔRg) when strained an amount ε is given by

$$\Delta Rg = Rg\, S\varepsilon \qquad (4)$$

where S is the gauge factor, then inserting a known resistance Rc in parallel with the gauges simulates a strain given by

$$\varepsilon = \frac{Rg^2}{S(Rg+Rc)} \qquad (5)$$

Thus from the horizontal traces a calibration curve of deflection against strain could be drawn. This calibration curve was then used to convert the deflection-time curve into a stress-time curve. As the oscilloscope was calibrated immediately before impact it was considered that errors due to any change in gain of the amplifiers would be negligibly small.

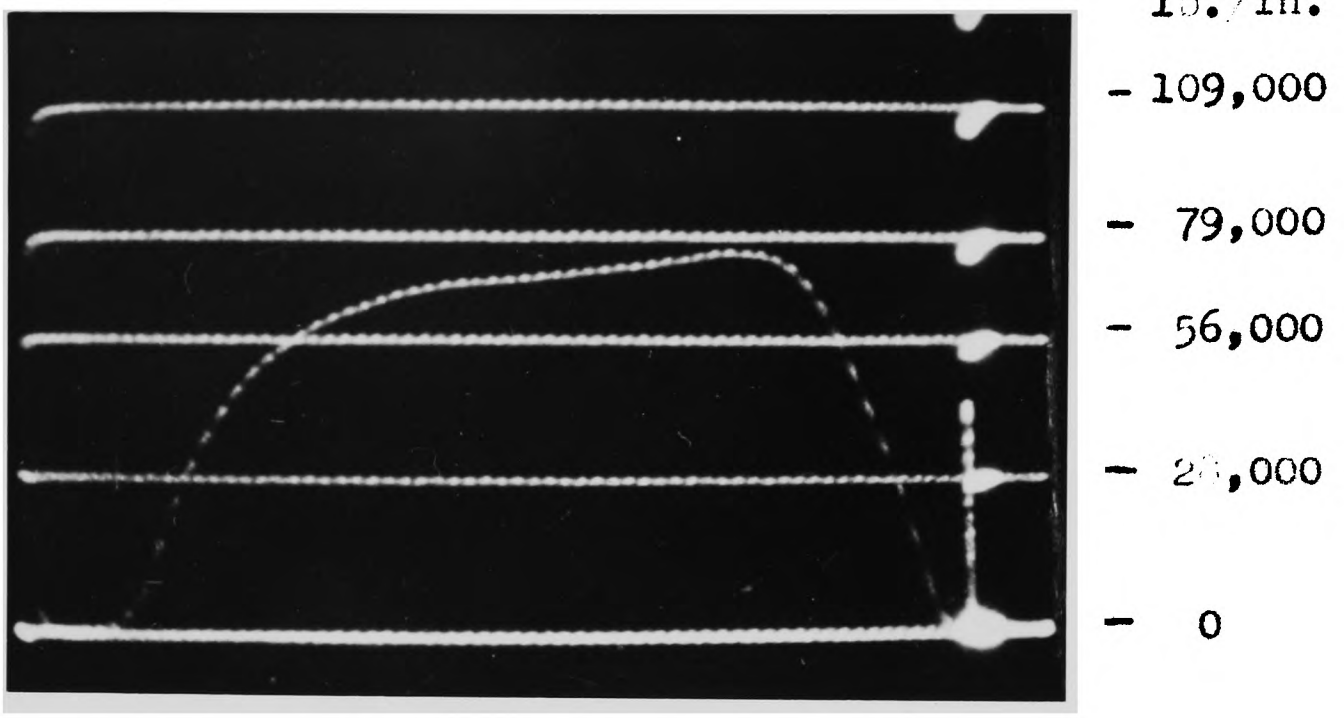
Figure 7 shows two elastic pulses and their respective calibration lines; the first pulse was obtained at room temperature and the second at $-41^{\circ}C$. Also shown in Figure 7 are the stresses corresponding to each horizontal trace.

(ii) Calibration of the gauges.

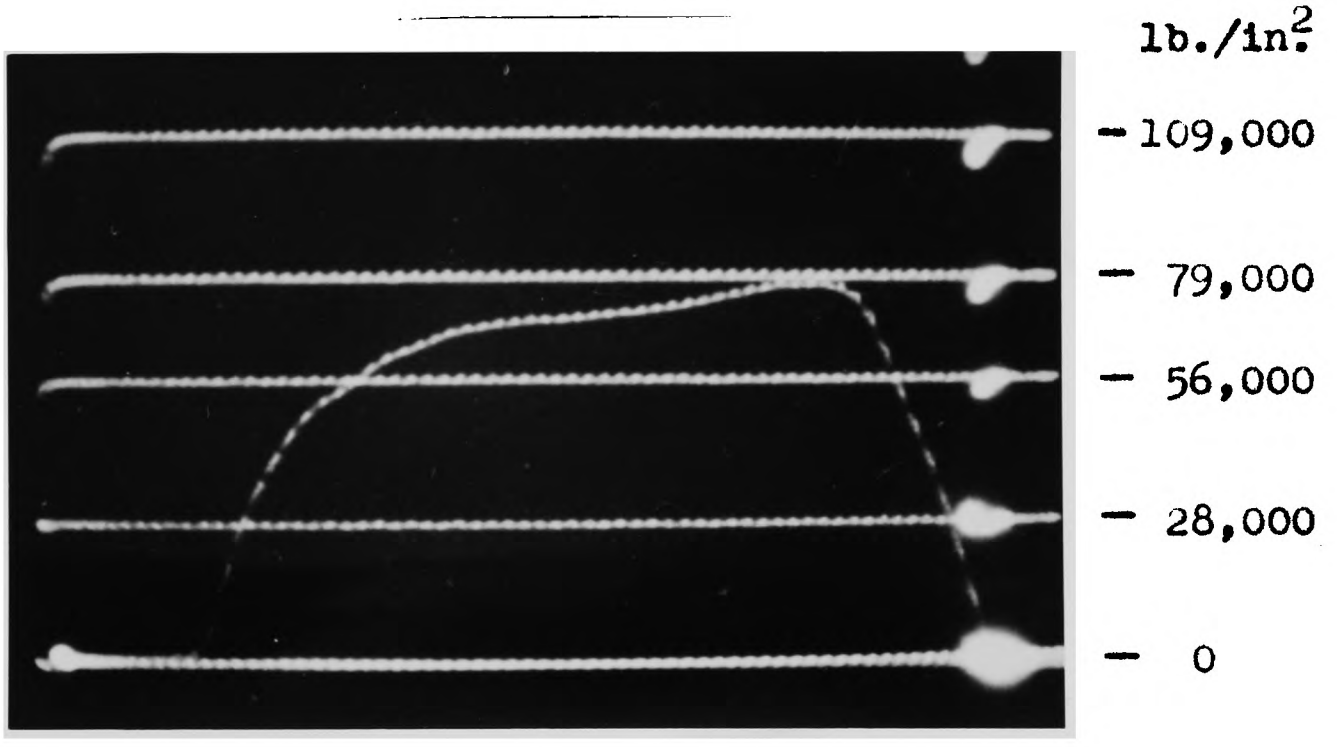
To check the value of the gauge factor S, as given by the maker, two methods were used. The first was by statically testing the gauges and comparing the strain recorded on a Huggenberger extensometer with that calculated using the given value of S. The second was by comparing the magnitude of the recorded elastic wave with the theoretical value given by equation 1. If the elastic peak stress compared within 2% of the theoretical, the given value of S was taken as correct.

For the second method values of the elastic modulus E, and the density ρ of the material of the weighbar and anvil bar were required. The density was found by conventional methods to be 0·0086 slugs/in.^{3}, and by determining the natural frequency of longitudinal vibrations of the anvil bar E was found to be $29{\cdot}6 \times 10^6$ lb./in^2. Thus the velocity of sound in the material ($c = \sqrt{\frac{E}{\rho}}$) was 201,000 in./sec.

For a constant velocity of impact, and for temperatures



7(a)



7(b)

FIGURE 7 Elastic records obtained at +15°C and -41°C for for an impact velocity of 238 in./sec.

(a) at +15°C. Rg = 376Ω. S = 1·94.
(b) at -41°C. Rg = 376Ω. S = 1·98 (calculated)
NB. Calibration stresses shown have been calculated assuming S = 1·94.

down to the lowest test temperature (-121°C), it was thought that the elastic stress-time waves would differ very little from one another. A theoretical estimate of the difference in the maximum stresses at room temperature and -121°C may be made using equation (1) and knowing the values of E and ρ at the two temperatures. Koster's (29) formula for the variation of the shear modulus G with temperature i.e.

$$G = (13{\cdot}30 - {\cdot}0032)\times 10^{6} \text{ lb./in}^2 \qquad (6)$$

indicates that at -121°C, G has increased 3.1% from the room temperature value. Assuming that Poisson's ratio is constant at both temperatures then E may be taken to have also increased 3.1%. Also taking a temperature coefficient of expansion of $= 1{\cdot}4 \times 10^{-5}/C^{o}$ for the steel then ρ is negligibly increased. Hence from equation 1 the stress maximum should be increased $\frac{3{\cdot}1}{2} = 1{\cdot}55\%$. In practice the difference will be even smaller than this since the impact end of the weighbar is at room temperature and not at -121°C, hence the stresses generated at the top of the weighbar, are the same at both temperatures and do not differ by 1.55% as assumed. Finally, as the maximum stresses differ only slightly, it appears reasonable to assume that the whole of the elastic stress wave, corresponding to a given impact velocity, will be little affected by temperature variation.

Using this assumption it is possible to find the variation in gauge factor at the low temperatures. To do this, elastic waves were recorded at + 15°C, -41°C, -84°C and -121°C for an impact velocity of 238 in./sec. The recorded pulses and calibration lines for the +15°C and -41°C tests are shown in Figure 7. It is seen that these elastic waves are almost identical in shape. By assuming that the magnitude of the two stress waves are the same, values of S were found at each test temperature. Figure 8 shows the gauge factors thus obtained, plotted against specimen temperature. It is seen that over the temperature range used in these tests S may be taken as being substantially constant. Using this assumption the pulses shown in Figure 7 give the maximum stresses at room temperature and -41°C as 76,000 lb./in.^{2} and 77,500 lb./in.^{2} respectively. The difference between these stress maxima is small and it was felt that assuming a constant gauge factor throughout would not introduce significant errors.

(iii) Calibration of the amplifiers.

The frequency response of the Solartron amplifier and extra push-pull stage is shown in Figure 9. It was known that, using the response curve for 21db attenuation

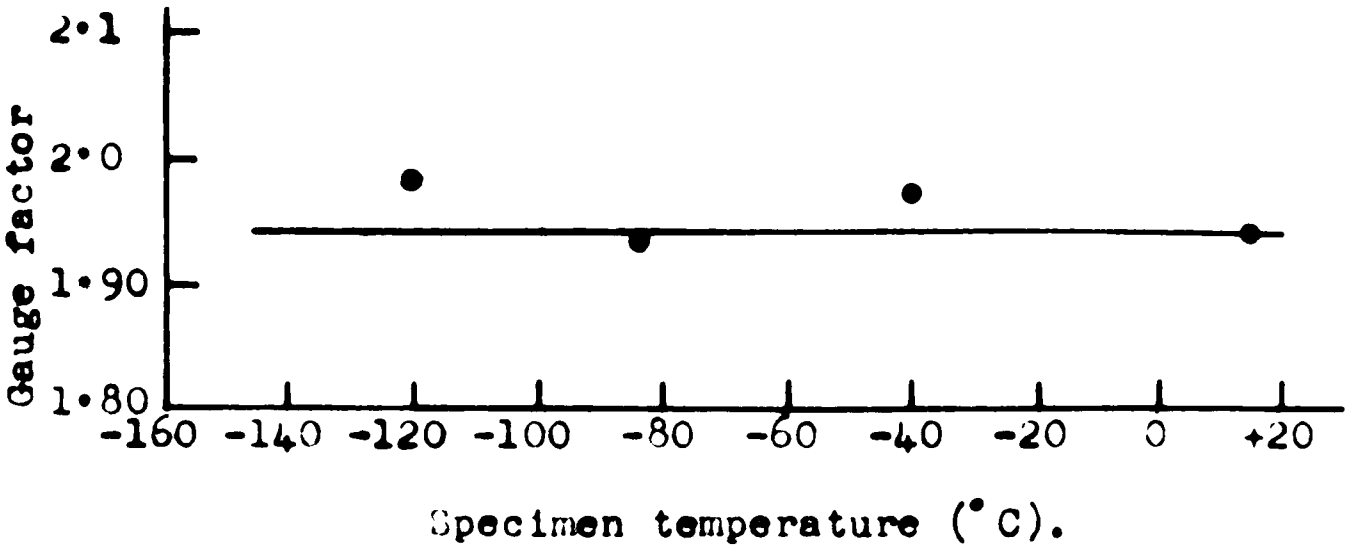


FIGURE 8 Variation of gauge factor with specimen temperature.

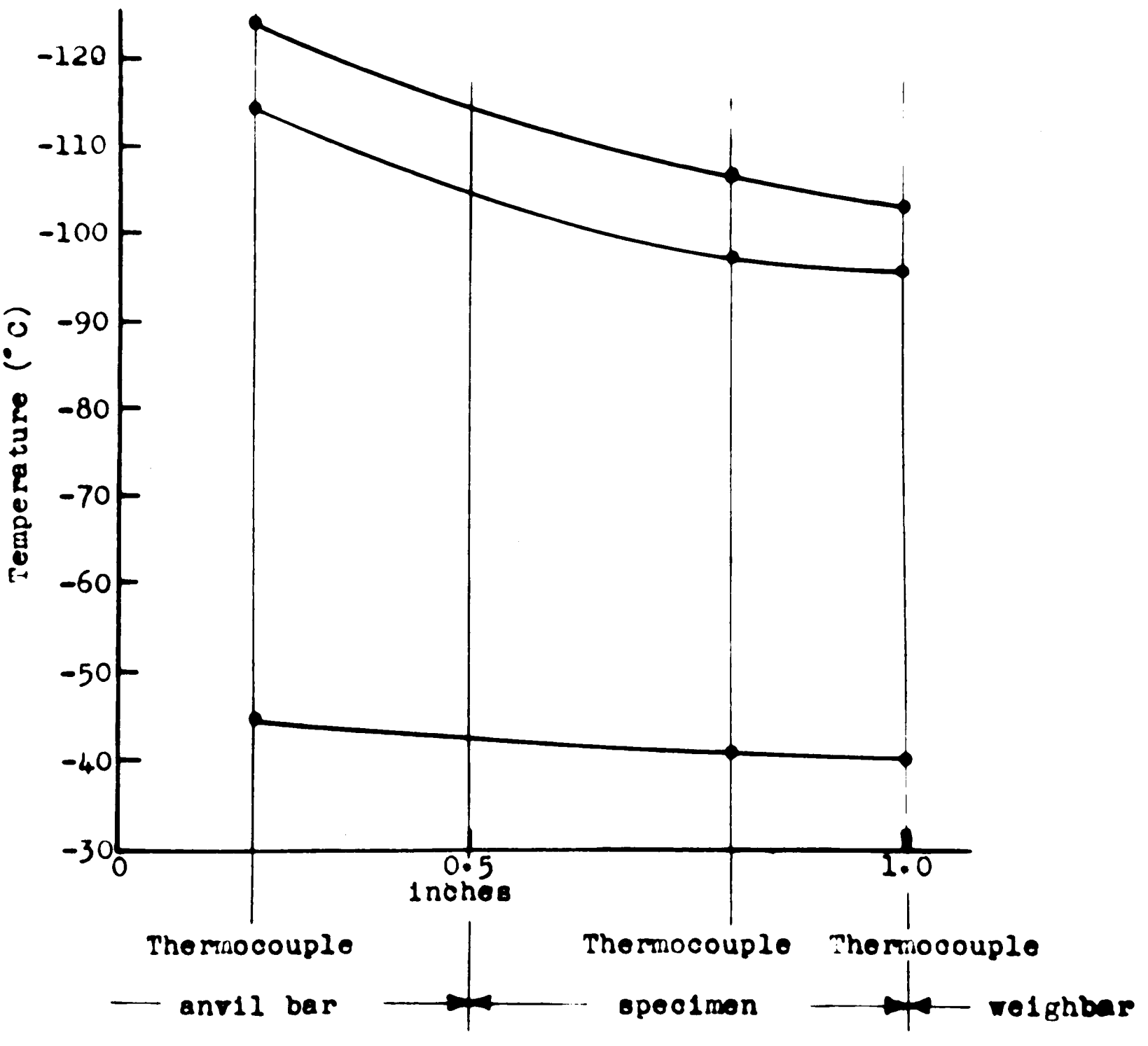


FIGURE 11 Variation of temperature along the specimen.

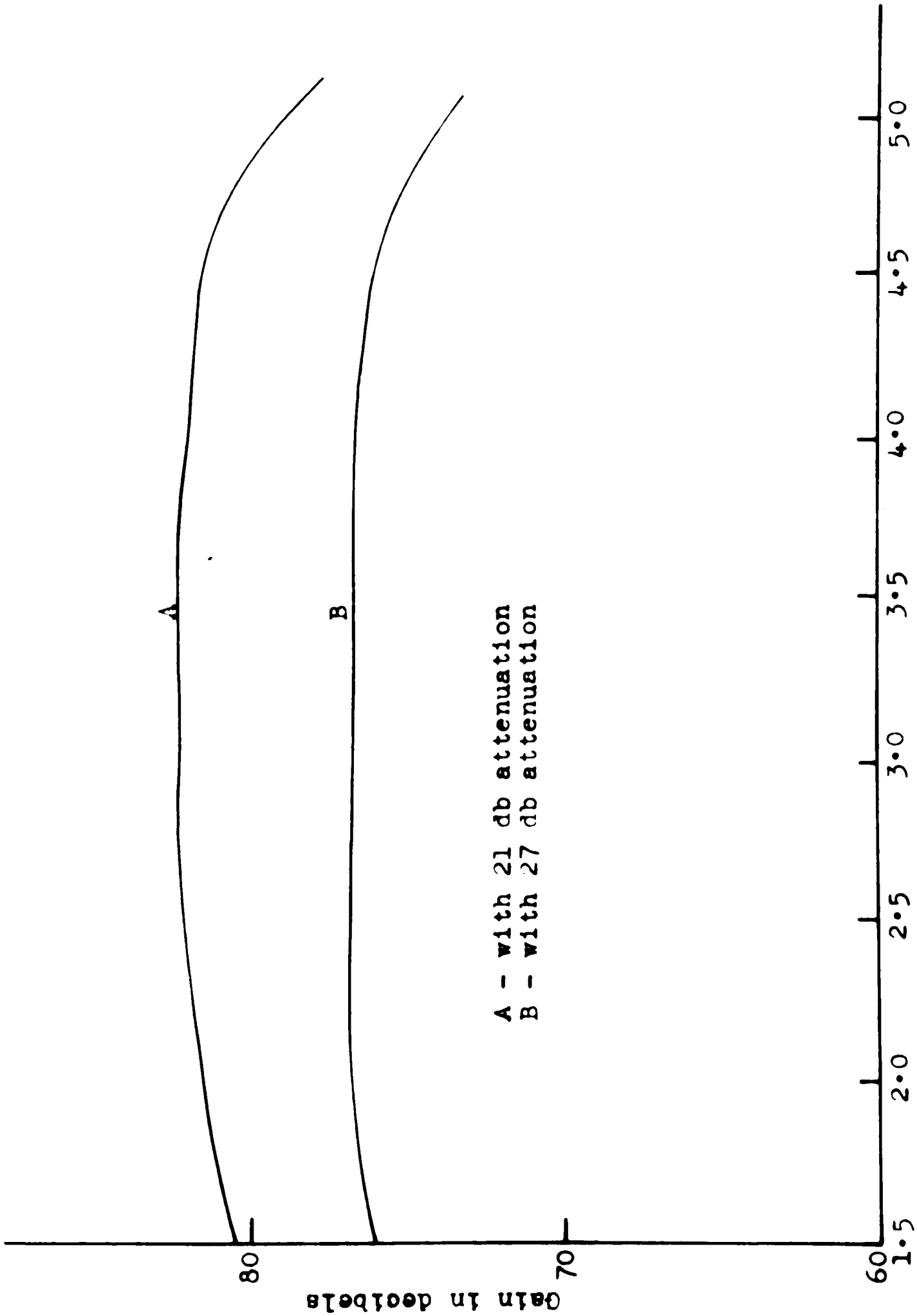


FIGURE 9 Amplifier frequency response.

the Fourier analysis of a square wave input of duration 120 microseconds gave an amplifier rise time of about 5 μsecs. The calibration lines (Figure 7) also show that the rise time for a step input is of this order. As the rise times of the pulses recorded in this thesis were of the order of 50 μsecs it was considered that the amplifier would faithfully reproduce the impact wave shape. This assumption had been checked by an earlier investigator (35) who applied a known wave shape to the amplifier and found that the amplified wave was only slightly distorted.

(iv) Calibration of the thermocouples.

These were calibrated at three fixed points, the ice point (0°C), the CO_2 point (-78·51°C) and the oxygen boiling point (-182·97°C). The calibration at the liquid oxygen point was perfectly straight forward, however, care had to be taken in calibrating the CO_2 point. As solid carbon dioxide is seldom surrounded by an atmosphere of pure CO_2 vapour, its temperature is considerably lower than the normal sublimation temperature. The fixed point temperature is only reached when the solid carbon dioxide has a vapour pressure equal to the partial pressure of the CO_2 vapour in the atmosphere immediately surrounding the solid. To obtain this sublimation temperature an electrical heating

coil (30 watts) was buried in the CO_2 near the bottom of the Dewar flask and about 2 inches below the thermocouple. The fixed point temperature was taken to have been reached when the e.m.f. reading was constant. This occurred after a time of about 12 minutes.

After having obtained values for the e.m.f. and temperature at the calibration points, the process of interpolating to obtain a continuous temperature — e.m.f. relationship over the whole range was facilitated by the use of a table giving the e.m.f. of a standard thermocouple. This standard thermocouple had been calibrated against a platinum resistance thermometer at the National Bureau of Standards, Washington D.C. (40). Figure 10 is the graph used to find the temperature corresponding to a given e.m.f. The abscissa represents the temperature and equivalent e.m.f. as given by the standard thermocouple. The ordinate is the e.m.f. of the standard thermocouple minus the e.m.f. of the test thermocouple at a particular temperature. Thus to find the temperature equivalent to a test e.m.f., a point is found on the abscissa such that its e.m.f. plus the vertical ordinate is equal to the given e.m.f. The temperature at this point is then read off.

It is seen from Figure 10 that the three test thermocouples calibrated very near the standard thermocouple —

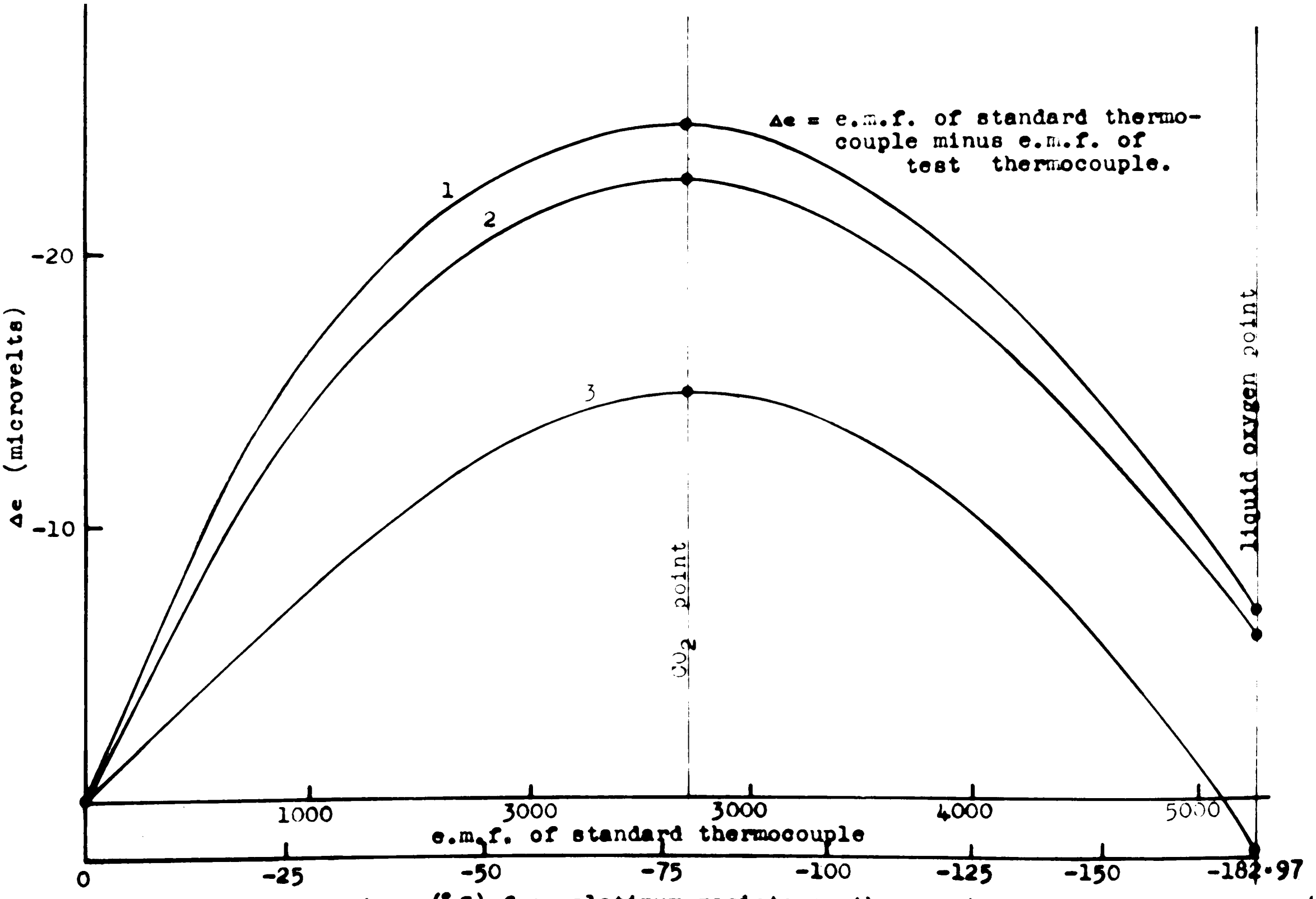


FIGURE 10 Thermocouple calibration curves.

the maximum variation at any temperature being only 25 μVolts.

(v) Temperature variation along the specimen.

From Figure 1 it is seen that the specimen is cooled by conduction and hence there must be a temperature gradient along the specimen axis. There will be radial temperature gradients as well, but these should be small compared with the gradient along the axis.

The thermocouple was always placed about $\frac{1}{8}$ inch from the top of the specimen. This was done because the temperature gradient does not affect the delay time-yield stress relationship. Yield occurs first at the top of the specimen, because not only does the stress wave reach here first but also the temperature is highest here. Hence in the delay time-yield stress investigation the temperature at the top of the specimen is the temperature required. However, in obtaining the dynamic stress-strain curves by recording stress-time curves on each specimen face it is important that the temperature throughout the specimen is substantially constant.

To investigate this variation in specimen temperature three thermocouples were fixed in position as shown by Figure 11. One was on the weighbar just above the specimen, one was approximately in the test position, and the third was on

the anvil bar below the specimen lower face. For three arbitrary test temperatures the variation of temperature along the specimen is shown in Figure 11. The variations in temperature from the average in each case were, 5·2% at -197°C, 2% at -99·5°C and 0·4 at -4°C. It was assumed that these variations were small enough not to cause any significant errors in the derived dynamic stress-strain curves.

(vi) The temperature rise during impact.

A certain proportion of the work done in plastically deforming a specimen must appear as heat energy. Hence during an impact the temperature of a specimen must rise slightly. Appendix II shows that the maximum increase in test temperature (absolute) that occurs in tests described throughout this thesis is 2°7 . Thus all the impact tests may be reasonably assumed to be constant temperature tests.

(2) Static tests.

(1) Calibration of the gauges.

(a) Maty cylinder gauge.

Owing to distortion of the plunger faces there was an error in the strain reading as obtained by the two static gauges. This error was found by comparing

the strain measured by the Baty cylinder gauge with the known strain of a high tensile test specimen. The error, which is only small, is a function of load and was applied as such in all static tests.

(b) Low temperature gauge.

This was calibrated at room temperature, and the calibration curve thus obtained was assumed to hold at the lower test temperatures. As the Wheatstone bridge circuit (Figure 6) is such that the gauges are temperature-compensated, the calibration will be valid at the low temperatures provided that the gauge factor remains constant. Figure 8 shows that down to -141°C such an assumption is very nearly correct. Hence the room temperature calibration was assumed to hold at all test temperatures. That it was valid was proved by the fact that the permanent deformation, as calculated from the room temperature calibration, compared favourably with that measured with a micrometer after the test.

The gauge was calibrated by two methods. The first was by simulating known specimen strains by squeezing the plunger-bearing faces together with two micrometers. A number of readings of strain and changes in the balancing resistances (R) were thus obtained and are shown plotted in Figure 12. The theoretical calibration line (Appendix 1)

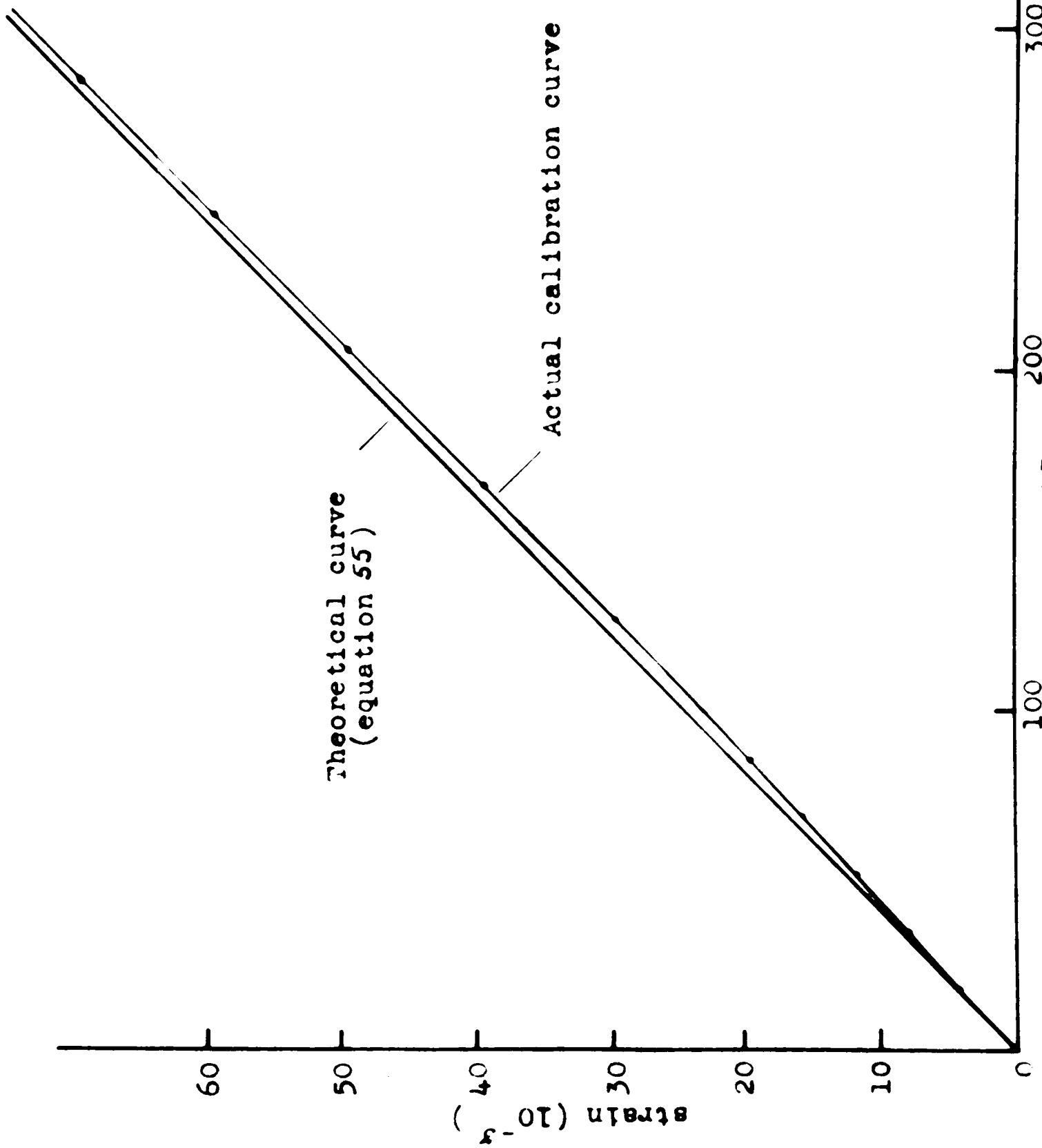


FIGURE 12 Calibration curve for low temperature strain gauge.

is also shown. The Figure shows that the actual calibration line is very nearly straight and does not differ to any great extent from the theoretical.

The second method was to yield a specimen at room temperature measuring the strain with both Baty cylinder gauge and the low temperature gauge. This method verified the use of the calibration line shown in Figure 12.

1-4. A DELAY-TIME THEORY

For the purposes of this thesis yield is defined as that point where the strain rate $\frac{d\varepsilon}{dt}$ increases suddenly as the stress rate $\frac{d\sigma}{dt}$ falls to zero. This occurs after a finite time of loading τ known as the delay-time.

According to Cottrell and Bilby's (25) theory of yield the dislocations in annealed ferrite are locked by carbon atoms. By making certain assumptions their theory shows that the mean time before a dislocation is released from its atmosphere is proportional to $e^{U/kT}$, where U is the activation energy for the applied stress σ, k is the Boltzmann's constant and T is the absolute temperature. It follows that at time t the total number of dislocations released is proportional to

$$\int_0^t e^{-U/kT}\, dt \qquad (7)$$

Campbell (13) suggested that yielding occurs when the density of released dislocations reaches a critical value. Thus yield is assumed to occur at a time τ (the delay time)

when

$$\int_0^{\tau} e^{-U/kT} dt = C = \text{constant} \qquad (8)$$

Now Yokobori (41) pointed out that the activation energy curves, as derived by Cottrell and Hilby from considerations of the mechanism of the release of a dislocation, may be approximately expressed by

$$U = -\frac{1}{n} \log_e (\sigma/\sigma_o) \qquad (9)$$

where σ_o is the yield stress at absolute zero and n is a constant. Therefore substituting this expression for U into equation (8) gives an expression for when yield occurs.

i.e. $$\int_0^{\tau} (\sigma)^{\alpha_T} dt = C (\sigma_o)^{\alpha_T} = c_T \qquad (10)$$

where $\alpha_T = \frac{1}{nkT}$ and c_T is constant at a constant temperature

Thus in constant strain-rate tests where $\dot{\varepsilon} = K^{d\varepsilon}/_{dt}$, the relationship between delay time τ and yield stress σ_y is given as

$$\tau = \frac{c_T}{(\sigma_y)^{\alpha_T}} \qquad (11)$$

Similarly for constant stress tests the relationship is given by

$$\tau = \frac{\sigma_T}{(\sigma_y)^{\alpha_T}} \qquad (12)$$

i.e. in both cases the theory predicts, at any given temperature, a straight line relationships between the logarithm of delay-time and the logarithm of yield stress.

It is to be noted that the above delay-time theory is only valid for times to yield less than about 0·1 second. It has been suggested (24, 42, 43, 44) that in tests in which yield occurs after a greater duration than this diffusion of carbon atoms may relock some of the dislocations after they have been released. The above theory does not take this into account.

Not all tests are constant strain rate or constant stress tests. The theory, however, permits a correlation between such 'general' tests and those performed at a constant strain rate or a constant stress. This may be done as follows. For any relationship $\sigma = f(t)$ where yield occurs at a stress σ_y after a time , then σ_y may be found from equation (10). Using this value of σ_y the equivalent time to yield at the same stress σ_y, in a constant strain rate test at the same test temperature, may be found from

equation (11). This method was used by Campbell and Duby (44), in collaboration with Dickson (43), to compare the delay-time theory with room temperature results obtained from tests on two steels, one a 0·24 C, steel and the other of the same composition (0·32%C) and heat treatment as that used in the present investigation. For the 0·24 C steel they found a value of α_{RT} = 13·0, and for the 0·32%C steel a value of α_{RT} = 12·5 appeared to be the most accurate, α_{RT} being the value of α_T at room temperature.

Other assessments of α_{RT} have also been made. Campbell (13) showed that Morrison's results (0·2% and 0·6%C steels) gave α_{RT} approximately equal to 19, whereas Vreeland, Wood and Clark's results (0·12 C steel) gave α_{RT} = 25. As both these researches were concerned with delay times in the region of 0·1 sec. it is possible that the above values of α_{RT} are over-estimates. Also there appears to be some evidence that the lower the carbon content of the steel the higher the value of α_{RT}.

To compare the delay time theory with the experimental results obtained in this thesis it is intended to first find an accurate room temperature value of α_{RT}. As α_T is in-

versely proportional to the absolute temperature this value of α_{RT} will give values of α_T corresponding to any temperature T. Hence using these values of α_T in equation (10) will give values of σ_T at the temperatures considered, thus if the theory holds, then for all tests at a constant temperature, these values of σ_T should be constant. Also the constants found at room temperature and a temperature T should be related by the following equation

i.e. $$\frac{\sigma_T}{\sigma_{RT}} = (\sigma_0)^{\alpha_T - \alpha_{RT}} \qquad (13)$$

To check this relationship a value of σ_0, the yield stress at absolute zero, is required. This is found by extrapolating the curve of static yield stress against temperature. (see section 2-2.)

1-5. METHOD OF WAVE ANALYSIS

In order to obtain dynamic stress-strain curves and delay time results for the steel the stress-time and particle velocity-time curves had to be found for both specimen faces. These curves were obtained by analysing the gauge outputs in a similar manner to that used by Campbell and Ruby (19). The method is reviewed below.

(i) General Theory.

The elastic wave motion in a long rod may be shown on a lagrange or (x, t) diagram, where x gives the position on the rod and t the time. In this x, t plane lines of slope $\frac{1}{c}$ ($\frac{dx}{dt} = c$) are such that $\rho cv + \sigma =$ constant (2α say), and those of slope $-\frac{1}{c}$ are such that $\rho cv - \sigma =$ constant (2β say).

Hence

$$\sigma = \alpha - \beta \qquad (14)$$

and

$$\rho cv = \alpha + \beta \qquad (15)$$

give the stress and particle velocity at any point x on the rod at any time t.

At a sudden change of section, as at section B (Figure 1), continuity considerations of force and velocity require

$$\sigma_1 = r\sigma_2 \qquad (16)$$

and $$v_1 = v_2 \qquad (17)$$

where $r = \frac{A_2}{A_1}$, the ratio of the cross-sectional area, suffixes referring to sections on either side of the discontinuity. Substituting values for σ and v from (14) and (15) and solving for α_2 and β_1 gives

$$\alpha_2 = \frac{2}{1+r}\alpha_1 - \frac{1-r}{1+r}\beta_2 \qquad (18)$$

and $$\beta_1 = \frac{1-r}{1+r}\alpha_1 + \frac{2r}{1+r}\beta_2 \qquad (19)$$

Consider two tests using the dynamic apparatus shown in Figure 1, the first on a high tensile plug, and the second on a test specimen. The stress waves generated at the end of the weighbars in the two tests are assumed to be identical. At Section B in the case of the first test $\beta_2 = 0$, hence from (18) and (14)

$$\alpha_2 = \frac{2}{1+r}\alpha_1 = \sigma_{2_0} \qquad (20)$$

where σ_{2_0} represents the elastic stress recorded at the gauges. In the second test when the specimen starts generating unloading waves β_2 is not zero and α_2 is given by (18) as

$$\alpha_2 = \frac{2}{1+r}\alpha_1 - \frac{1-r}{1+r}\beta_2 \qquad (21)$$

i.e. $$\alpha_2 = \sigma_{2_o} - \frac{1-r}{1+r}\beta_2 \qquad (21)$$ cont.

from (20).

The weighbar used in this investigation consists of three sections, of cross-sectional areas A_o, A_1 and A_2 such that $A_o > A_1 > A_2$, thus for the first test considered above the elastic stress wave recorded at the gauges is magnified from that generated at the impact end. This magnification is given by (20) as

$$MF = \frac{2}{1+\frac{A_2}{A_o}} \times \frac{2}{1+\frac{A_2}{A_1}} \qquad (22)$$

where MF is the magnification factor. The diameter of the middle section of the weighbar was chosen to give a maximum value of MF, i.e. A_1, was chosen so that

$$\frac{dMF}{dA_1} = 0$$

i.e. $$A_1^2 = A_o A_2$$

For the chosen values of the diameters D_o and D_2, i.e. 0·990 inches and 0·375 inches, this equation gives $D_1 = 0·609$ inches. These changes of section correspond to a stress magnification factor of 2·10.

(11) <u>The analysis of the stress-time and particle velocity-time curves</u>.

(a) <u>Upper face</u>.

Figure 13 shows the Lagrange diagram for the dynamic apparatus, letter suffixes referring to the points shown.

Let V represent the point at which the elastic and test records first diverge. Then the stresses recorded at the gauges during the interval OV give the stress and particle velocity ($v = \frac{q}{\rho c}$) on the upper face directly. For times greater than OV the specimen is generating unloading waves. These waves, generated at the specimen upper face, travel up to section B (Figure 1) where part of the wave is reflected and part transmitted. Consider any point P, on section 1-1 above the characteristic VW, from (21)

$$\alpha_p = \sigma_{p_o} - \frac{1-r}{1+r}\beta_R \qquad (23)$$

and from (14)

$$\sigma_{p_o} - \frac{1}{2} = \beta_p + \frac{1-r}{1+r}\beta_R \qquad (24)$$

where as before σ_{p_o} represents the stress recorded at the gauges using a high tensile plug instead of the specimen.

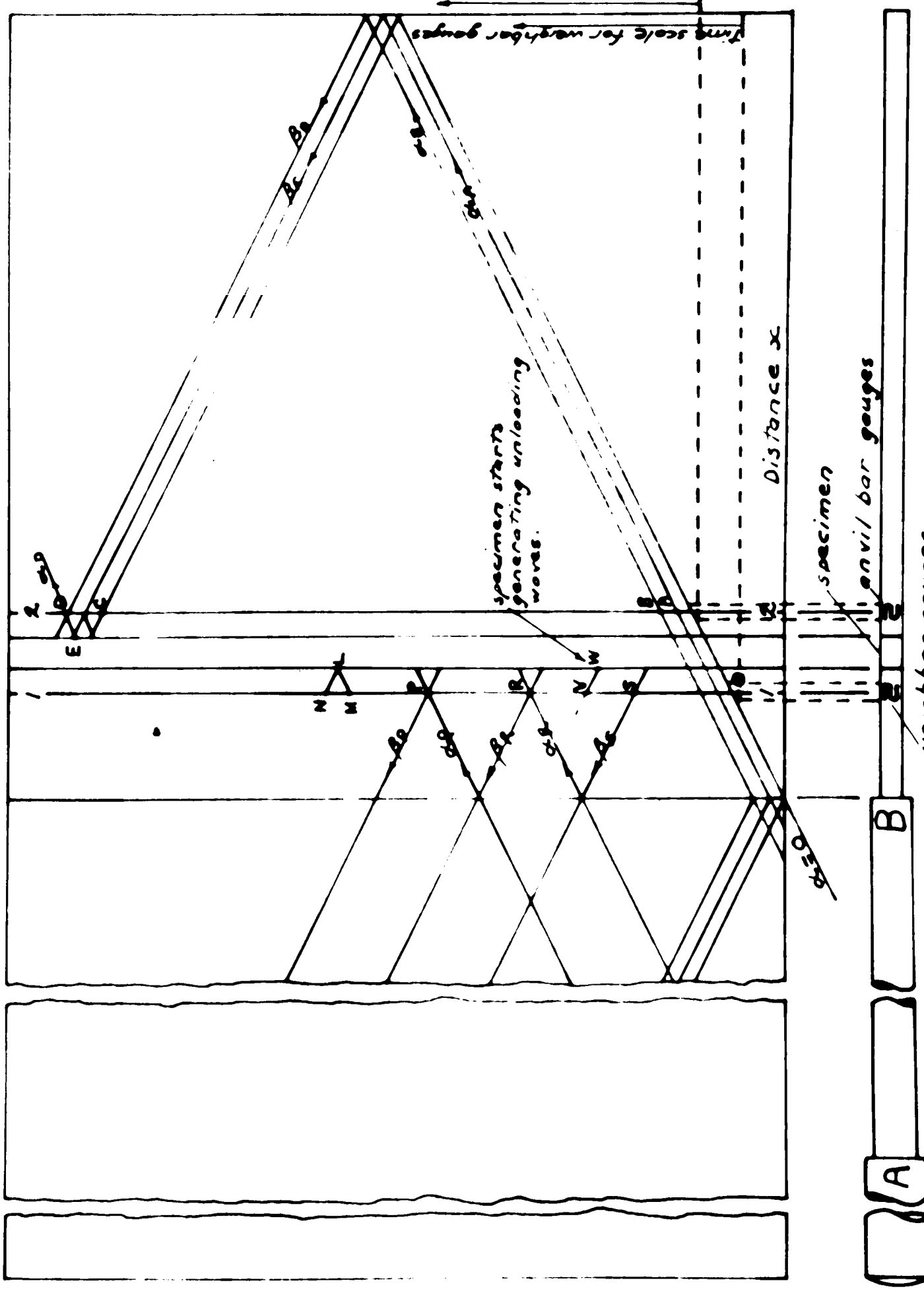


FIGURE 13 Lagrange diagram showing method of calculating α and β.

Similarly at R

$$\alpha_R = \sigma_{R_o} - \frac{1-r}{1+r}\beta_s \tag{25}$$

and $$\sigma_{R_o} - \sigma_R = \beta_R + \frac{1-r}{1-r}\beta_s \tag{26}$$

However as S is below the characteristic VW $\beta_s = 0$, and hence from (26)

$$\alpha_R = \sigma_{R_o} \tag{27}$$

and $$\sigma_{R_o} - \sigma_R = \beta_R \tag{28}$$

Thus as σ_{R_o} and σ_R are known from the elastic and test records respectively then β_R may be found. Similarly using this value of β_R, the known values of σ_{p_o} and σ_p, equations (23) and (24) give α_p and β_p. In this manner values of α and β may be plotted against time at the gauge sections 1-1. The stress-time and particle velocity-time curves on the specimen upper face are then easily obtained as follows.

Consider point L. From equations (14) and (15)

$$\sigma_L = \alpha_M - \beta_N \tag{29}$$

and $$\rho c v_L = \alpha_M + \beta_N \tag{30}$$

hence as α_M and β_N are known σ_L and v_L may be calculated.

In a like manner the stress and particle velocity at other points on the specimen upper face may be found, thus giving the required stress-time and particle velocity-time curves.

(b) Lower face.

The method used to find the stress-time and particle velocity-time curves for the specimen lower face is described below.

Until the unloading wave from the free end of the anvil bar reaches the gauges (point C) the stress and particle velocity on the specimen face are recorded directly. However, for any point D above C the following analysis must be used. Consider the point D

From (14)

$$\sigma_D = \alpha_D - \beta_D$$

$$= \alpha_D - \sigma_B \qquad (31)$$

as $\beta_D = \sigma_B$, assuming perfect reflection at the free end of the anvil bar. Thus as σ_D and σ_B are known, α_D and β_D may be determined. Hence the values of α and β can be found for all values of time along section 2-2. From these curves the stress and particle velocity at a point E (say) on the specimen lower face may be found from (14) and (15)

i.e. $$\sigma_E = \alpha_E - \beta_E$$

$$= \sigma_D + \sigma_B - \sigma_A \qquad (32)$$

and $$\rho c v_E = \alpha_E + \beta_E$$

$$= \sigma_D + \sigma_B + \sigma_A \qquad (33)$$

as $$\alpha_E = \alpha_D = \sigma_D + \sigma_B$$

and $$\beta_E = \alpha_A = \sigma_A$$

In this manner complete stress-time and particle velocity-time curves may be found for the specimen loaded face.

(iii) Dynamic stress-strain curves.

To obtain a dynamic stress-strain curve, a curve of mean stress against time, and a curve of strain against time for the specimen have to be found.

The mean stress-time curve is obtained by averaging the stress-time curves for the two specimen faces, as found by the methods outlined above.

The strain-time curve may be found as follows. The average strain-rate for the specimen at a given instant is

given by

$$\frac{de}{dt} = v_u - v_l \qquad (34)$$

where v_u is the particle velocity on the specimen upper face and v_l is the particle velocity on the specimen lower face. Thus the average strain at time t is given by

$$e = \int_0^t \frac{(v_u - v_l)}{0.5} dt \qquad (35)$$

Hence by integrating the difference between the two particle velocity-time curves a curve of specimen strain against time may be found.

From these curves of mean stress against time and strain against time, the dynamic stress-strain curves are found by plotting stresses against strain at corresponding times.

(iv) Variation of yield stress with delay-time.

As yield first occurs at the specimen upper face, only the elastic and weighbar records need be analysed to obtain values of the yield stress and delay-time. Also, as the yield stress has been defined as that point where $\frac{dq}{dt} = 0$ (section 1-4), the above records need only be analysed up to the maximum stress. It will be seen later (section 2-3) that the yield stresses obtained in this manner are a few

percent higher than those shown on the corresponding dynamic stress-strain curves. This is due to the fact that the stress wave propagated through a specimen is always slightly smaller than that applied to the specimen upper face. Hence the maximum stress (apparent yield stress), obtained from the average stress-time curve for the specimen, is always less than the maximum stress on the specimen upper face (true yield stress). Also as the maximum stress at the specimen lower face does not occur at the same time as the maximum stress at the specimen upper face, the 'time to yield' obtained from the dynamic stress-strain curve differs slightly from the 'delay-time' as found from the stress-time curve for the specimen upper face.

1-5. TESTING TECHNIQUE

(1) Static.

The specimen was lapped in contact with the plungers and centered by means of a brass ring. The container, formed by bolting the two turned boxes on to the steel block, was then filled with liquid oxygen until the specimen temperature, as indicated by the thermocouple e.m.f., was in the region of that required. The constant feed apparatus was then turned on and the flow of liquid oxygen adjusted until the best temperature was obtained. No liquid oxygen escaped from the container as the joints were tight. Also, with central loading the plungers did not seize up in the block as the liquid oxygen acted as a lubricant and prevented ice formation. During loading the flow of liquid oxygen was adjusted to maintain a constant specimen temperature. The criterion for central loading throughout the test was that the block could rotate on the plungers.

Theoretically, as the low temperature strain gauge (Figures 4 and 5) is temperature-compensated, then varying the specimen temperature at a constant load should have no effect on the bridge balance. In practice, however, it was found that the strain gauge was not perfectly temperature-

compensated. This was attributed to uneven distortion of the rings as the temperature was lowered. Hence to obtain accurate results the temperature had to be maintained substantially constant throughout the test. This was done by the method described above and it was found that the temperature could be kept constant to within $\pm 3^{\circ}C$.

(ii) Dynamic.

To obtain a delay-time result at a given impact velocity and test temperature only the elastic and weighbar records were required, however, to obtain the dynamic stress-strain curve an anvil bar record, was also needed. As the elastic record, corresponding to a given impact velocity, is negligibly altered by altering the specimen temperature, a room temperature elastic wave served (for the particular impact velocity under consideration) as the elastic wave at all temperatures.

The specimen was first lapped in contact with the high-tensile steel weighbar and anvil bar, a thin layer of oil being applied between the surfaces. At the lower test temperatures a difficulty was met with, in that the oil would freeze and upon impact would cause slight irregularities in the weighbar records. This difficulty was overcome by using only a very fine film of oil, just sufficient

for the surfaces to 'stick' together. Also as the temperature of test became lower and the rubber sleeves clamped to the bar became less effective, it became increasingly difficult to stop the anvil bar after impact. Hence in these tests stricter clamping methods had to be used to prevent the strain gauges from being stripped off the anvil bar.

In the static test after dynamic compression the specimen was removed and retested statically within a few minutes, whereas in the repeated impact tests the time between impacts varied between eight and thirteen minutes. If any time-taking difficulties were met with, the specimen was put in liquid oxygen until ready to be retested — thus preventing undue ageing between tests.

(iii) Micrographic examination of specimens.

A flat approximately 0·1 inch wide was first mechanically prepared on the specimen, the final polish being obtained with microid polishing alumina. This flat was then polished electrolytically in a perchloric acid — acetic anhydride electrolyte. This electrolyte was chosen as it gave maximum throwing power. The voltage across the cell was 50 volts, the current 25-30 ma. and the time of polishing 2-3 minutes. Finally the specimen was etched in picral.

PART II

2-1. [illegible]

The steel used in the present investigation was York Gate 2185 supplied by the Mechanical Engineering Department of the University of Bristol. This medium carbon steel had the following composition

C	Si	Mn	S	P
0·32%	0·235%	0·62%	0·037%	0·025

The bar supplied was $2\frac{1}{2}$ inches in diameter and was rough-machined into eight $\frac{5}{8}$ inch diameter rods, which were stress relieved for one hour at 600°C. After cooling in the furnace, the rods were machined and ground to either $\frac{1}{2}$ inch or $\frac{3}{8}$ inch diameter, before receiving a final vacuum anneal at 850°C for thirty minutes.

Micrographs of this steel revealed its homogeneous nature. Inhomogenities such as inclusions and decarburised zones were virtually absent, and hence scatter in the results due to these should have been reduced to a minimum. Slight variations in the results as obtained by different batches of specimens were, however, noticed. These can probably be attributed to slight differences in heat treatment.

2-2. STATIC TESTS

(1) Experimental Results.

(1) Test results.

The static properties of the steel were investigated at a number of temperatures. The apparatus used, its calibration and the techniques necessary in its application have been described in sections 1-2, 1-3 and 1-6 respectively.

Static stress-strain curves were found at temperatures of +15°C (room temperature), -41°C, -81°C, -121°C and -183°C. At all these temperatures the load was applied at an approximately constant rate. The room temperature stress-strain curve was found by using the Baty cylinder gauge to measure the strains, whereas the lower temperature stress-strain curves were obtained by using the strain gauge shown in Figures 4 and 5. The stress-strain curves found in this manner are shown in Figure 14.

It is seen that the whole of the stress-strain curves are raised as the test temperature becomes lower. At -183°C the upper yield stress has increased to 106,000 lb./in², 2·4 times the room temperature value. After yield the ratio of the stresses, at the same strain, decreases slightly as the strain increases. Also the stress-strain curves in

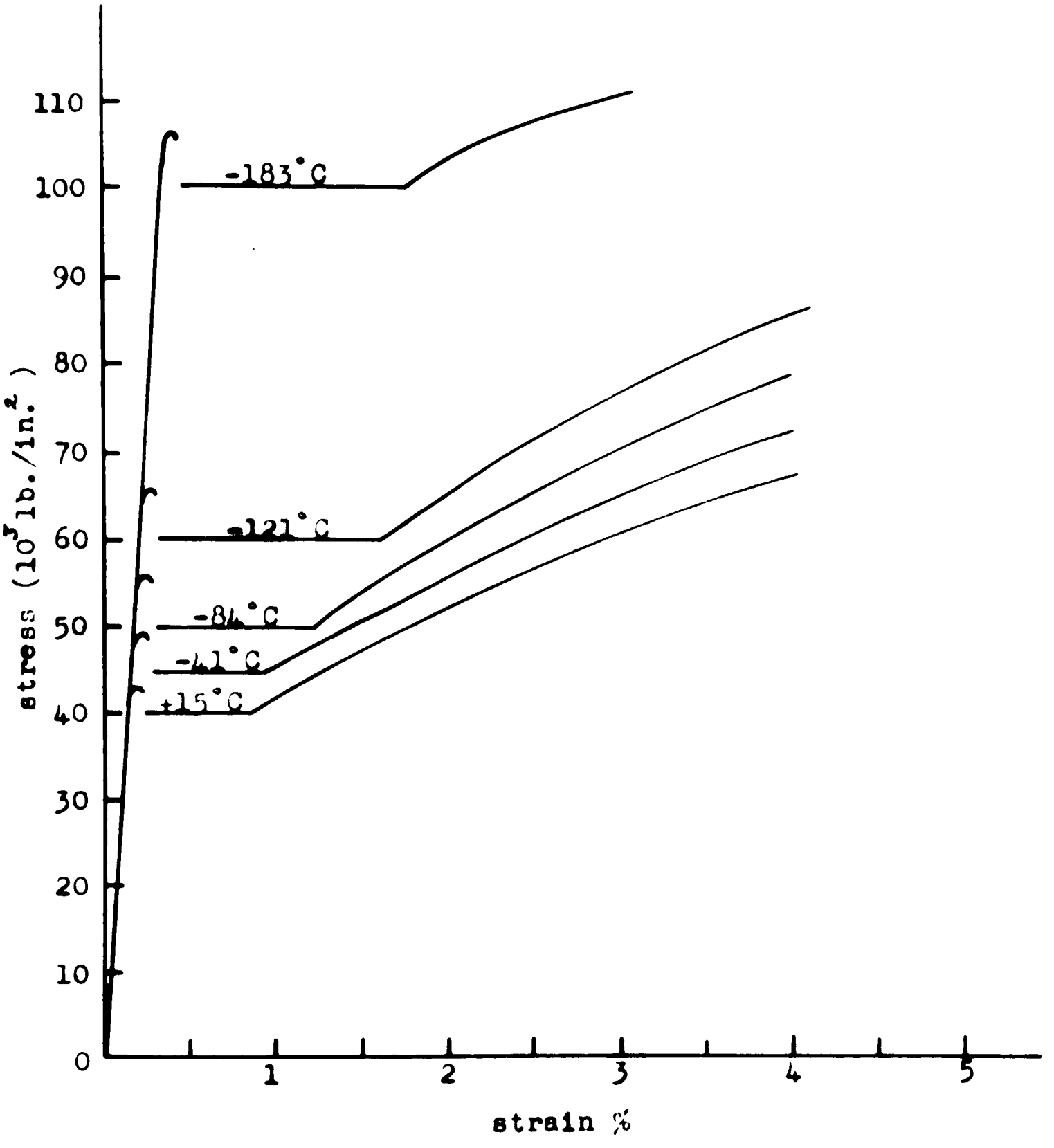


FIGURE 14 Static stress-strain curves obtained at a number of test temperatures.

Figure 14 show that not only does the lower yield stress increase as the test temperature becomes lower, but also the yield point strain becomes greater.

In order to obtain an estimate of σ_o, the upper yield stress at absolute zero, the logarithm of the yield stresses, corresponding to the above static stress-strain curves, are shown in Figure 15 (curve C) plotted against their respective test temperatures (absolute). To obtain the shape of this curve accurately, a further set of tests was performed in which only the upper yield stresses were found. Some of these tests were carried out at the temperatures at which the whole stress-strain curves were obtained and some at different temperatures. The results corresponding to these tests are also shown in Figure 15. From the values of the yield stresses obtained in tests at identical temperatures it is seen that the scatter in the results is small.

(11) Micrographic examination.

A number of specimens, with 'flats' prepared as described in section 1-6, were tested statically at various temperatures. By examined the prepared 'flats' before and after test it was possible to compare the mechanism of deformation at the various test temperatures.

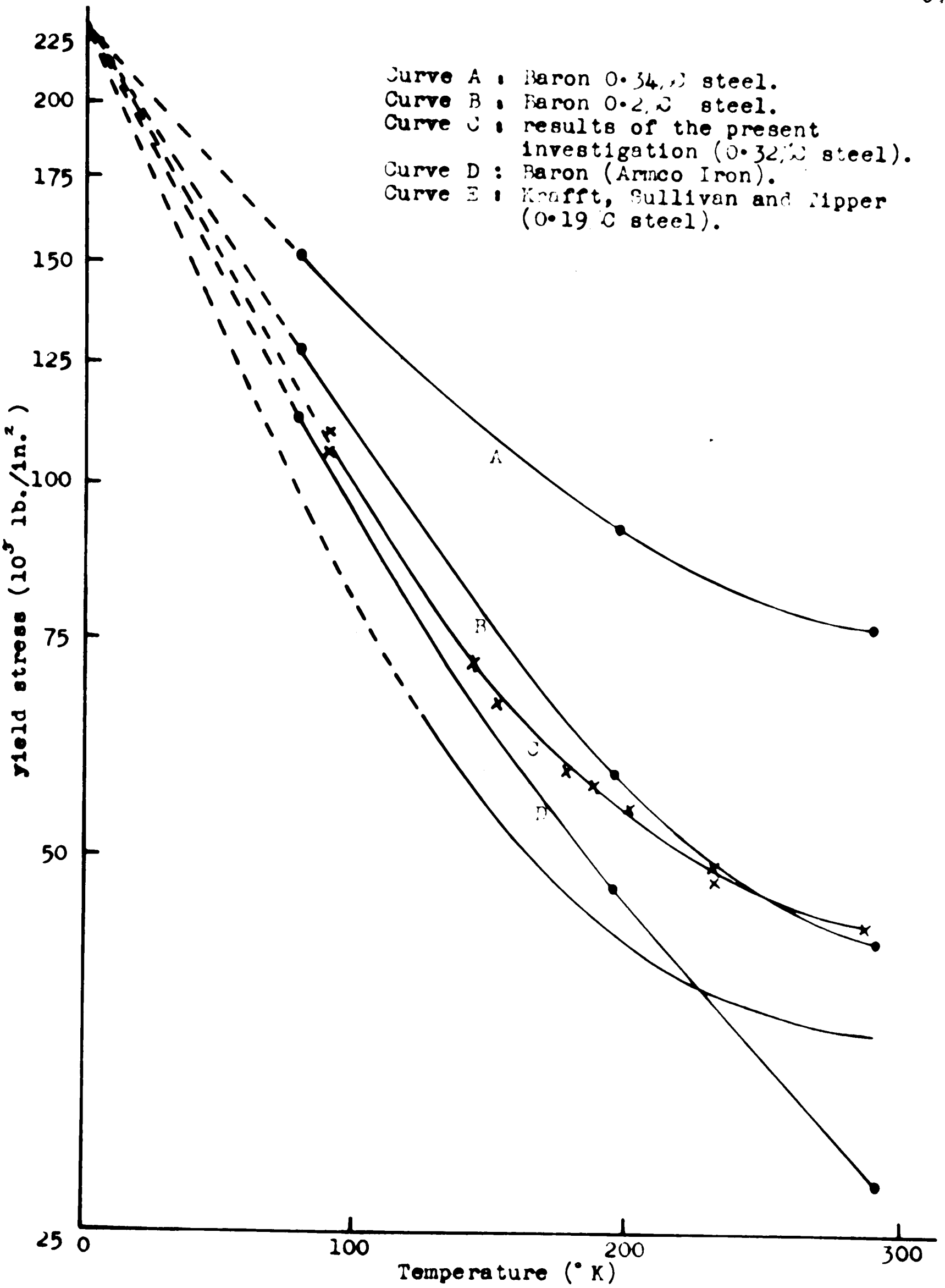
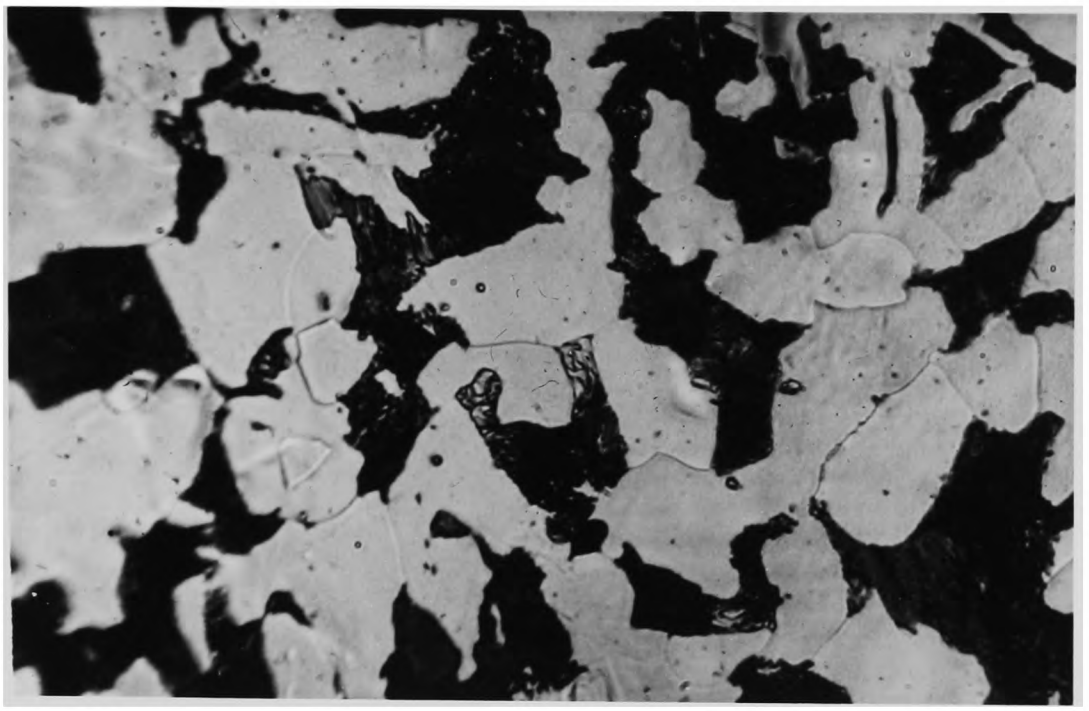


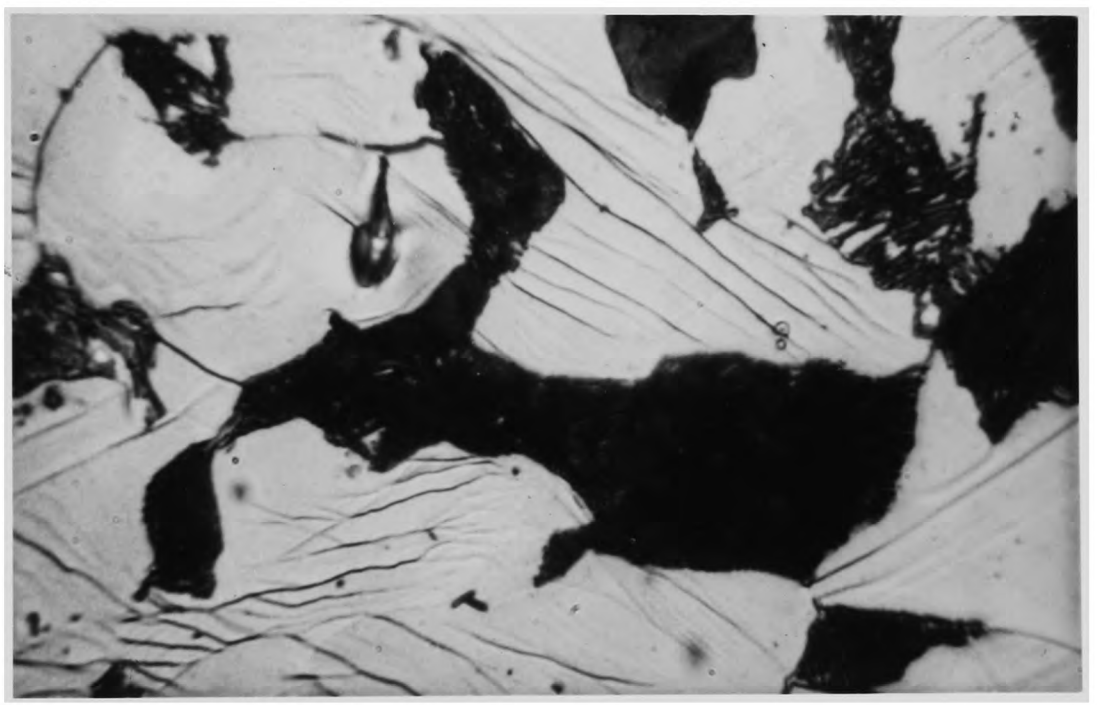
FIGURE 15 Variation of the upper yield stress with temperature.

Figure 16(a) shows the microstructure of a steel specimen before deformation, and Figure 16(b) a portion of the same prepared surface after 4% static deformation at +15°C. It is seen that deformation occurred by coarse slip in the ferrite, the slip lines often being forked. Some multiple slip is also evident. Similarly Figures 17(a) and 17(b) show microstructures of another specimen after 4% static deformation at -183°C. The magnification in Figures 16(a) is ×550 and that in Figures 16(b), 17(a) and 17(b) is ×1400. A comparison of Figures 16(b) with 17(a) and 17(b) shows that at -183°C the specimen deforms by a much finer slip than that by which the steel deforms at room temperature. Also there is far less multiple slip at -183°C than at room temperature.

An examination of the prepared flat after deformation at -183°C failed to show the formation of any twins. As these may have been disguised by slip lines, it was decided to prepare for examination the specimen used to find the stress-strain curve at -183°C. When examined this surface also failed to show the formation of twins. Similarly most of the specimens used to find either the static-strain curves, or yield stress variation with temperature, were prepared for metallographic examination and examined thoroughly. Twins were not observed in any of these



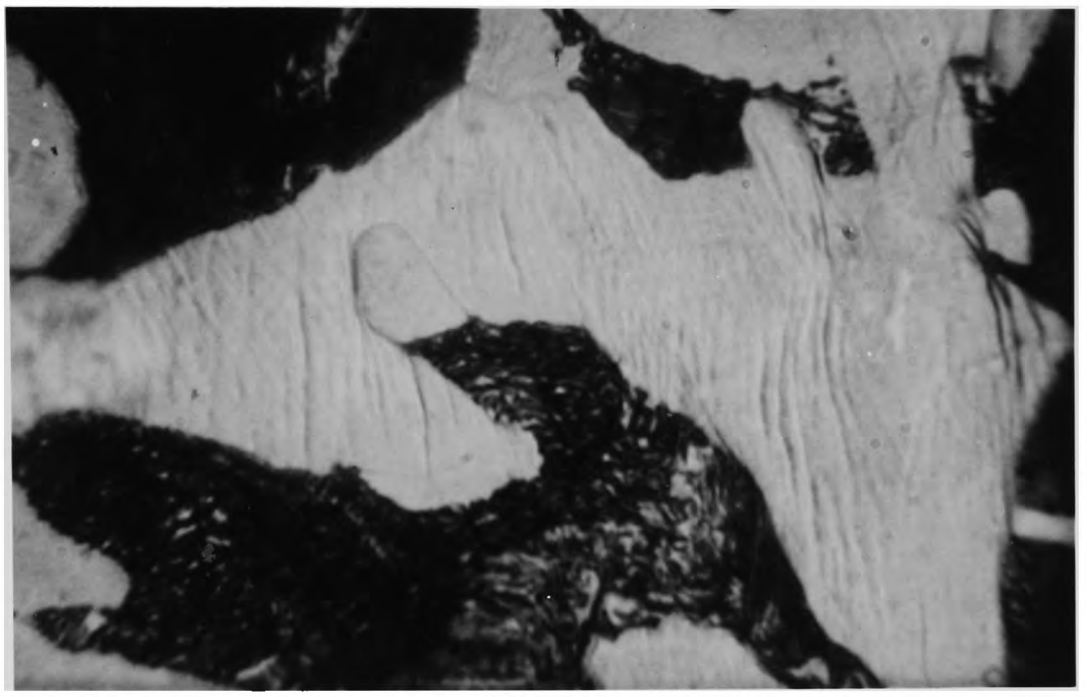
16 (a)



16 (b)

FIGURE 16 Micrographs taken before and after static deformation at +15°C.

(a) Before test. Magnification = ×550
(b) After 4% strain. Magnification = ×1400



17(a)



17(b)

FIGURE 17 Micrographs taken after static deformation at -183°C.

(a) and (b) After 4% strain. Magnification = ×1400

specimens and it was thus concluded that twinning was not a mechanism of static deformation even at the lowest test temperature used.

(2) Discussions of Results.

(1) In their theory of the yield strength of iron, Cottrell and Bilby (44) presented a relationship between the static upper yield stress and the test temperature. The theory predicted that at constant strain rate yield will occur when the value of $\frac{U}{kT}$ reaches a constant value, where the symbols have the meaning assigned in section 1-4. Yokobori's (41) expression for the activation energy U, (equation 9) thus gives the relationship between test temperature and yield stress as

$$T \propto \log\sigma_0 - \log\sigma_y$$

i.e. the theory predicts a straight line relationship between the absolute test temperature and the logarithm of the yield stress, the intercept on the Y-axis being equal to the logarithm of σ_0.

To enable a comparison to be made between the present results and the above theory, the logarithms of the yield stresses have been plotted against absolute temperature in

Figure 15. Also shown in Figure 15 are results obtained by other investigators (24, 26) in similar tests on iron or steel. It is seen that for temperatures above about -100°C the curve representing the present results is by no means straight as the theory predicts. At first this appears surprising as the results of McAdam and Mebs (7) for tests undertaken on ingot iron and 0.04%C steel agree remarkably well with the theory. However, the results of other investigators, as plotted in Figure 15, also show discrepancies from the predicted straight line relationship. The present results and those of the investigators cited above appear to show two general trends. The first is that the higher the carbon content of the steel the less is the temperature dependence of the upper yield stress, and the second is that the higher the carbon content the greater is the discrepancy between the actual results, and the straight line relationship as predicted by the above theory. To a large extent it is considered that both of these tendencies are due to the influence of the pearlite on the strength properties of the steel. In particular, as the carbon content of the steel increases, the greater becomes the ratio of pearlite to ferrite, and hence the greater must be the discrepancy between the yield theory (based on ferrite alone) and the experimental results.

Finally, by extrapolating the curves in Figure 15 to the absolute zero it is seen that σ_o may be taken as essentially independent of carbon content and in the range 220,000 lb./in^2 to 240,000 lb./in^2

(ii) It has been observed Figures 16(b) and 17(b) that the lower the test temperature the finer the slip in the ferrite. This may be explained by the fact that the lower the test temperature, the higher the stress to yield and hence the greater the disturbances when yield occurs. These disturbances, which are caused by source dislocations breaking free and generating free dislocation rings, assist nearby sources to operate, thus the greater the disturbance the greater the total number of sources activated and hence the finer the slip.

In 1950 Frank and Read (46) showed that dislocations tended to form a superlattice in crystals, such that all components of the superlattice could act as dislocation generators. Mott (47) gave the shear stress $\Delta\sigma$ required to activate a Frank-Read source as

$$\Delta\sigma = \frac{Gb}{\ell} \qquad (36)$$

where b is the Burger's vector of the dislocation and ℓ

is the source length. As the freed sources must generate dislocation rings under the influence of the applied lower yield stress, it is reasonable to assume that $\Delta\sigma$ is approximately proportional to this lower yield stress. Thus as the slip is finer and hence ℓ is smaller as the test temperature becomes lower, then from equation (36) the lower yield stress must increase as the test temperature falls. Figure 14 shows that this does occur.

The existence of a greater lower yield strain as the temperature becomes lower may be explained from the work of Eshelby, Frank and Nabarro (48). The lower yield extension is terminated when the back stress on the sources, due to dislocations piled up against obstacles, completely neutralises the applied stress $\Delta\sigma$. According to Eshelby, Frank and Nabarro this occurs when the shear displacement δ, due to dislocation movement in a slip band of length L, is given by

$$\delta = \frac{\pi L (\Delta\sigma) k}{G} \qquad (37)$$

where k is a numerical factor always near to unity. Again taking $\Delta\sigma$ as being approximately proportional to the lower yield stress and substituting its value from equation (36) we obtain an expression for the shear displacement when

the source ceases to activate

i.e. $$\delta = \frac{Ek}{\ell} \qquad (30)$$

Hence as decreases as the test temperature falls then the shear displacement and hence the lower yield strain should increase as indeed it does (Figure 14).

(iii) As no twins were evident in the specimens tested at temperatures of -183°C and above, it may be assumed that if a critical shear stress for twinning does exist (24, 26) it must be above the yield stress at -183°C i.e. above 106,000 lb./in^2

2-3. DYNAMIC STRESS-STRAIN CURVES

(1) General

To obtain a dynamic stress-strain curve, corresponding to a given impact velocity and temperature of test, the relevant elastic, weighbar and anvil bar records were analysed in the manner described in section 1-5. Stress-strain curves were found for up to three impact velocities at four different temperatures of test. The impact velocities used were 430 in./sec., 470 in./sec., and 503 in./sec., and the test temperatures were +13°C, -41°C, -84°C and -121°C respectively. At -121°C yield was found to occur only at an impact velocity of 503 in./sec., and hence only the dynamic stress-strain curve corresponding to this particular impact velocity is presented. For the same reason, at -84°C only the stress-strain curves at 470 in./sec., and 503 in./sec., were obtained.

In general two or more weighbar and anvil bar records were obtained at each temperature and impact velocity. The records obtained at each gauge were found to be consistant to ±1% at room temperature and to ±2% at lower temperatures. The average record at each gauge position was used to obtain the dynamic stress-strain curves. Also, as shown in section 1-3 (Figure 7), the elastic wave, corresponding to

a given impact velocity, is altered very little by changes in the test temperature. Hence, in finding the dynamic stress-strain curve at a particular temperature, the elastic record used was the average of those found at room temperature at the impact velocity under consideration.

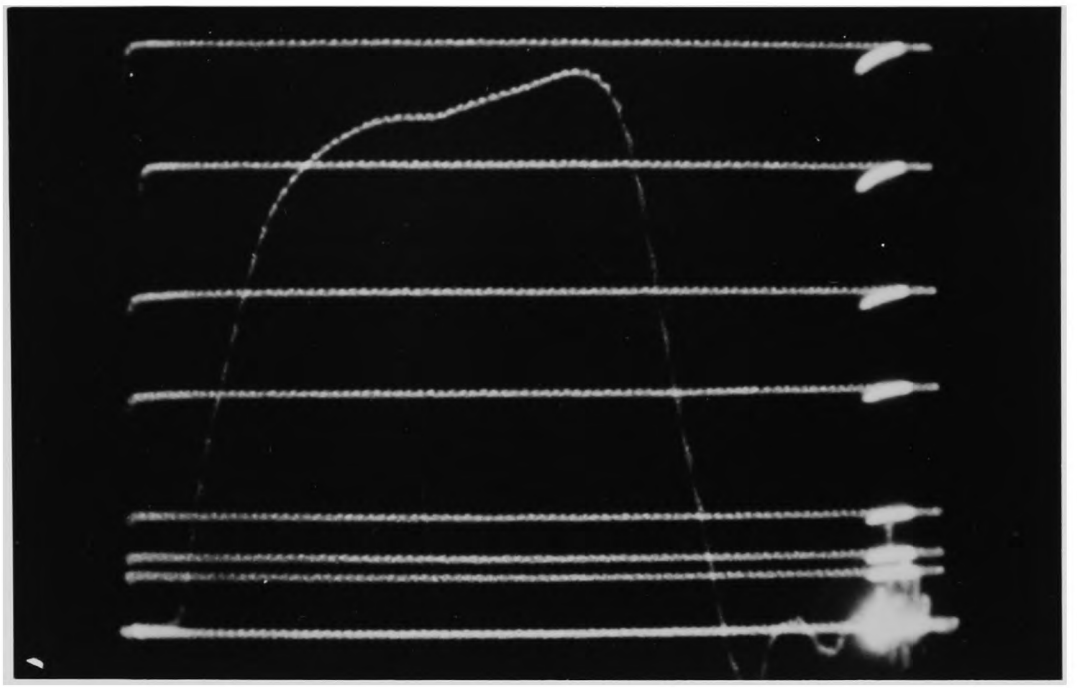
(2) Experimental Results

(i) Room temperature results.

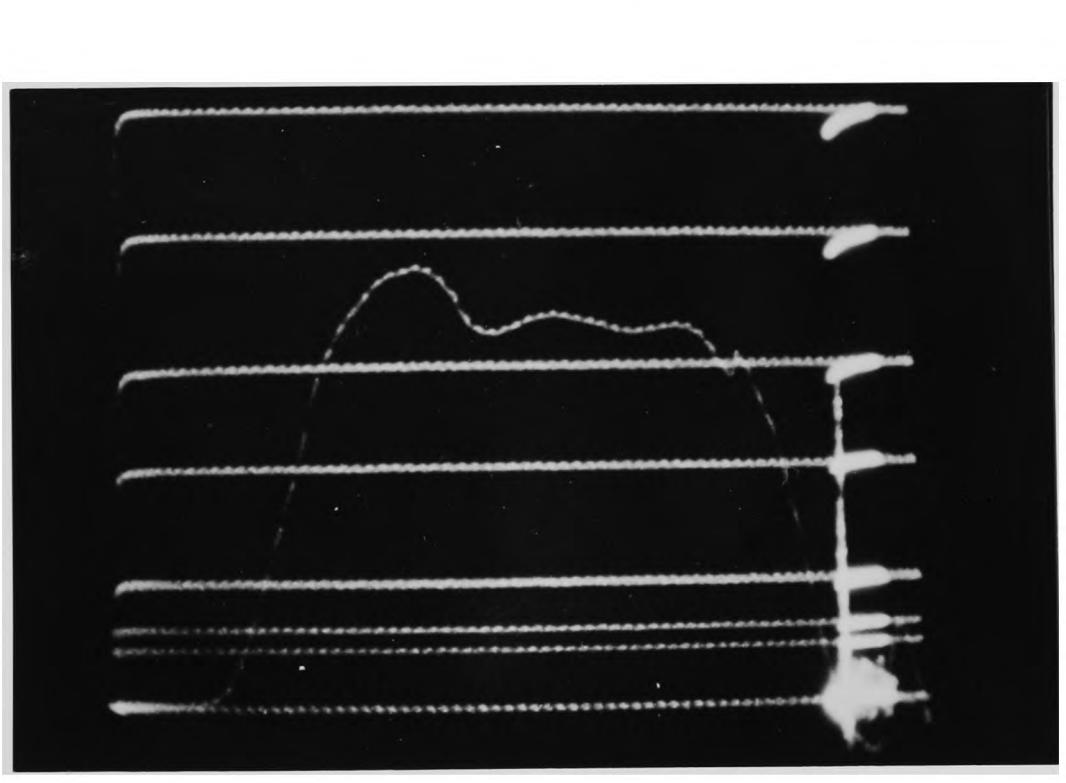
(a) Dynamic stress-strain curves. ($+15^{\circ}C$)

The following is an outline of the method by which the stress-strain curve was obtained at an impact velocity of 430 in./sec. It is not thought necessary to give details of how the stress-strain curves were obtained at the other two impact velocities but merely to present the final results.

Figure 18 shows the relevant gauge records and their respective calibration lines for an impact velocity of 430 in./sec. Figure 18(a) shows the elastic record, Figure 18(b) the anvil bar record, and Figures 18(c) and 18(d) two weighbar records, the traces being interrupted every two microseconds. Figures 18(c) and 18(d), both weighbar records, indicate the consistency of the records that were obtained; it is seen that at no time do the stresses differ



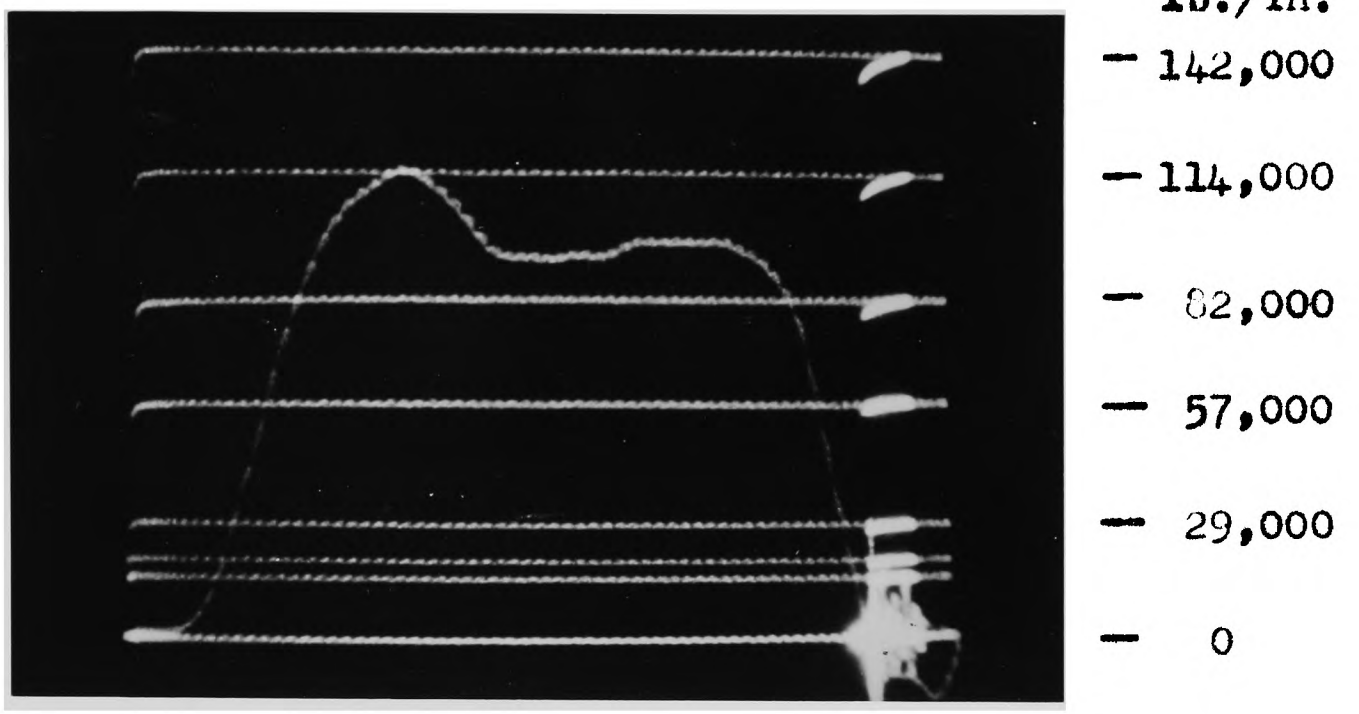
18(a)



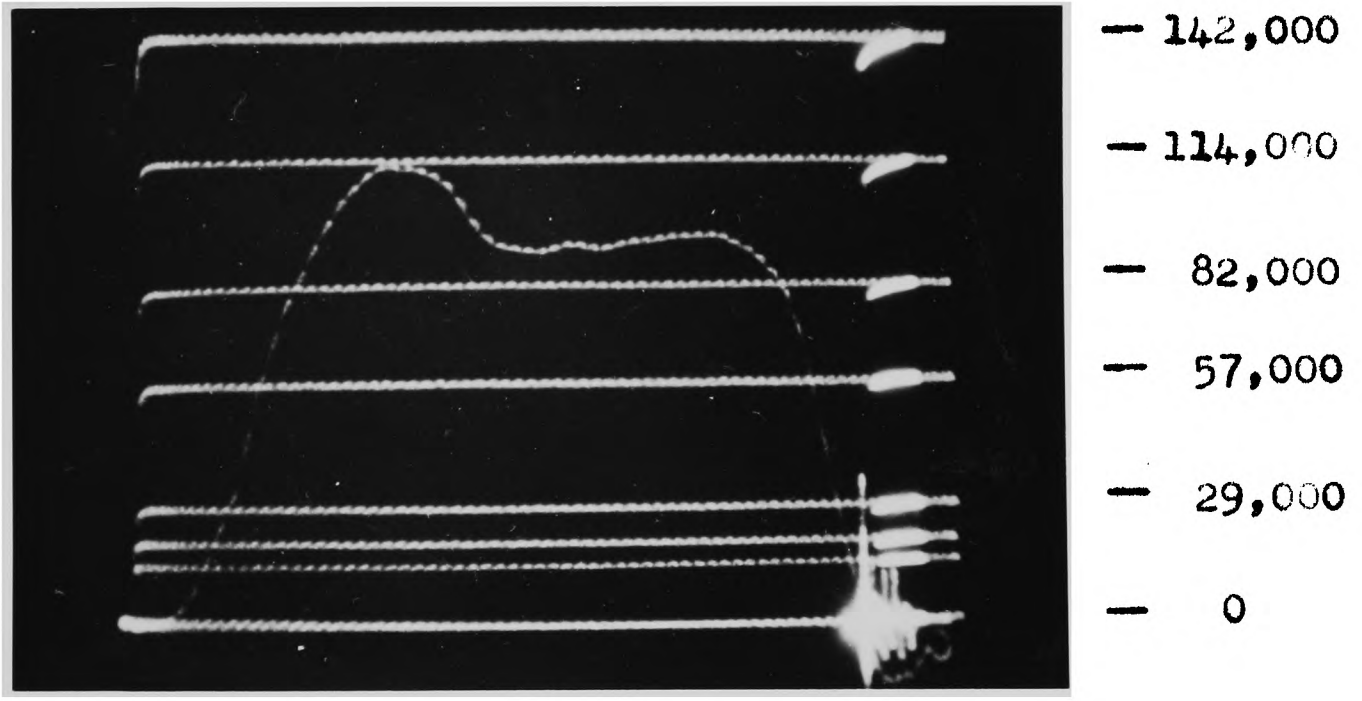
18(b)

FIGURE 18 Records obtained at +15 C for an impact velocity of 430 in./sec.

(a) Elastic record. Rg ≑ 369Ω S = 1·94
(b) Anvil bar record. Rg ≑ 369Ω = 1·94.



18(c)



18(d)

FIGURE 18 (continued)

(c) and (d) Weighbar records. $R_g \doteq 376\Omega$
$S = 1{\cdot}94$.

by much more than 1%. Using the gauge factor, the known value of E and the values of the calibrating resistances, a calibration curve was drawn for each record, relating vertical deflection to stress at the gauge position (equation 5). By means of these calibration curves, the records were converted to stress-time curves. The average elastic and neighbar stress-time curves thus obtained are shown in Figure 19 as curves A and B respectively. From these curves the stress-time curve for the specimen upper face (curve C) was obtained by the method of wave analysis described in section 1-5. From curve C it is seen that the true yield stress (stress maximum by definition) is 108,000 lb./in^2 and occurs after a time of 33 microseconds. Figure 19 also shows that the fronts of the recorded and analysed waves differ slightly. This is due to the finite length of the gauges.

Figure 20 shows the stress-time and particle velocity-time curves (xpc) for both specimen faces obtained by the method of wave analysis as described in section 1-5. Curves B and C are the stress-time and particle velocity-time curves respectively for the specimen upper face, and curves D and E are the stress-time and particle velocity-time curves for the specimen lower face. The time base for these curves is the time measured from the arrival of the inci-

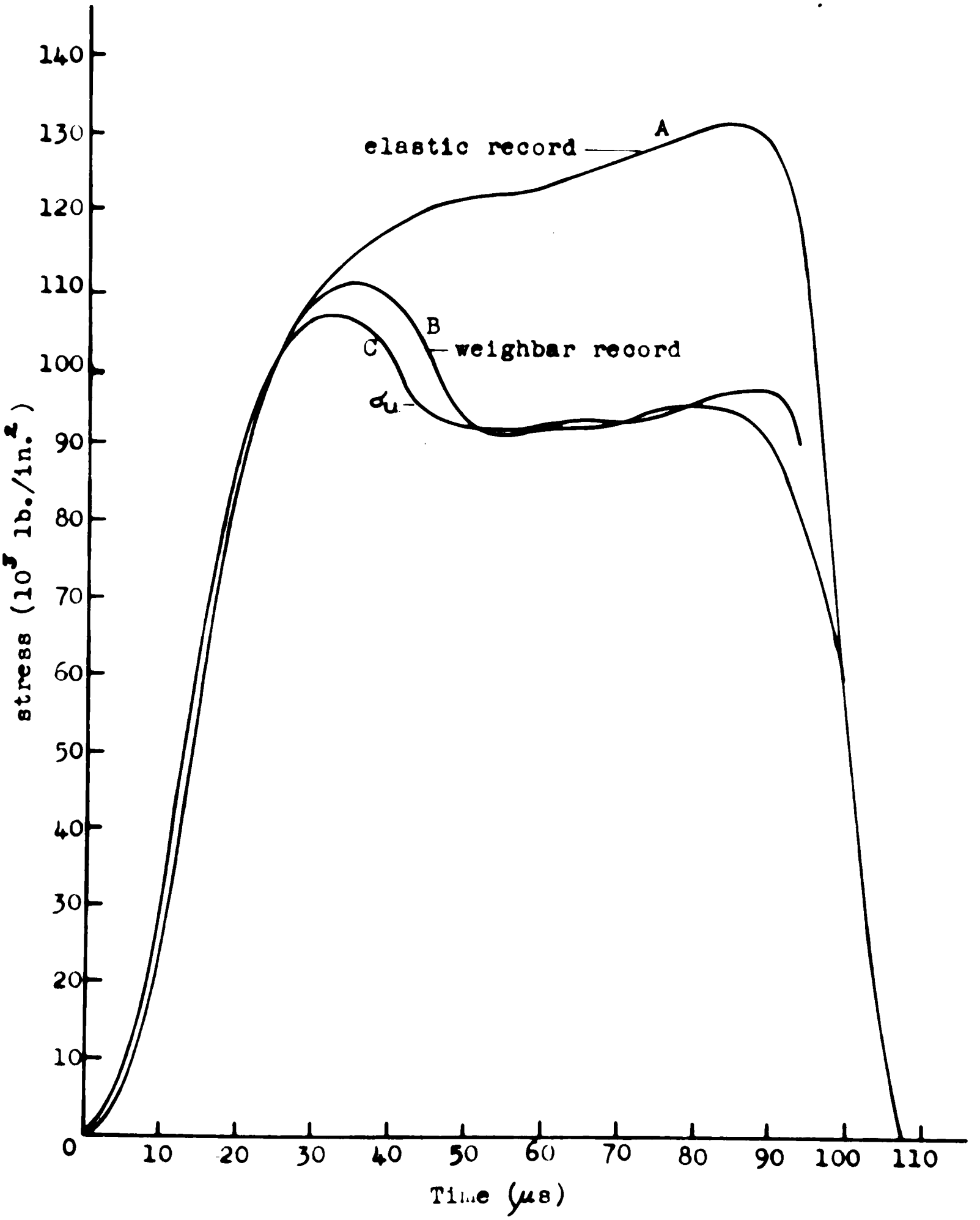


FIGURE 19 Average elastic record weighbar record and stress-time curve for the specimen upper face - impact velocity = 430 in./sec, temperature = +15 C.

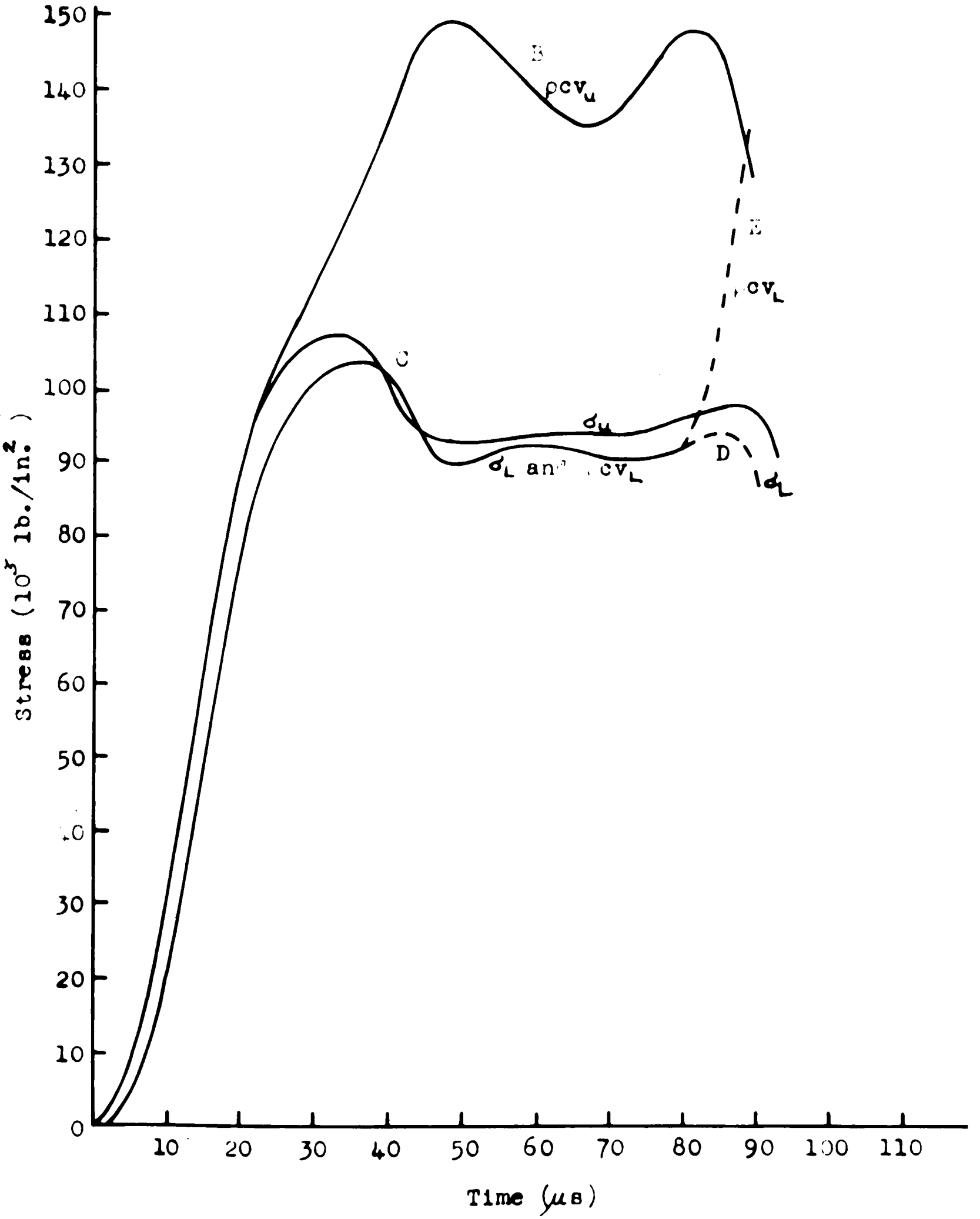


FIGURE 20 Derived stress and particle velocity curves for the specimen faces. (430 in./sec. and +15°C)

dent wave at the specimen upper face. Hence the stress-time and velocity time curves for the lower face do not commence until t=2·5 microseconds, the time for a wave to travel the length of the specimen. As expected, it is seen from Figure 20 that the stress-time curves σ_u and σ_L differ very little.

The difference between the particle velocities on the faces of the specimen ($v_u - v_L$) is proportional to the rate at which the specimen is being strained (equation 34). This variation of the strain rate is plotted in Figure 21; the maximum strain rate is approximately 800/sec., and the average is 440/sec. As the specimen strain ϵ at time t is given by the area under this curve from 0 to t microseconds, the specimen strains corresponding to various times were found. Also the mean stress on the specimen at time t was obtained by taking the arithmetic mean of the stresses given by curves B and D in Figure 20. These average stress and strain values are tabulated in Table I and are plotted as a stress-strain curve in Figure 22 (curve C); the time in microseconds corresponding to different parts of the curve are indicated. The permanent strain shown was obtained from micrometer measurements of the specimen before and after impact.

Also shown in Figure 22 are the room temperature static

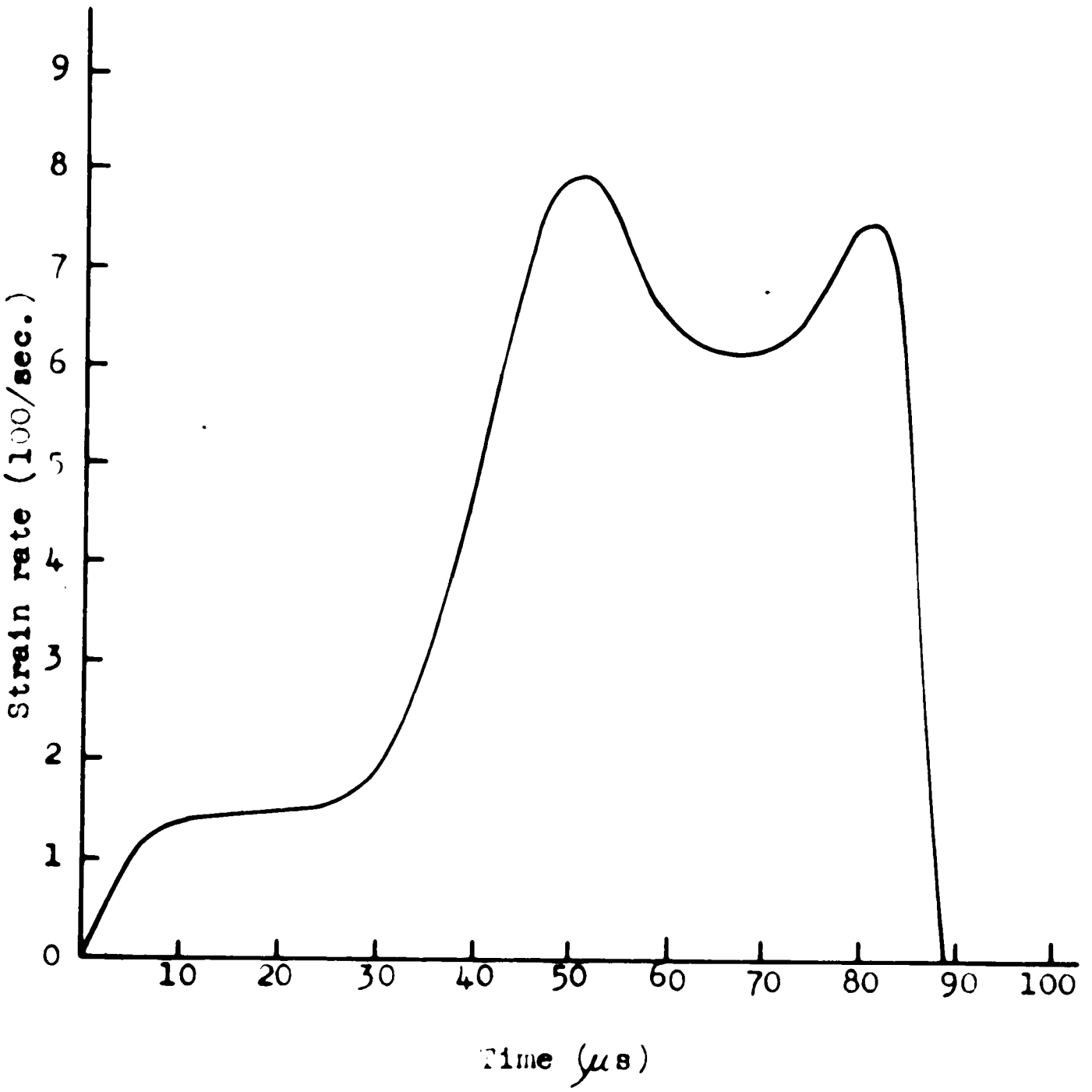


FIGURE 21 Strain rate curve (+15° C and 430 in./sec.)

TABLE I

Dynamic stress and strain values

(+15°C and at 430 in./sec.)

time μ secs	strain %	average stress 10^3 lb./in.^{2}
20	0•50	86•0
30	0•50	104•5
40	0•78	100•0
50	1•45	91•5
60	2•17	92•0
70	2•83	92•5
80	3•55	95•0
88	3•95	96•0

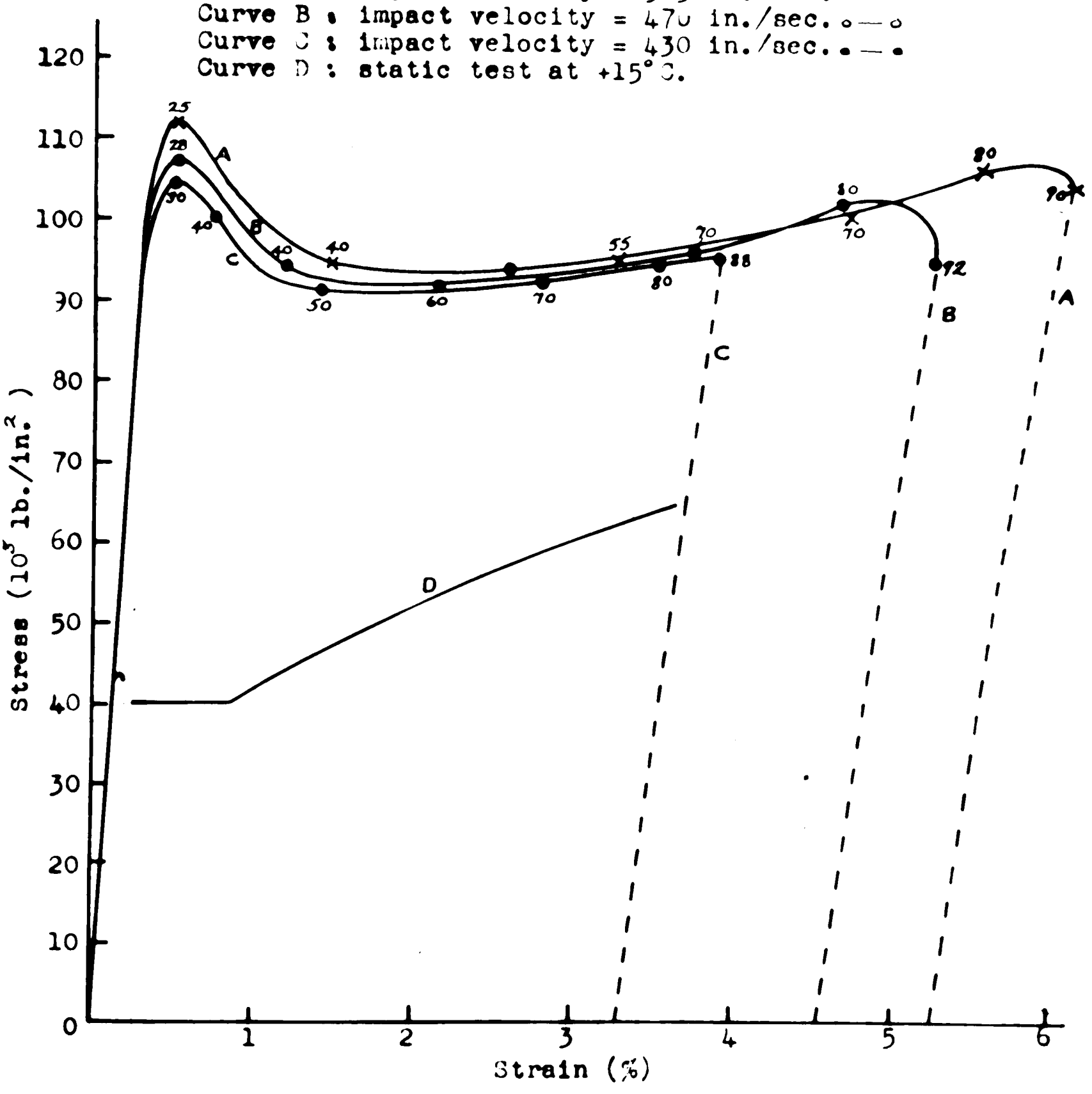


FIGURE 22 Dynamic stress-strain curves at +15° C.

stress-strain curve (Figure 14) and the dynamic stress-strain curves corresponding to impact velocities of 470 in./sec., and 503 in./sec. These latter curves were found in a similar manner to that described for an impact velocity of 430 in./sec.

(b) Micrographic examination.

Several specimens were prepared for micrographic examination before impact. Figure 23(a) shows a portion of a prepared surface prior to impact and Figure 23(b) the same field of view after impact at 503 in./sec. By comparing the two micrographs it is seen that the mechanism of deformation appears to have been very fine slip. Also it is noticeable that the impact has caused certain amount of localised shear near one of the grain boundaries. These characteristics of dynamic deformations at room temperature were observed in most of the specimens examined; in no case were twins found.

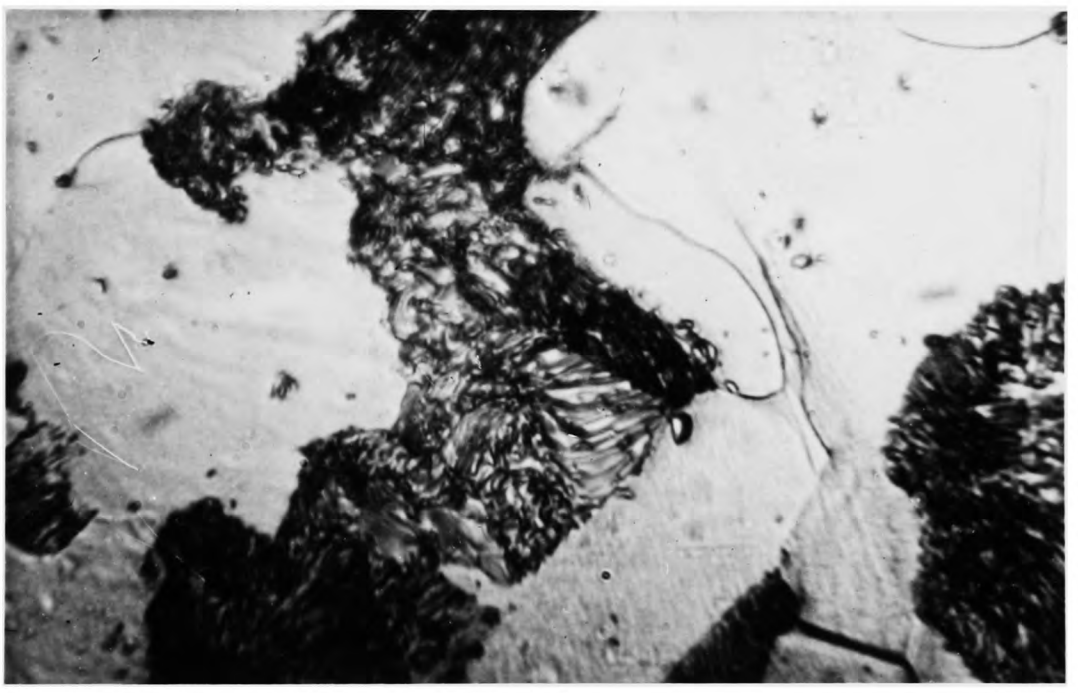
(11) Results obtained at -41°C.

(a) Dynamic stress-strain curves.

The gauge records obtained at this temperature were analysed in the same manner as were the room temperature records. Details of the analysis for an impact



23(a)



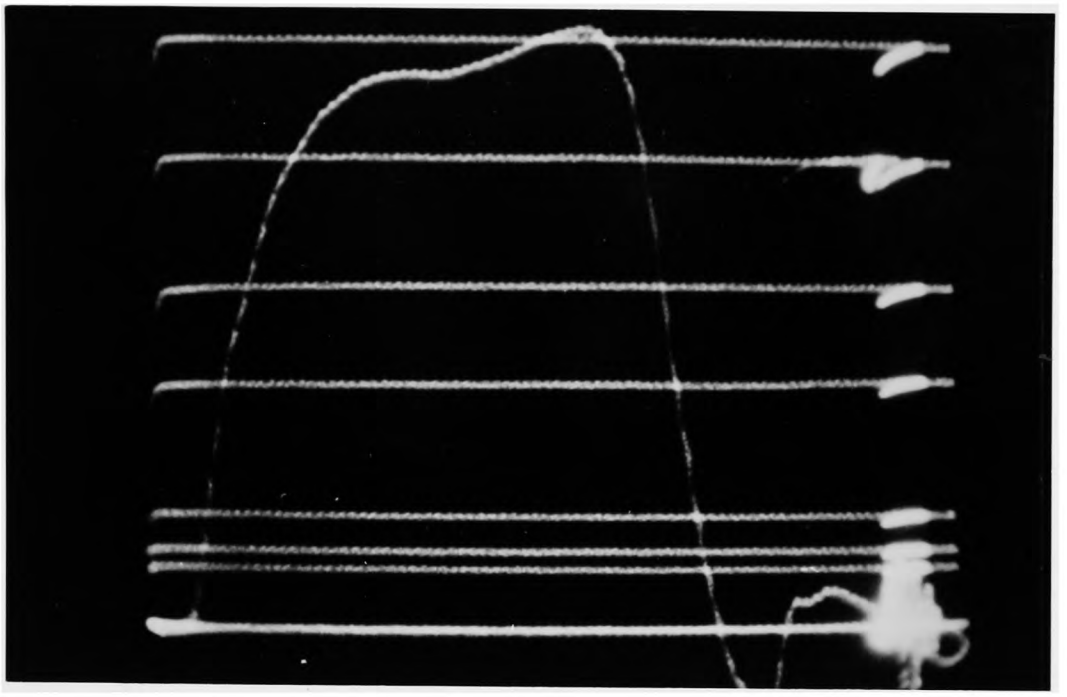
23(b)

FIGURE 23 Micrographs taken before and after impact at 503 in./sec. and +15°C.

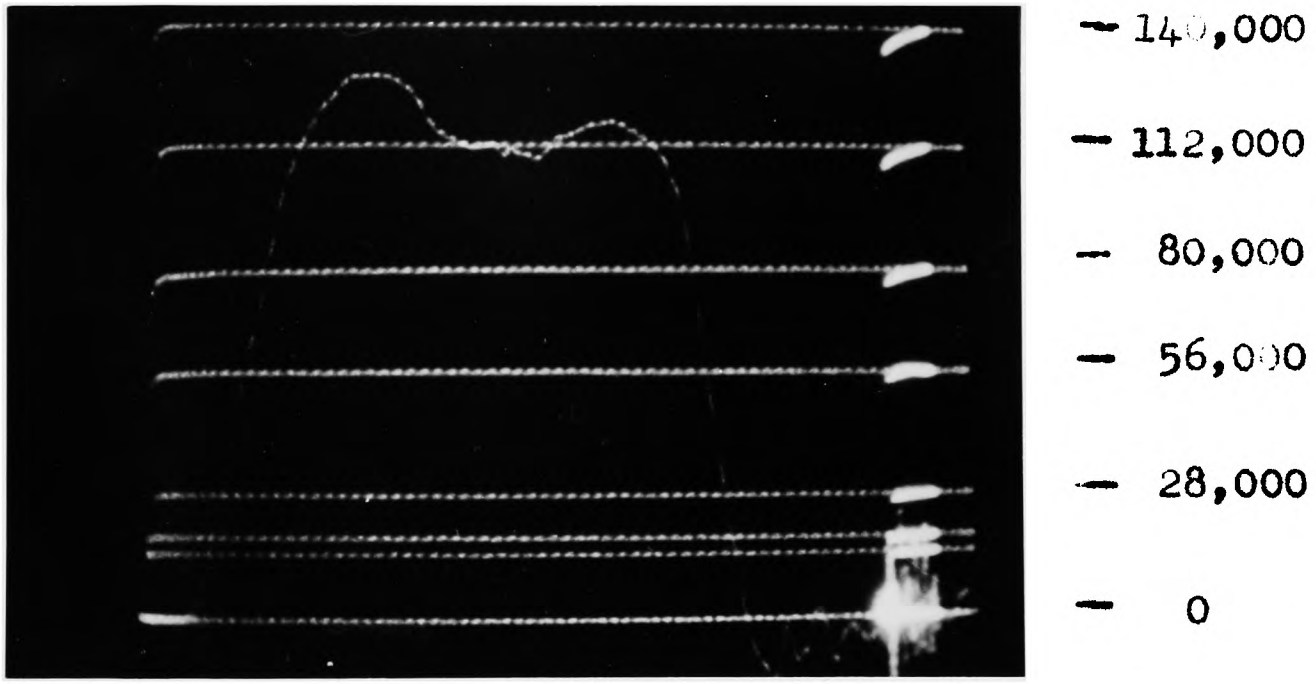
(a) Before test. Magnification = ×1400
(b) After 5.2% dynamic strain. Magnification = ×1400

velocity of 470 in./sec., are given below.

Figures 24(a), 24(b), 24(c) represent, for an impact velocity of 470 in./sec., an elastic record, a weighbar record, and an anvil bar record respectively. The stress-time curves obtained from the average elastic and weighbar records are shown in Figure 25 as curves A and B; also shown in this Figure is the stress-time curve (curve C) for the specimen upper face as derived from an analysis of curves A and B. Figure 26 shows the stress-time curves and particle velocity time curves for the specimen upper and lower faces. As at +15°C the difference in the stress-time curves for each specimen face is small. The mean stress on the specimen at a given time t was taken as the average of the stresses as given by curves B and D in Figure 25. From the plotted curve of the difference of the particle velocities (Figure 27) the maximum strain-rate was found to be 700/sec., and the average strain-rate was 380/sec. The strain at any time t was found by graphical integrations of the area under this strain rate curve up to time t (equation 34). The dynamic stress-strain curve thus obtained is shown in Figure 28; also shown in this figure are the dynamic stress-strain curves corresponding to impact velocities of 430 in./sec., and 503 in./sec., and the static stress-strain curve for the same test temperature.



24(a)

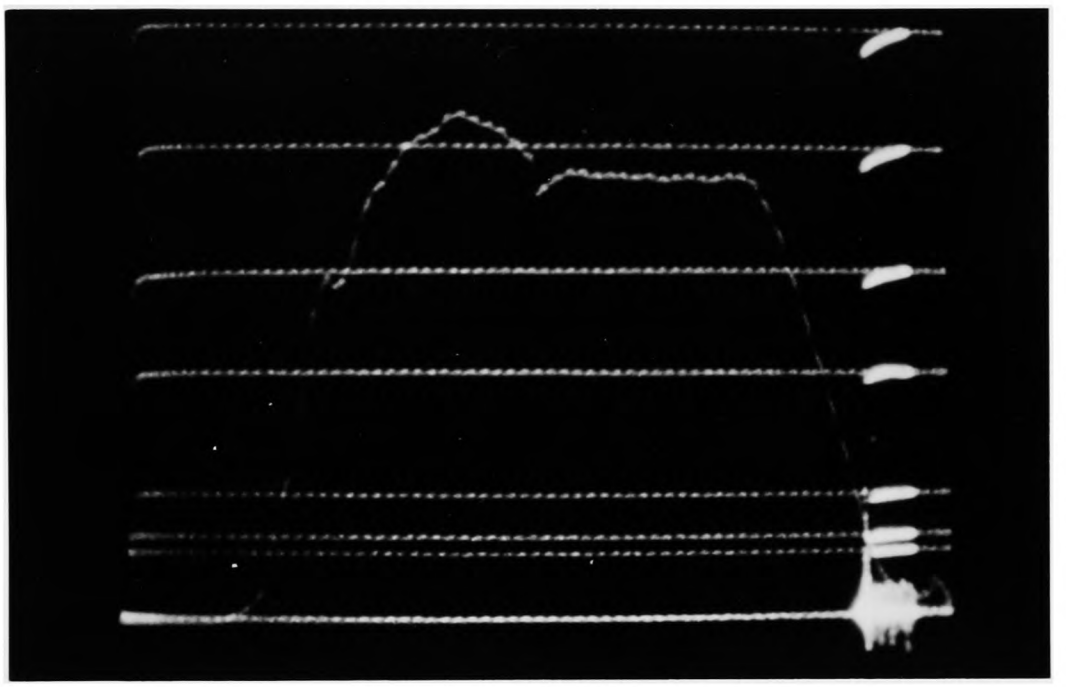


24(b)

FIGURE 24 Records obtained at -41°C and +15°C for an impact velocity of 470 in./sec.

(a) Elastic record at +15°C. Rg ≒ 376Ω
S = 1·94.

(b) Weighbar record at -41°C. Rg ≒ 369Ω
S = 1·94.



24(c)

FIGURE 24 (continued)

(c) Anvil bar record at -41°C. R_g = 369Ω
S = 1·94.

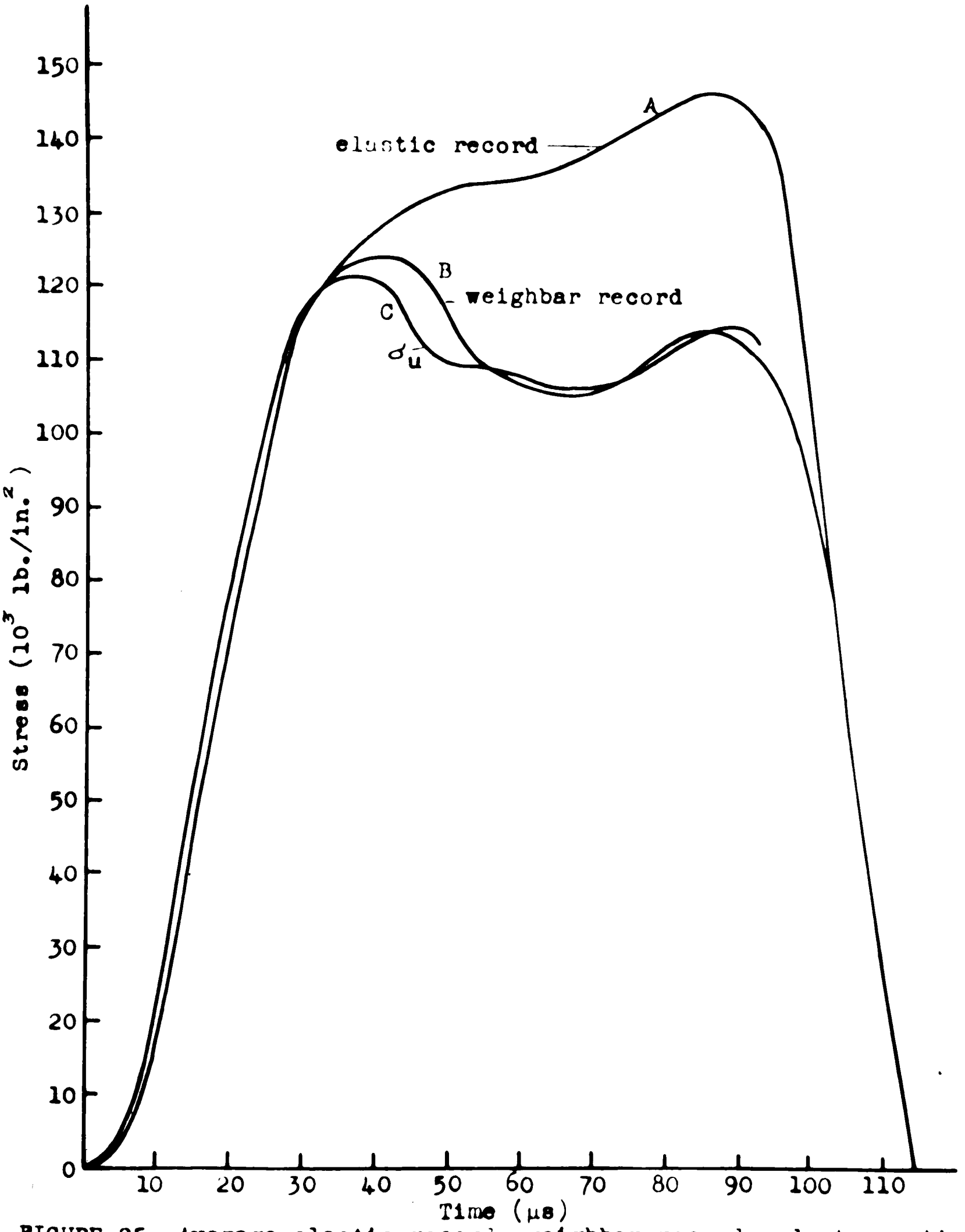


FIGURE 25 Average elastic record, weighbar record, and stress-time curve for the specimen upper face - impact velocity =470 in./sec. temperature = -41°C.

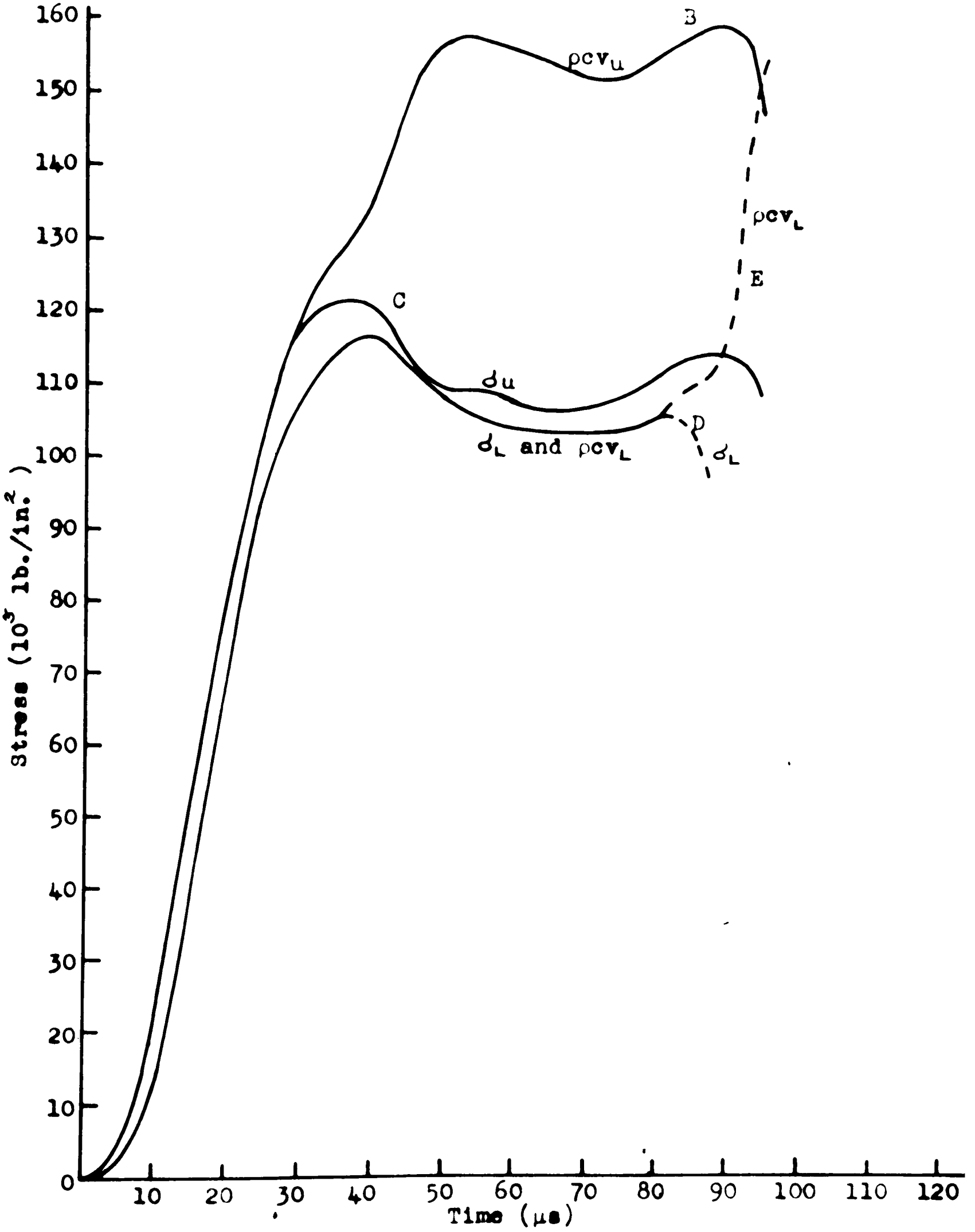


FIGURE 26 Derived stress and particle velocity curves for the specimen faces (470 in./sec. and -41° C).

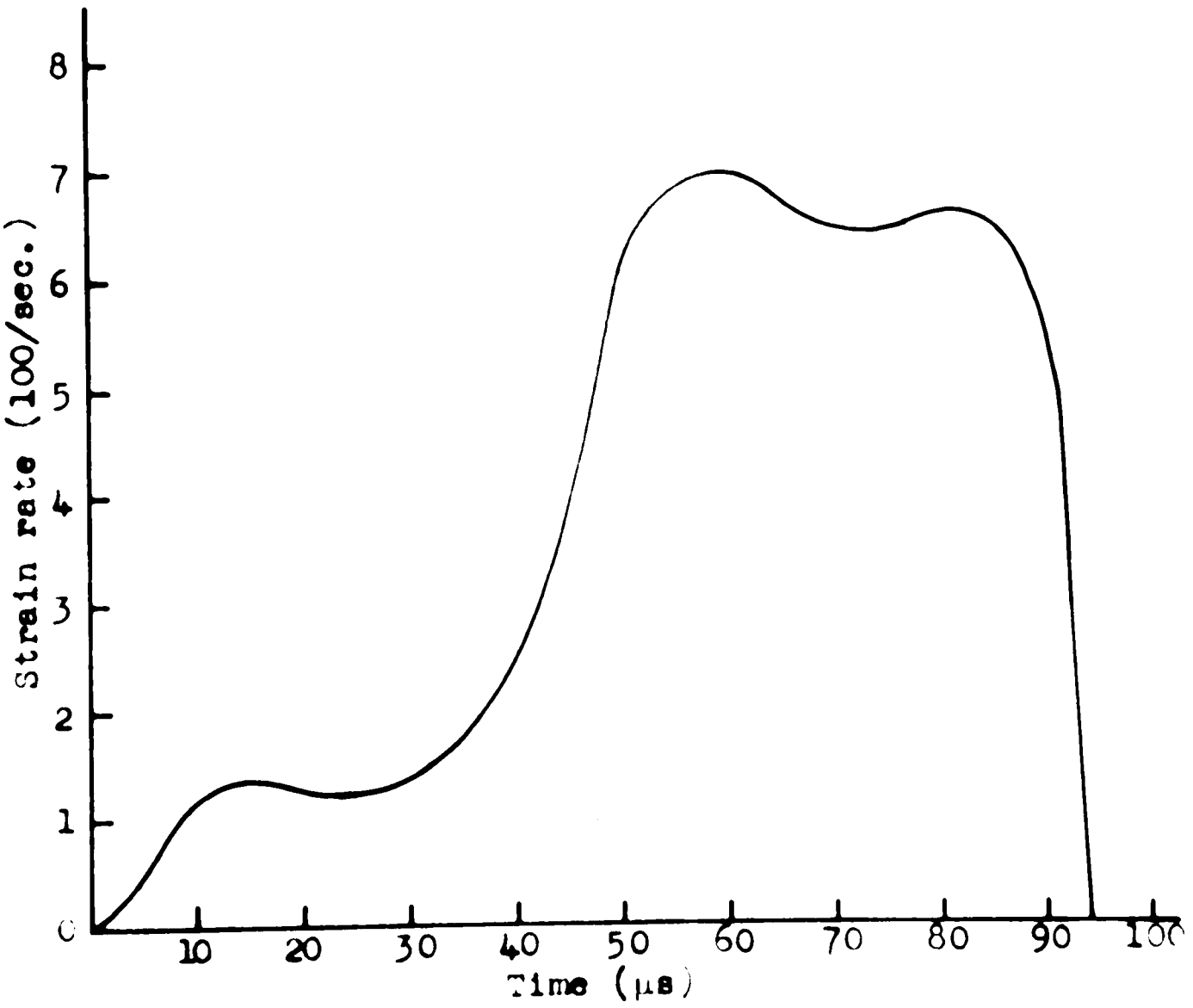


FIGURE 27 Strain rate curve (470 in./sec. and -41° C).

Curve A : impact velocity = 503 in./sec. ×—×
Curve B : impact velocity = 47[illegible] in./sec. ○—○
Curve C : impact velocity = 43[illegible] in./sec. ●—●
Curve D : static stress-strain curve at -41° C.

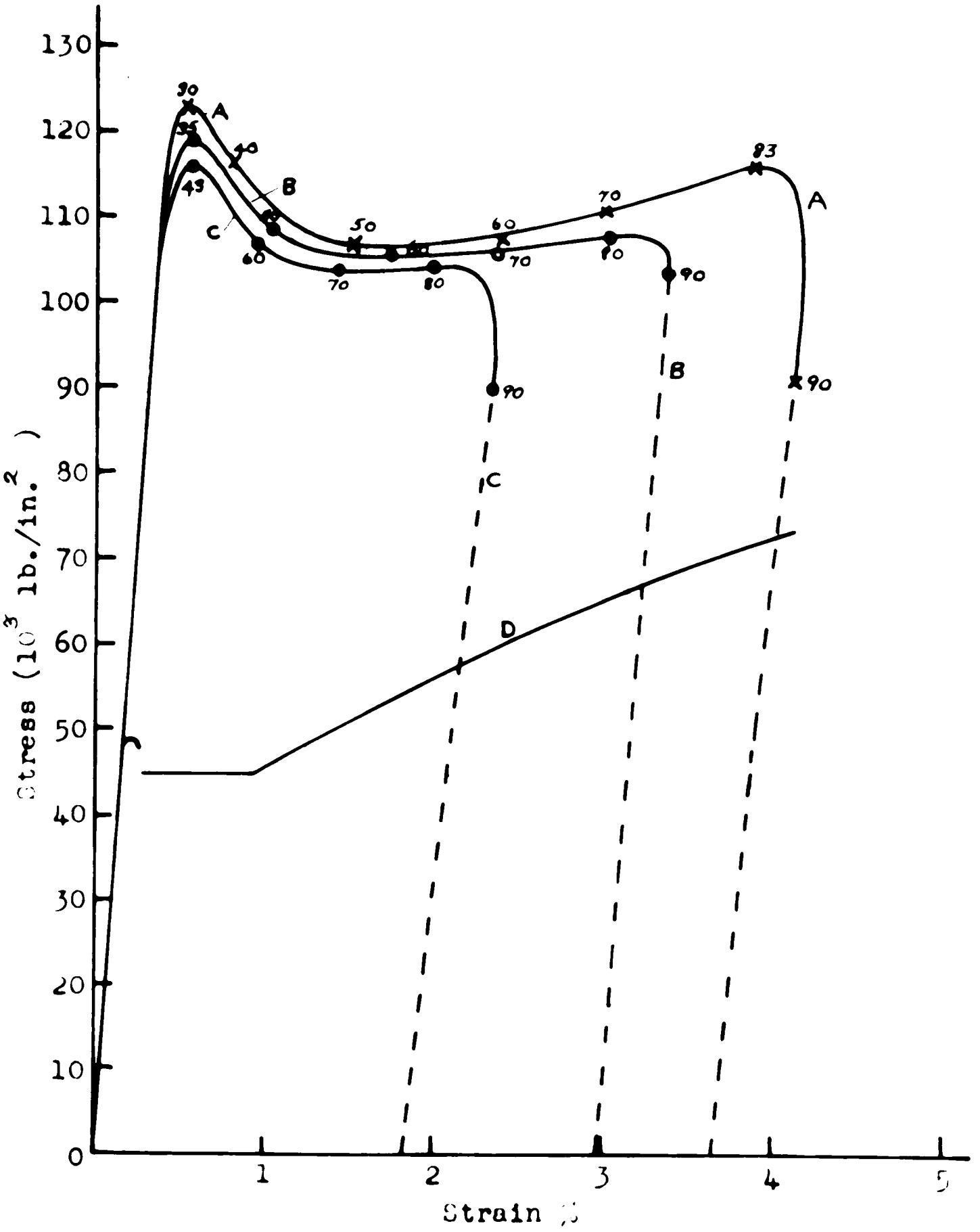


FIGURE 28. Dynamic stress-strain curves at -41° C.

(b) Micrographic examination.

As the temperature of test became lower, the deformation produced by a given impact velocity was reduced. At -41°C an impact velocity of 503 in./sec., gave 3.7% deformation compared to 5.2% produced by the same impact velocity at room temperature. It thus became more difficult to observe the fine slip in specimens impacted at -41°C than in specimens deformed at room temperature.

No twins were observed in specimens tested at impact velocities of 430 in./sec., and 470 in./sec, however, two twins were found in a specimen impacted at 503 in./sec. It thus appears that at -41°C, if not at all test temperatures, the stress at which twins appear must be in the vicinity of 128,000 lb./in.^{2}, the highest stress sustained in an impact at 503 in./sec.

(111) Results obtained at -84°C.

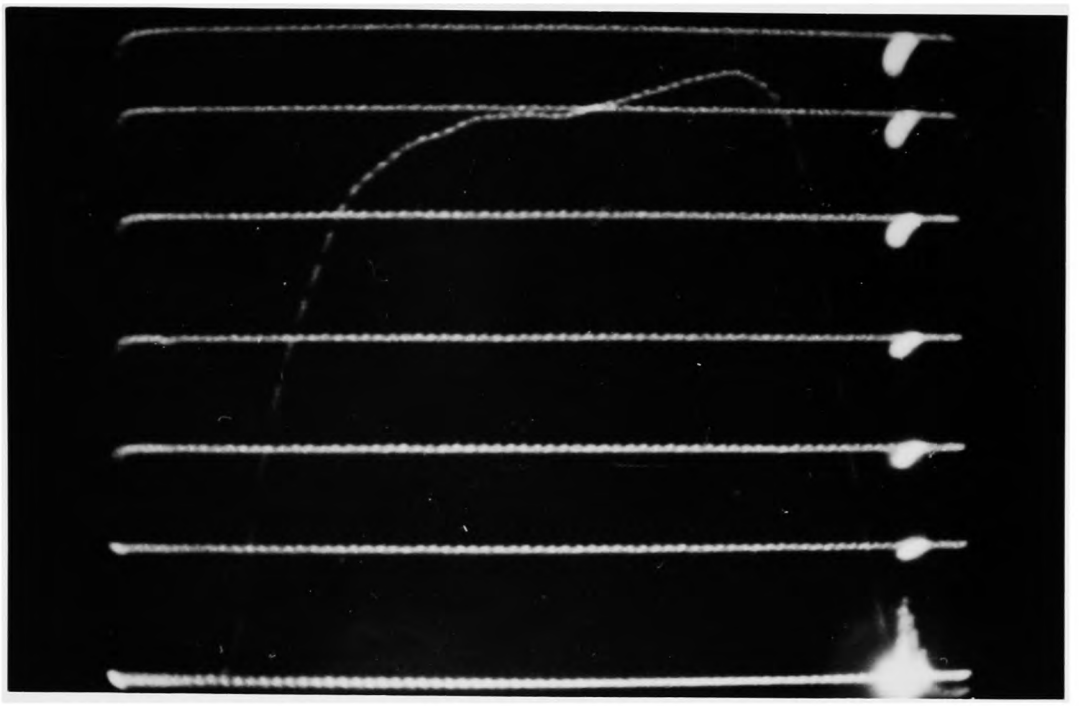
(a) Dynamic stress-strain curves.

At this temperature it became a little more difficult to obtain smooth weighbar and anvil bar records. This was attributed to the freezing of the thin layer of oil at the specimen faces. If great care was taken in lapping the specimen in contact with the weighbar

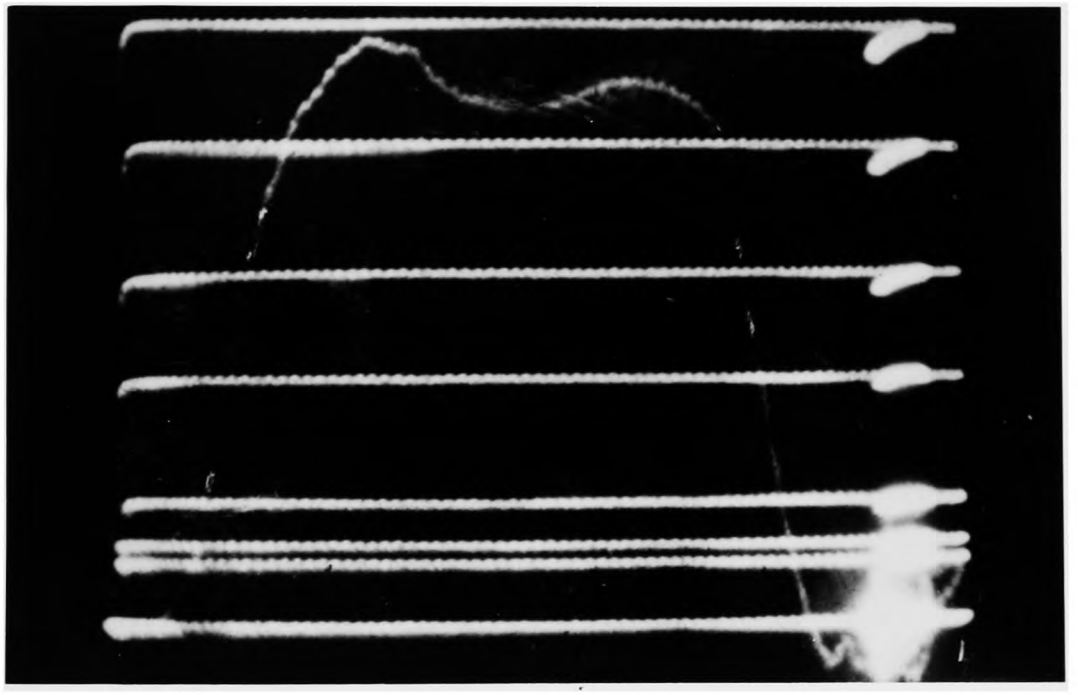
and anvil bar, and only a very thin layer of oil placed at the specimen faces, this difficulty could be overcome.

Figures 29(a), 29(b), 29(c) show an elastic record, a weighbar record and an anvil bar record for an impact velocity of 503 in./sec. The anvil bar record is not a very good one, however, it does show the effect on the record of imperfect contact at the specimen faces due to the oil freezing. Figure 30 shows the elastic and weighbar stress-time curves as well as the analysed stress-time curve for the specimen upper face, it is seen that yield occurred after 38 microseconds at 133,000 lb./in^2. At room temperature, at the same impact velocity, yield occurred after 27 microseconds at 113,000 lb./in^2. Thus the upper yield stress and delay-time have both been considerably increased by lowering the test temperature.

The stress-time curves and the particle velocity-time curves, for the specimen upper and lower faces, are shown in Figure 31. Figure 33 shows the dynamic stress-strain curve obtained from the curves in Figure 31, it also shows the dynamic stress-strain curve corresponding to an impact velocity of 470 in./sec., and the static stress-strain curve found at -84°C. For the specimen impacted at a velocity of 503 in./sec, the average strain-rate curve (Figure 32) gives the maximum strain rate as 65 /sec., and



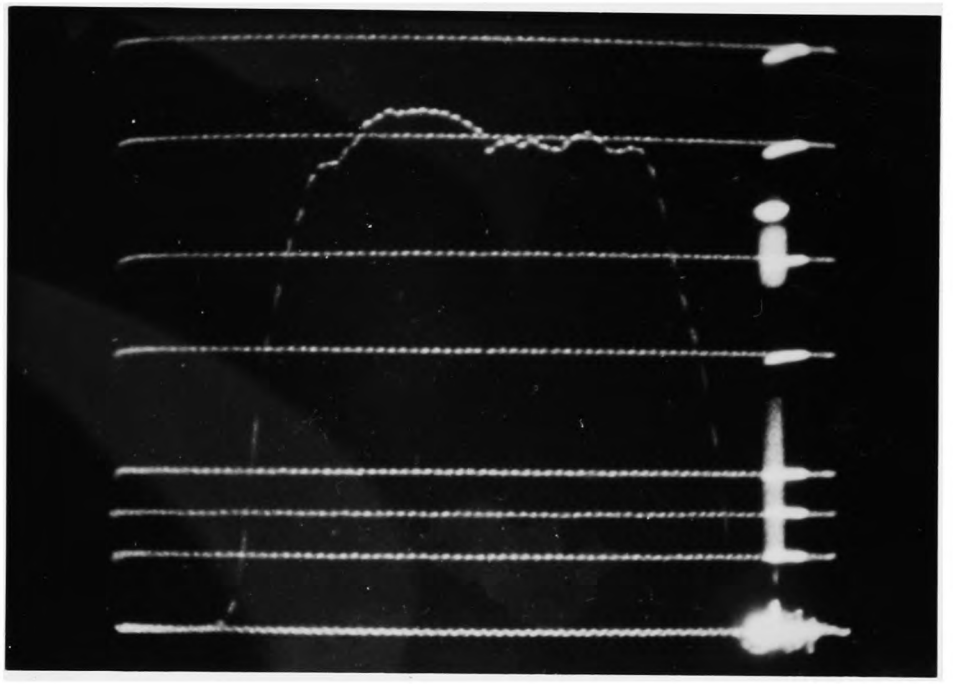
29(a)



29(b)

FIGURE 29 Records obtained at +15°C and -84°C for an impact velocity of 503 in./sec.

(a) Elastic record at +15°C. Rg ≒ 376Ω S = 1·94.
(b) Neighbar record at -84°C. Rg ≒ 3[illegible]Ω S = 1·94.



29(c)

FIGURE 29 (continued)

(c) Anvil bar record at -84°C.
Rg = 376Ω S = 1·86.

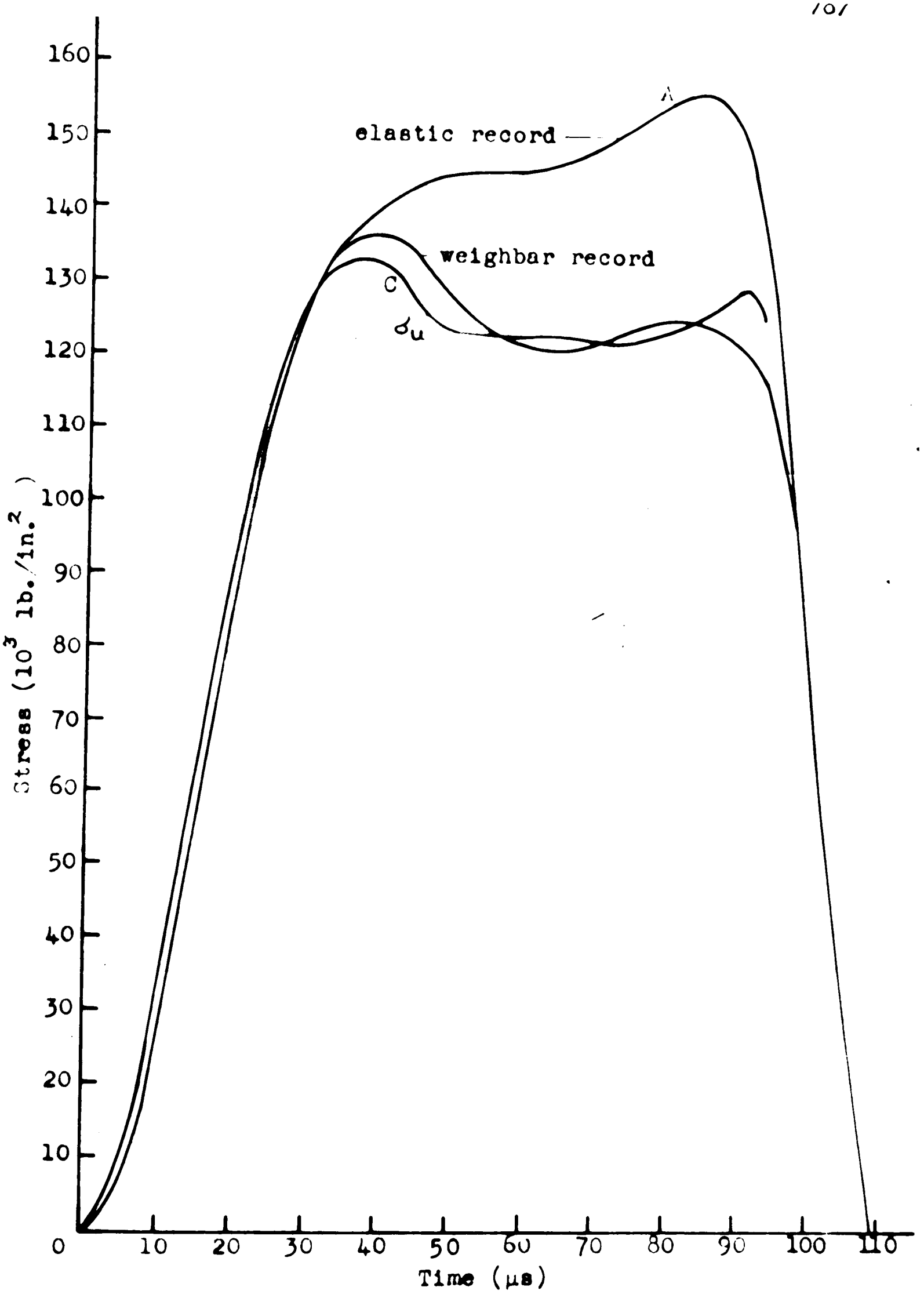


FIGURE 30 Average elastic record, weighbar record and stress-time curve for the specimen upper-face - impact velocity = 503 in./sec., temperature = -84° C.

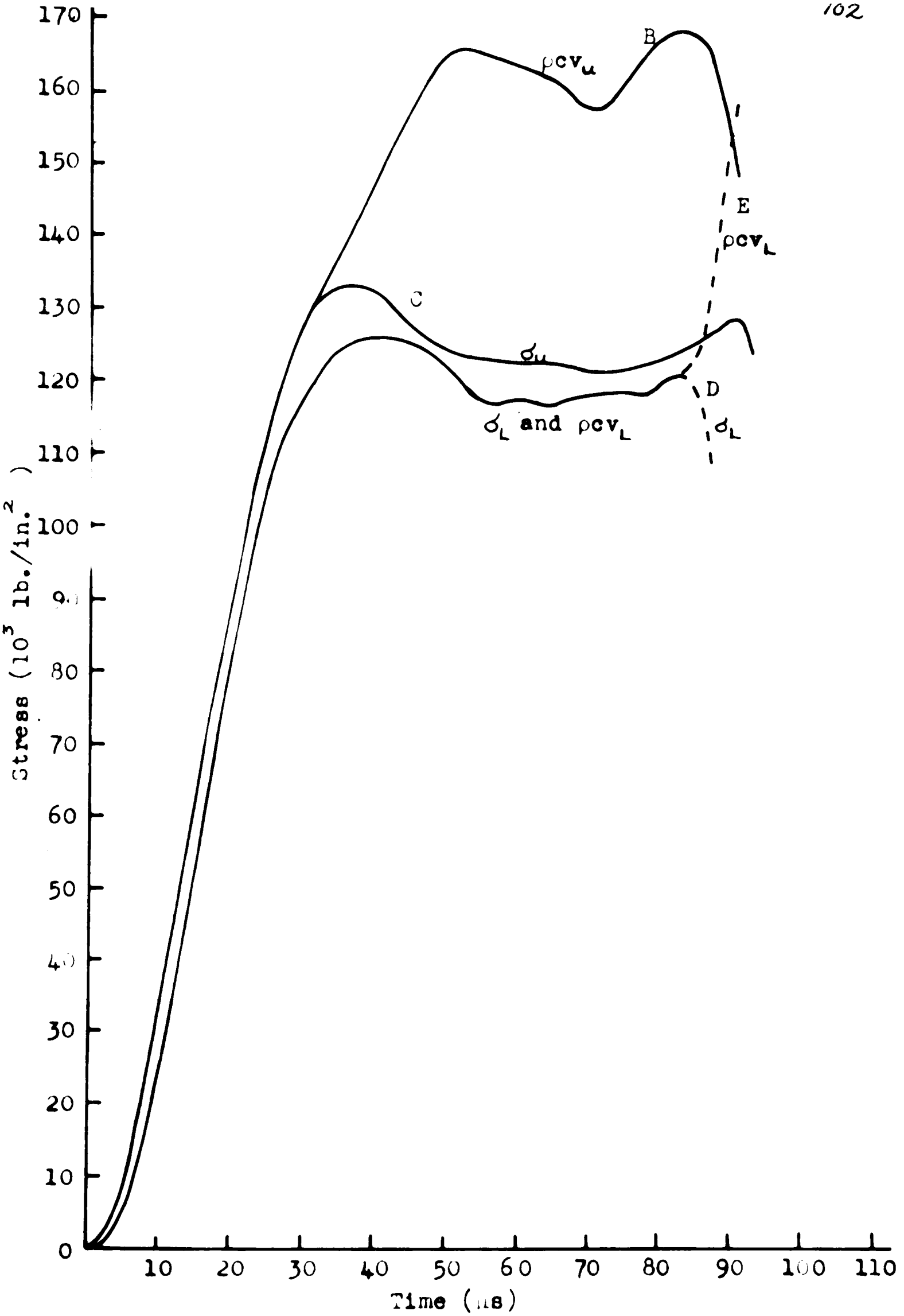


FIGURE 31 Derived stress and particle velocity curves for the specimen faces (503 in./sec. and -84° C).

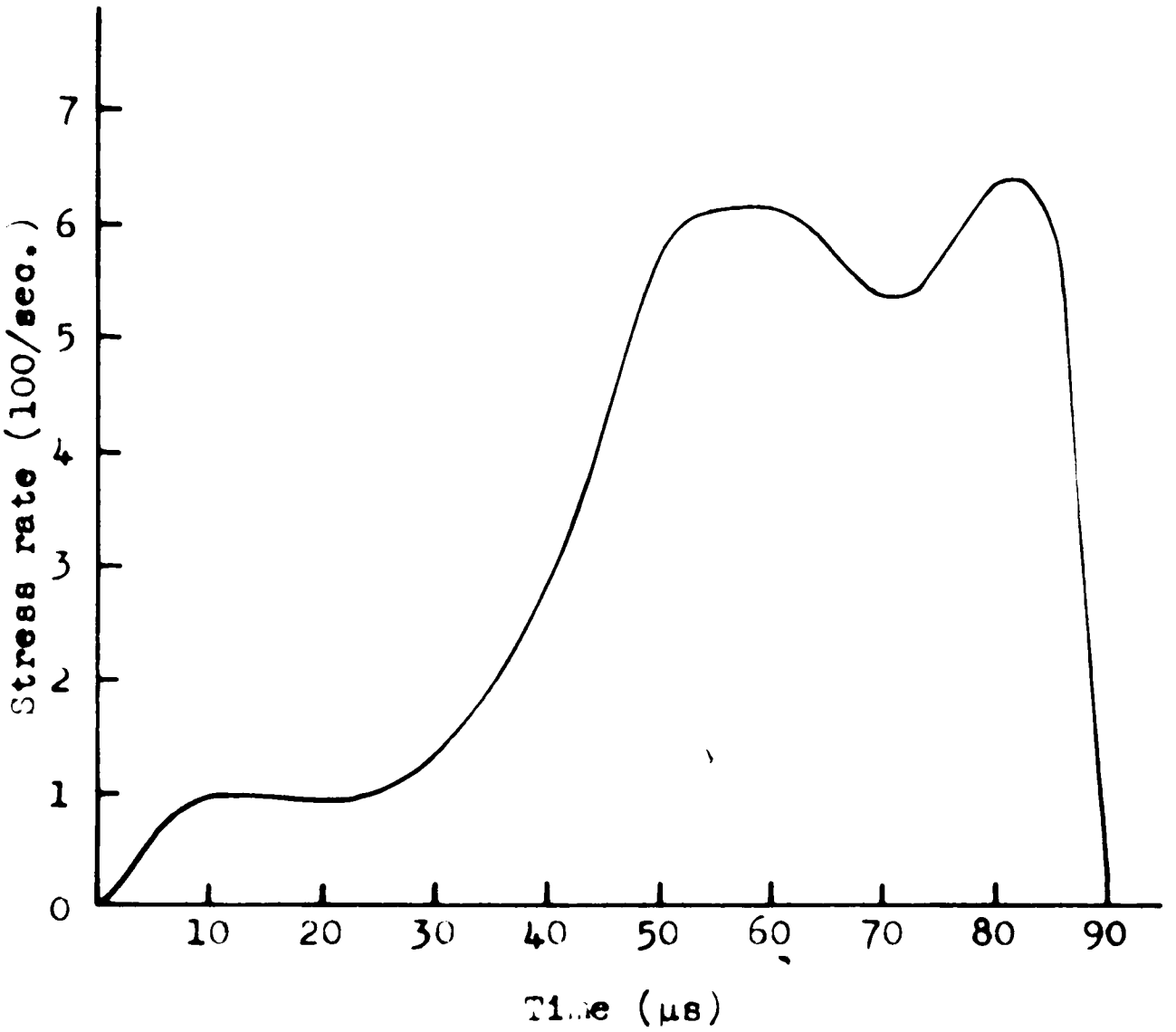


FIGURE 32 Strain rate curve (503 in./sec. and -84° C).

Curve A : impact velocity = 503 in./sec. × — ×
Curve B : impact velocity = 470 in./sec. ○ — ○
Curve C : static stress-strain curve at -84° C.

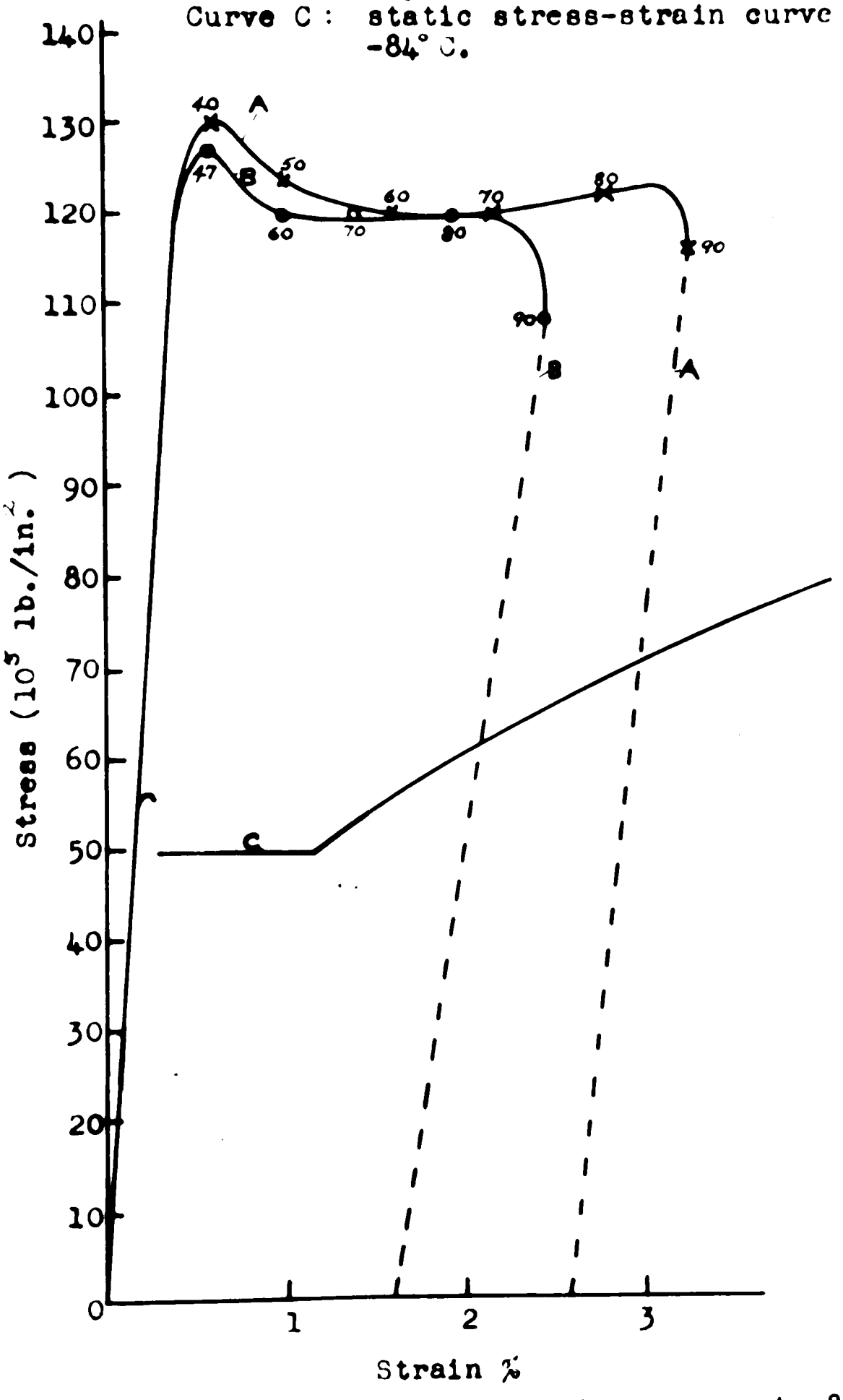


FIGURE 53 Dynamic stress-strain curves at -84° C.

the average strain rate as 290/sec.

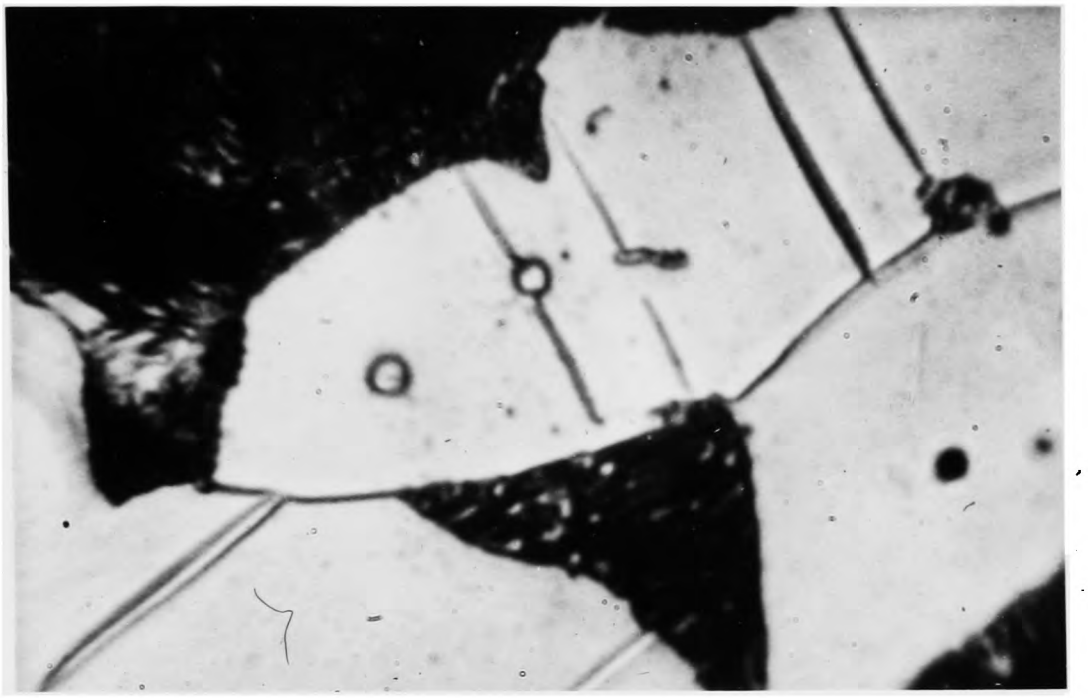
(b) Micrographic examination.

Figure 34(a) shows twins formed in a specimen impacted at a velocity of 503 in./sec. and at -84°C. The twins observed were all in crystals near the upper face of the specimen, no twins were found on the lower three-quarters of the prepared flat. A few twins were also observed near the upper face of a specimen impacted at 47[illegible] in./sec., at -84°C. In addition to twinning there was also some indication of fine slip in micrographs taken after impact at both velocities (Figure 34(b). In general this slip was too fine to be resolved.

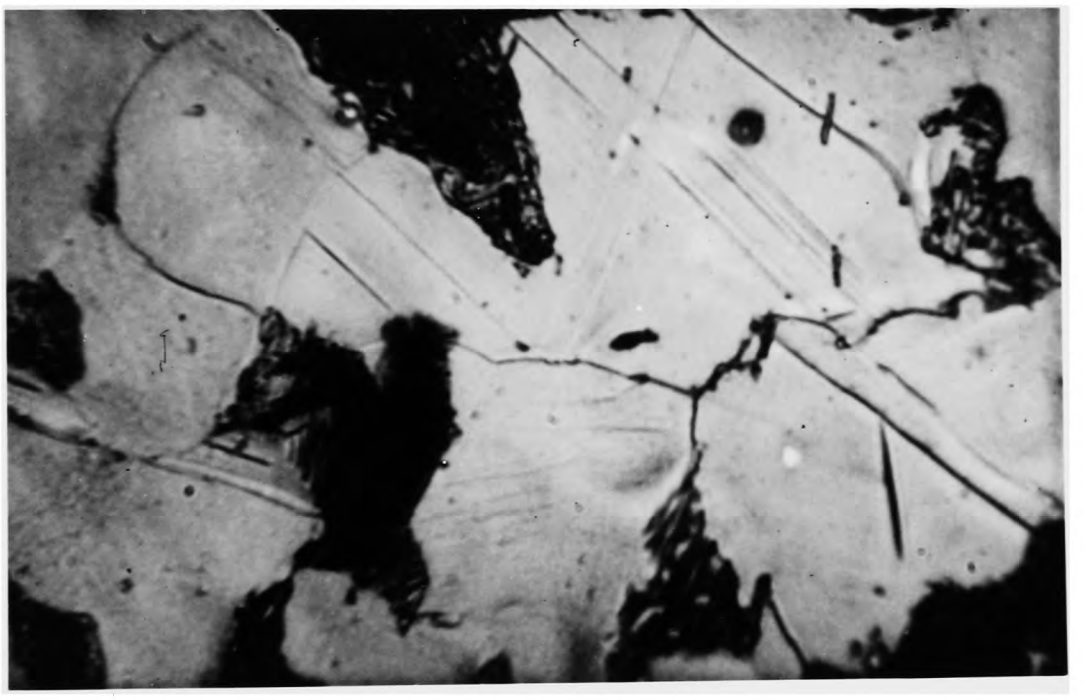
(iv) Results obtained at -121°C.

(a) Dynamic stress-strain curve.

At this temperature the difficulties met in obtaining smooth records were greater than at -84°C. Figures 35(a) and 35(b) show weighbar records obtained at an impact velocity of 503 in./sec., the first was obtained at -121°C and the second at +15°C. A comparison of these two figures gives an indication of the increase in strength of the steel at -121°C. The sequence of figures in obtaining the dynamic stress-strain curve is the same as used in



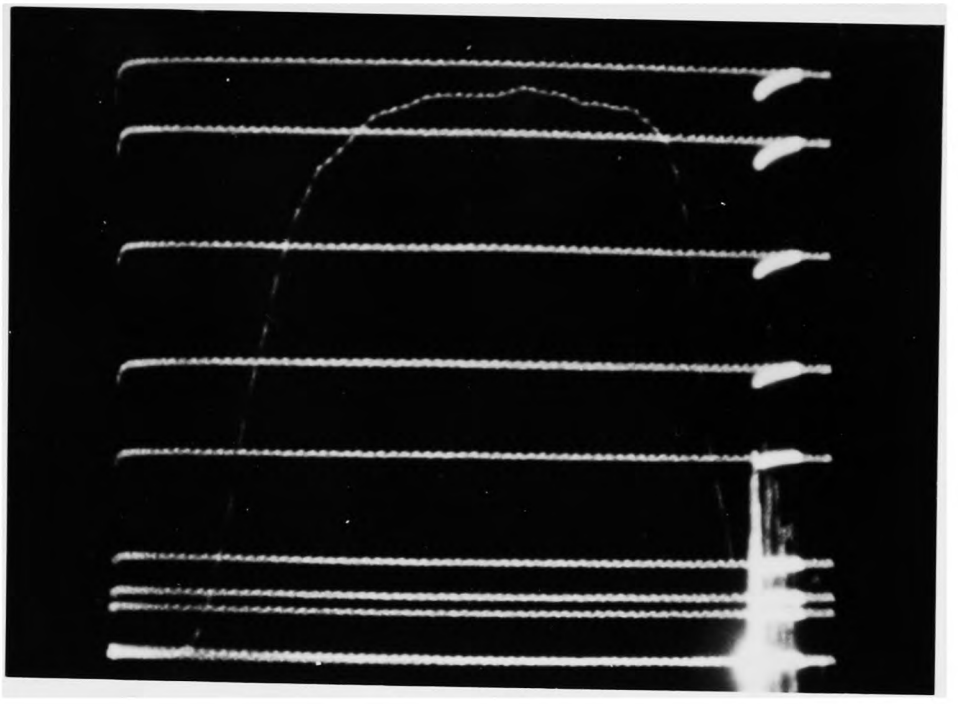
34(a)



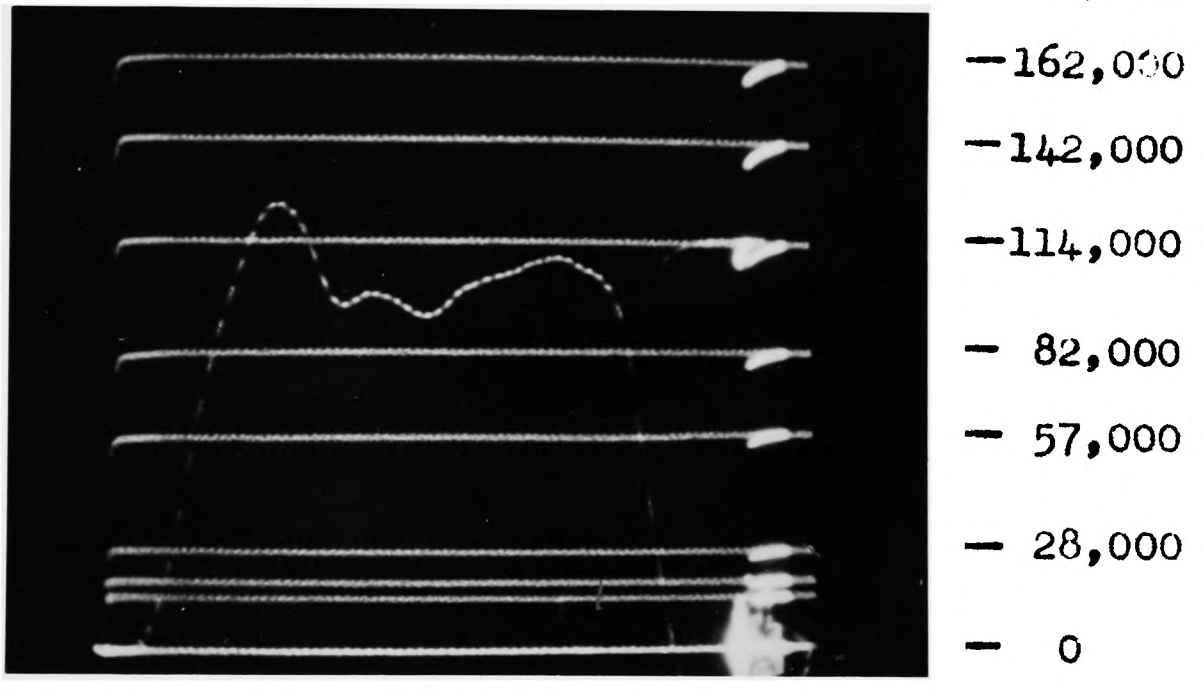
34(b)

FIGURE 34 Micrographs taken after impact at 503 in./sec. and -84°C.

(a) Magnification = ×2800
(b) Magnification = ×1400



35(a)



35(b)

FIGURE 35 Records obtained at -121°C and +15°C for an impact velocity of 503 in./sec.

(a) Weighbar record at -121°C. Rg ≒ 362 Ω
S = 1·94.

(b) Weighbar record at +15°C. Rg ≒ 376 Ω
S = 1·94.

finding the stress-strain curves at the other test temperatures. Figure 36 shows the elastic and weighbar stress-time curves as well as the stress-time curve for the specimen upper face as obtained by analysis, Figure 37 gives the stress-time and particle velocity-time curves for the specimen upper and lower faces, and Figure 38 shows the dynamic stress-strain curve obtained from the curves in Figure 37. To compare this dynamic stress-strain curve with that obtained under static conditions at the same test temperature, the static stress-strain curve found at $-121^{\circ}C$ is also shown in Figure 38. Due to the freezing of the layers of oil at the specimen faces, part of the anvil bar record obtained was of poor quality. This portion of the curve had to be estimated and is thus shown dotted in Figure 39.

(b) Micrographic examination.

Quite a large number of twins were observed in a specimen impacted under the above conditions. Whereas after impact at $-84^{\circ}C$ the twins had been localised near the upper face of the specimen, at $-121^{\circ}C$ twins were observed along the whole length of the prepared surface.

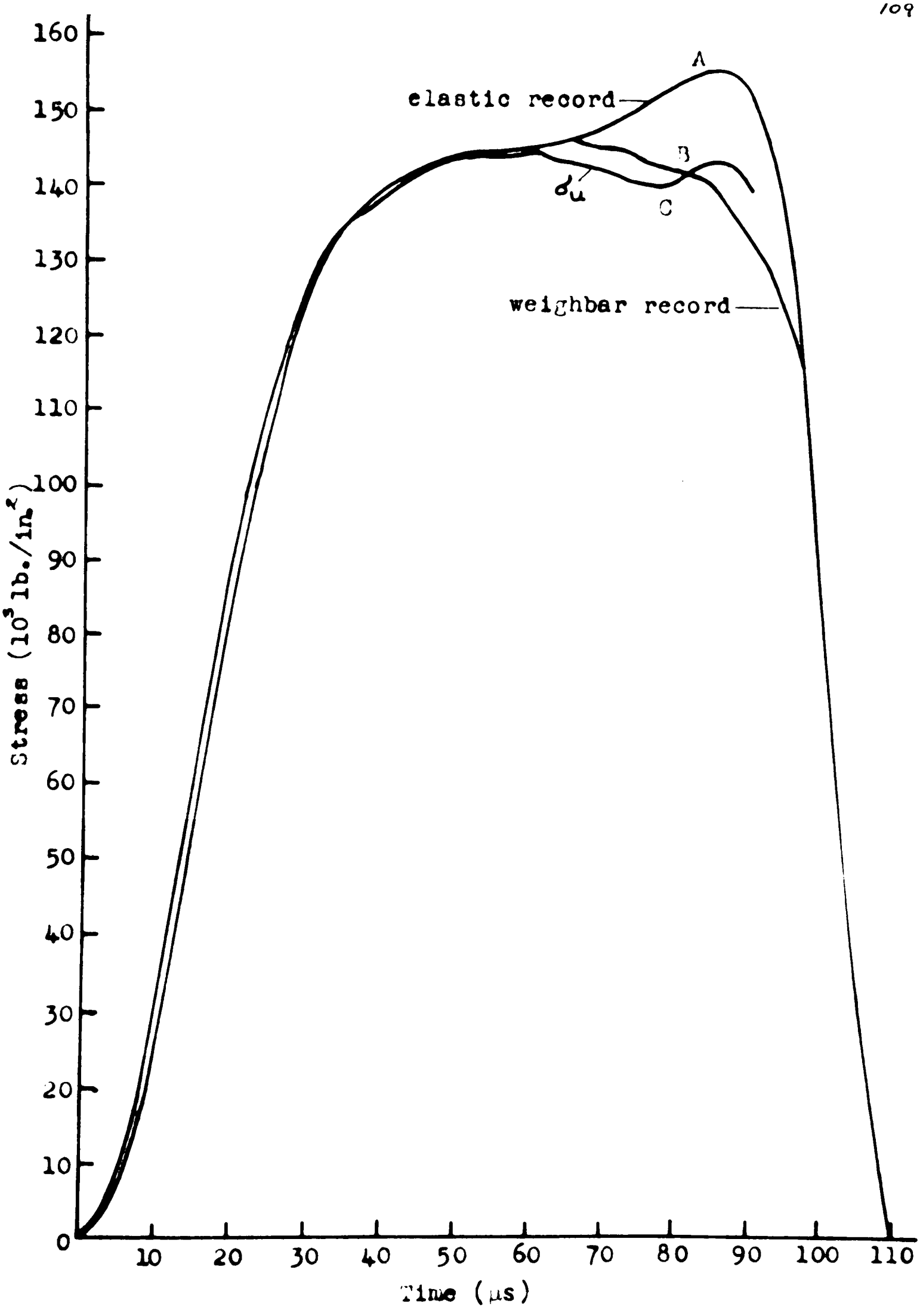


FIGURE 36 Average elastic record, weighbar record, and stress time curve for the specimen upper face - impact velocity = 503 in./sec. temperature = -121° C.

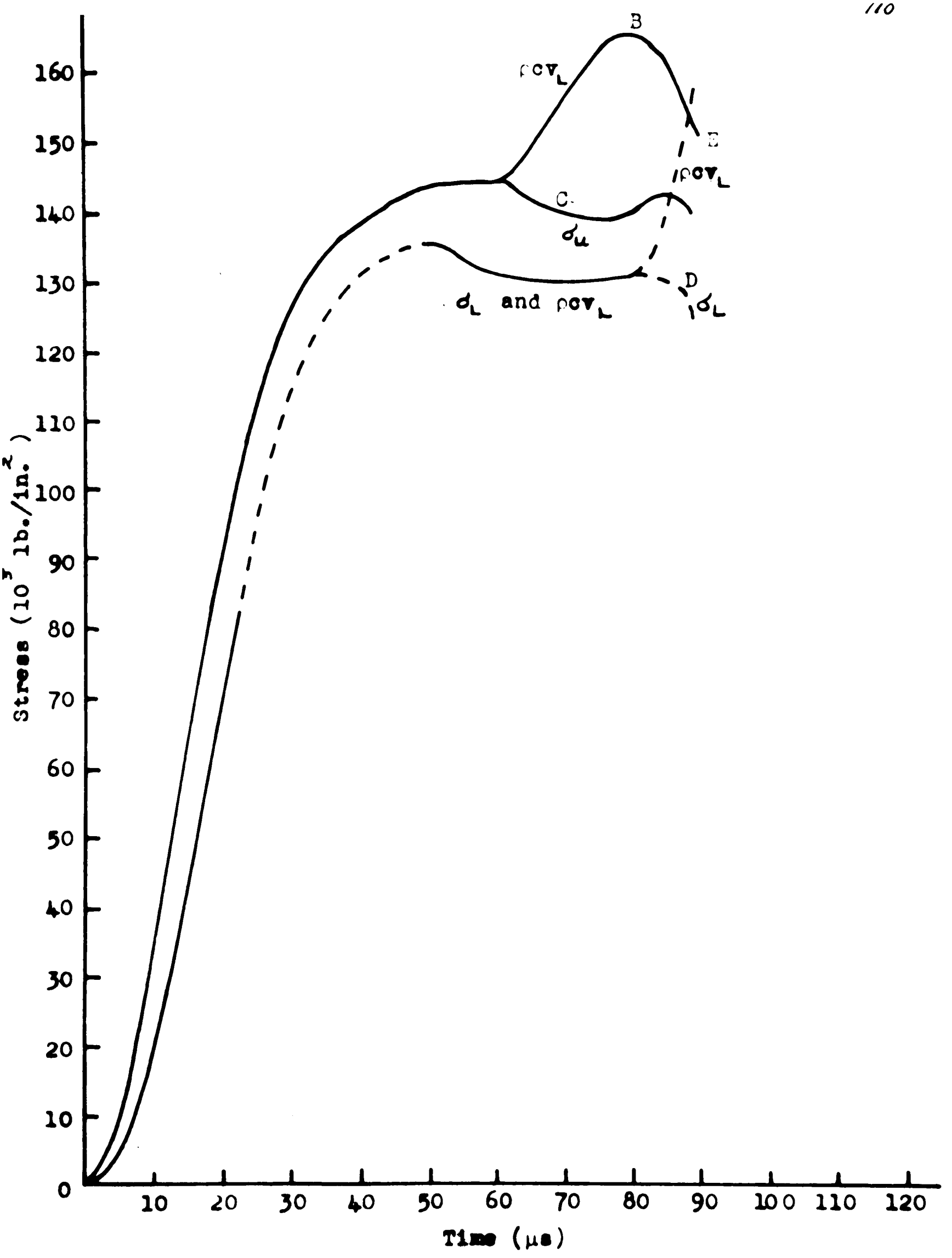


FIGURE 37 Derived stress and particle velocity curves for the specimen faces (503 in./sec. and -121° C).

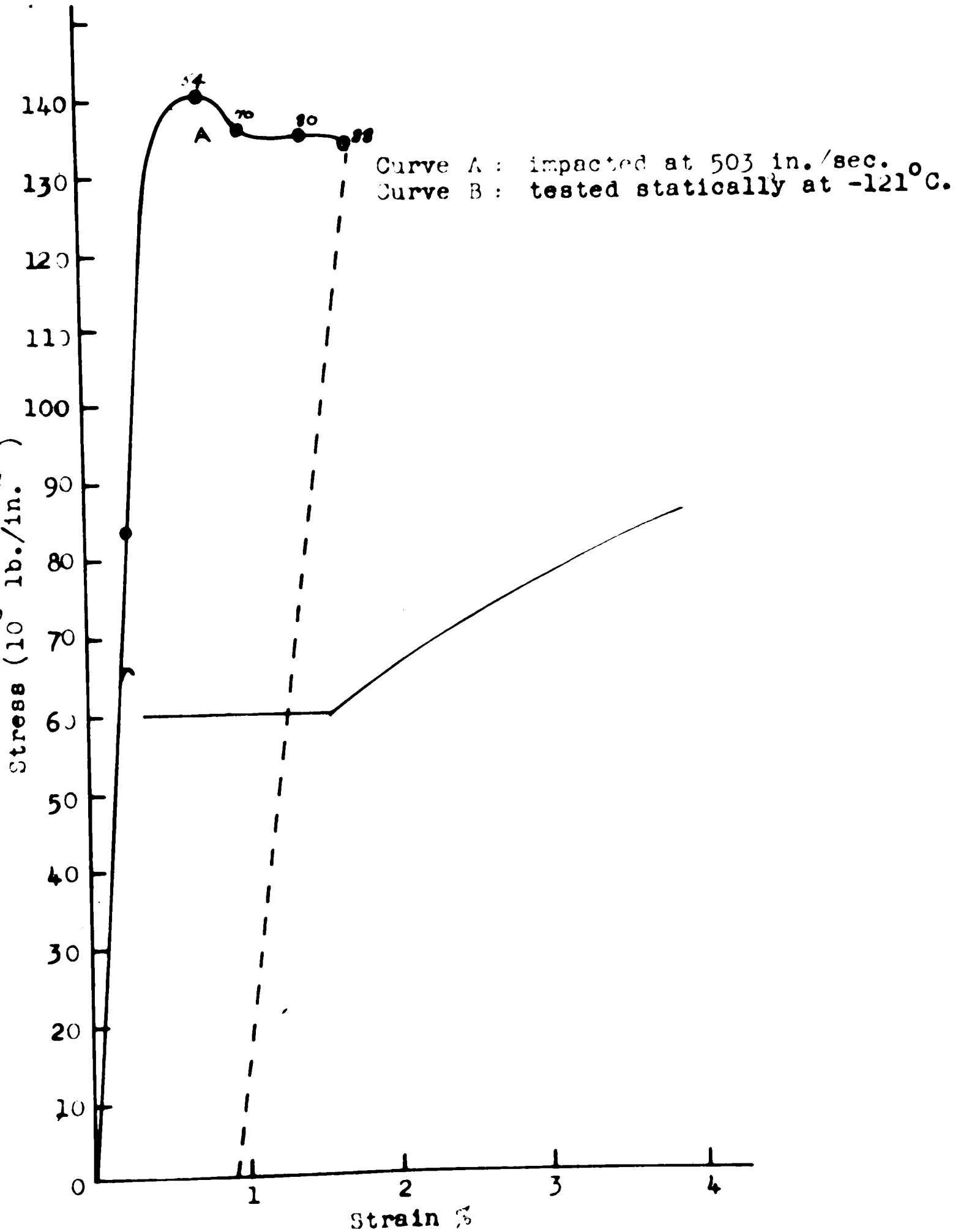


FIGURE 38 Dynamic stress-strain curve at -121° C.

(3) Discussion of results.

(1) The dynamic stress-strain curves obtained show that the steel is able to sustain very high rapidly-applied stresses before yield will occur. For a given impact velocity, the lower the temperature the higher the yield stress. It is also seen that not only is the yield stress raised above the static value, but also the stresses after yield are much higher than the static stresses corresponding to given strains at the same test temperature.

Table II has been drawn up to compare the dynamic stress-strain curves as plotted in Figures 22, 28, 33, and 38. In this table the following characteristics of the dynamic stress-strain curves are tabulated. the test temperature, the impact velocity, the time to yield, the dynamic upper and lower yield stresses, the ratio of the dynamic to the static upper yield stresses at the temperature concerned, the maximum and average strain rates, and the permanent deformation produced. From this table it is seen that for identical velocities of impact, as the test temperature is lowered the time to yield and the upper and lower yield stresses increase. It is to be noted that the values of time to yield and upper yield stress tabulated are the values taken from the dynamic stress-strain curves and thus differ slightly from the correct values as obtained

TABLE II

A comparison of the dynamic stress-strain curves obtained at various temperatures and impact velocities.

Temperature of test °C	Impact velocity in./sec.	time to yield μ sec.	dynamic upper yield stress (apparent) 10^3 lb./in.^{2}	dynamic lower yield stress 10^3 lb./in.^{2}	ratio of dynamic to static upper yield stresses	Maximum strain-rate per sec.	Average strain-rate per sec.	permanent deformation %
	503	25	113	94	2·57	1220	670	5·2
+15°C	470	28	108	91	2·45	970	570	4·6
	430	30	105	92	2·38	800	440	3·3
	503	30	125	107	2·49	950	470	3·7
-41°C	470	35	119	105	2·42	700	380	2·9
	430	43	116	104	2·36	560	260	1·8
	503	40	130	120	2·32	650	350	2·6
-84°C	470	47	127	120	2·26	540	260	1·6
-121°C	503	54	141	135	2·13	470	270	1·9

from the elastic and weighbar records alone (see section 1-5, (iv)). These true values will be considered later in section 2-6 in terms of a delay-time theory. Table II also shows that for a constant velocity of impact, the permanent deformation, the ratio of dynamic upper yield stress to static upper yield stress at the same temperature, and the maximum and average strain are reduced as the temperature is lowered. These are, in general, characteristics consistent with the observations of other investigators.

(ii) The accuracy of the above results depends on the validity of the wave analysis used. Possible errors are due to: non uniformity in stress distribution across the rod, variations in the phase and group velocities for those components of the stress-wave with short wavelengths, and imperfect reflection of the specimen unloading wave at the weighbar change of section F. (Figure 1)

For the transmission of a steady sinusoidal wave, Davies (49) has shown that the longitudinal strain at the surface of a bar gives an accurate measure of the average longitudinal stress, provided that the wavelength of the wave is greater than about five times the diameter of the bar. He has also shown that the fall in phase and group velocities from the value c is less than 2 for waves with

wavelengths again greater than five times the diameter of the bar. Wavelengths less than five times the diameter of the anvil bar correspond to frequencies greater than 106,000 kc/s. From a Fourier analysis of a square wave of durations 110 microseconds it was found that the percentage of components with frequencies greater than 106,000 kc/s is very small. Assuming that for the actual loading wave forms (Figure 18 etc.) the components of frequencies greater than 106,000 kc/s are also very small, it was considered that not only would wave distortion due to dispersion be negligible, but also the gauges would give an accurate measure of the average longitudinal stress. It was also considered that any errors due to imperfect reflection at section B (Figure 1) of the weighbar would be small, as the reflected wave amplitude is never greater than about one-quarter of the loading wave amplitude.

(iii) At room temperature the main mechanism of deformation in dynamic tests appears to be fine slip. This is in accordance with the results found by Campbell, Duby and Puttick (30) for steel of the same composition and heat treatment as that used in this investigation. The apparent grain boundary movement observed after dynamic deformation was attributed by these investigators to a localised shear

imposed by the requirements of continuity.

To explain the fine slip observed after impact, an argument similar to that used to explain the fine slip observed after static tests at -183°C may be used. When a source dislocation breaks free and begins generating free dislocation rings, the resulting disturbance assists nearby sources to operate. It is reasonable to expect that, at the higher stresses associated with yielding in dynamic tests or static tests at low temperatures, the disturbances at yield are greater than in a static test at room temperature. Also neighbouring dislocations would require a smaller amount of additional energy from such disturbances to enable them to generate, since the stresses at the sources are high. It is thus thought that when the yield stress is high the total number of sources that are activated during yielding will be much greater than the number activated during yielding at low stresses. Hence the number of slip planes will be increased and the amount of slip per plane reduced. The resulting deformation would be by fine slip.

At test temperatures lower than room temperature fine slip was also observed, however, this slip became more and more difficult to resolve as the test temperature was lowered. This was because the permanent deformation, produced by a

given impact velocity, decreased with test temperature. (Table II).

Some twinning was also evident in some of the low temperature impacts. Whether or not these twins were formed at a critical resolved shear stress will be considered in a later section (section 2-7). It is of interest to note that in the tests in which twins were found the dynamic stress-strain curves are smooth and do not exhibit saw-tooth features due to twin formation, a phenomenon observed in low temperature static tests by some investigators (8, 9). It is thought that the number of twins formed was not great enough to influence the shape of the dynamic stress-strain curves to any great extent.

(iv) It maybe seen from the derived dynamic stress-strain curves (Figures 22, 28, 33, 38) that the slopes of the unloading lines are less than the value of the elastic modulus E. This phenomenon has also been observed by Campbell and Duby (19).

2-4. STATIC PROPERTIES OF MILD STEEL AFTER DYNAMIC COMPRESSION.

(1) General

It appears that no systematic investigation has previously been made of the static stress-strain behaviour of steel after it has been subjected to rapidly applied loads of various magnitudes. In the tests described in this section the steel specimens were dynamically compressed by stresses of the order 10^5 lb./in.^{2} which were maintained for about 100 microseconds. In some of these tests the specimen yielded, but in others no appreciable permanent deformation occurred. The specimens were tested statically within a few minutes of the dynamic stressing, in order to eliminate ageing effects. A few tests were also carried out at low temperatures, in order to determine the effect of increasing the magnitude and duration of the impact stress, while maintaining the permanent strain constant.

(2) Experimental Results

(1) Effect of impacting at room temperature.

A series of room temperature impacts was carried

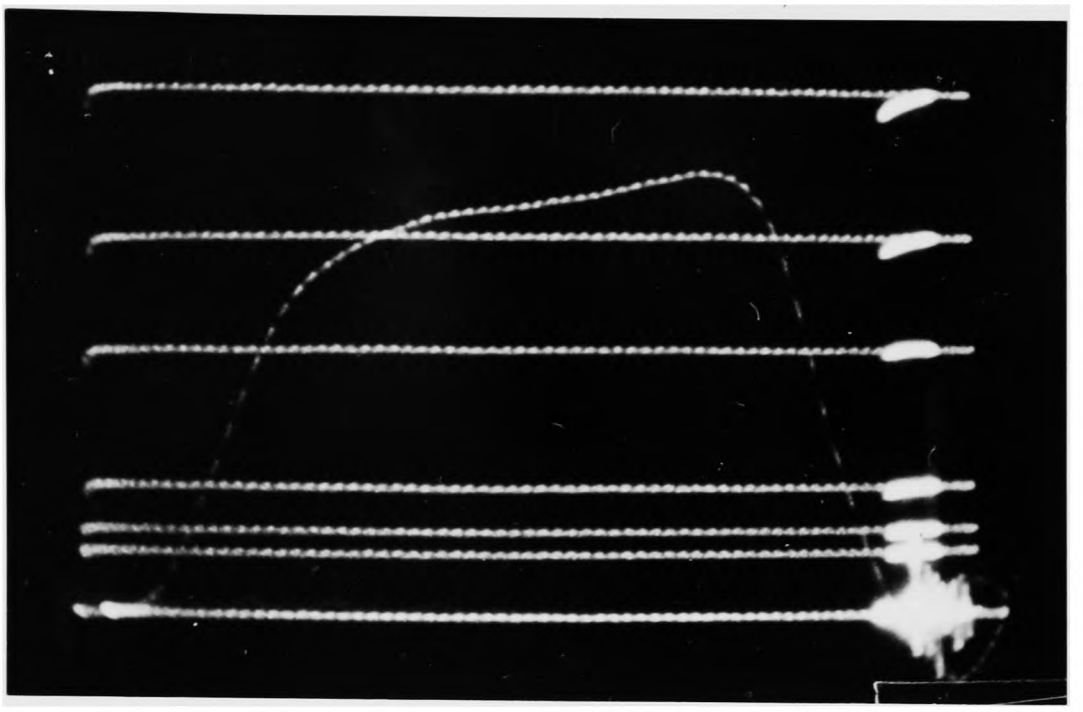
out, on the test specimens and on the high tensile steel plug at impact velocities ranging from 277 in./sec., to 365 in./sec. Static compression tests were performed on the specimens immediately after the impact tests.

Figure 39 shows typical stress-time records that were obtained. Records 39(a), 39(b) and 39(c) were obtained in tests on different annealed specimens, record 39(d) was obtained using the high-tensile steel plug.

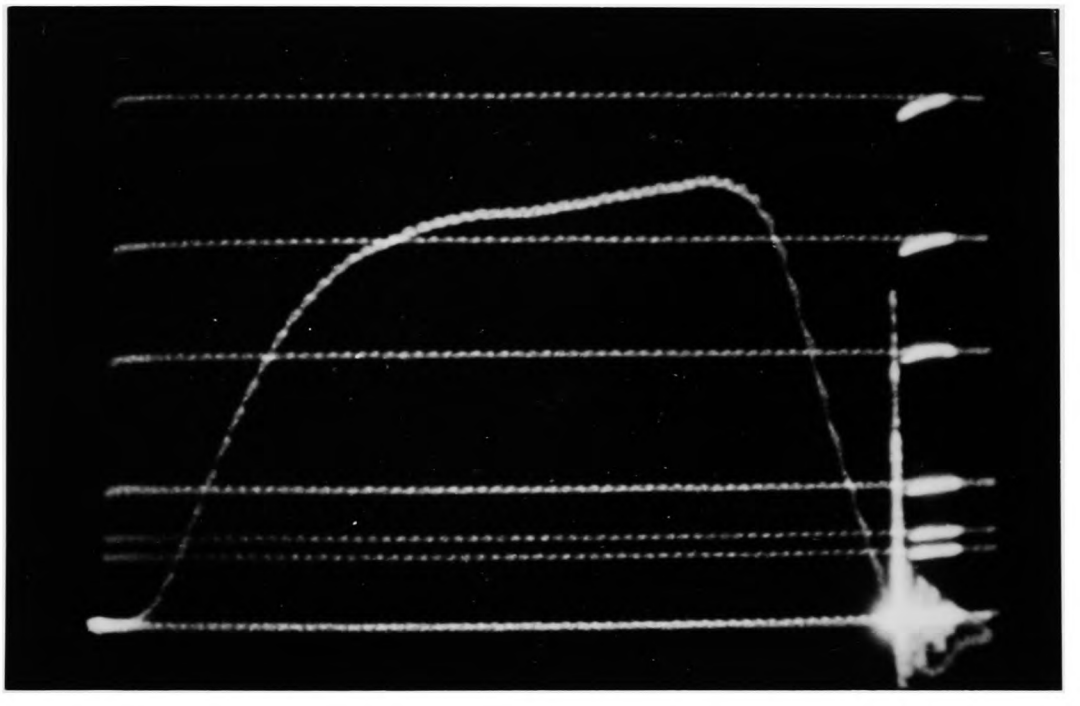
Records 39(a) and 39(b) refer to tests at an impact velocity of 308 in./sec., in which no appreciable yielding of the specimens occurred. They show that the wave shape is accurately repeatable, the greatest difference between records 39(a) and 39(b) being about 2% of the maximum stress. Neither of these records differs by more than this from the elastic wave shape, as recorded in a test on the high-tensile steel plug at the same impact velocity.

Records 39(c) and 39(d) refer to tests at an impact velocity of 340 in./sec. The difference in the two wave shapes is due to yielding of the specimen in the test which gave record 39(c).

By means of the calibration curves the records were converted to stress-time curves. Figure 40 shows the stress-time curves obtained at seven impact velocities. It is to be observed that until an impact velocity of



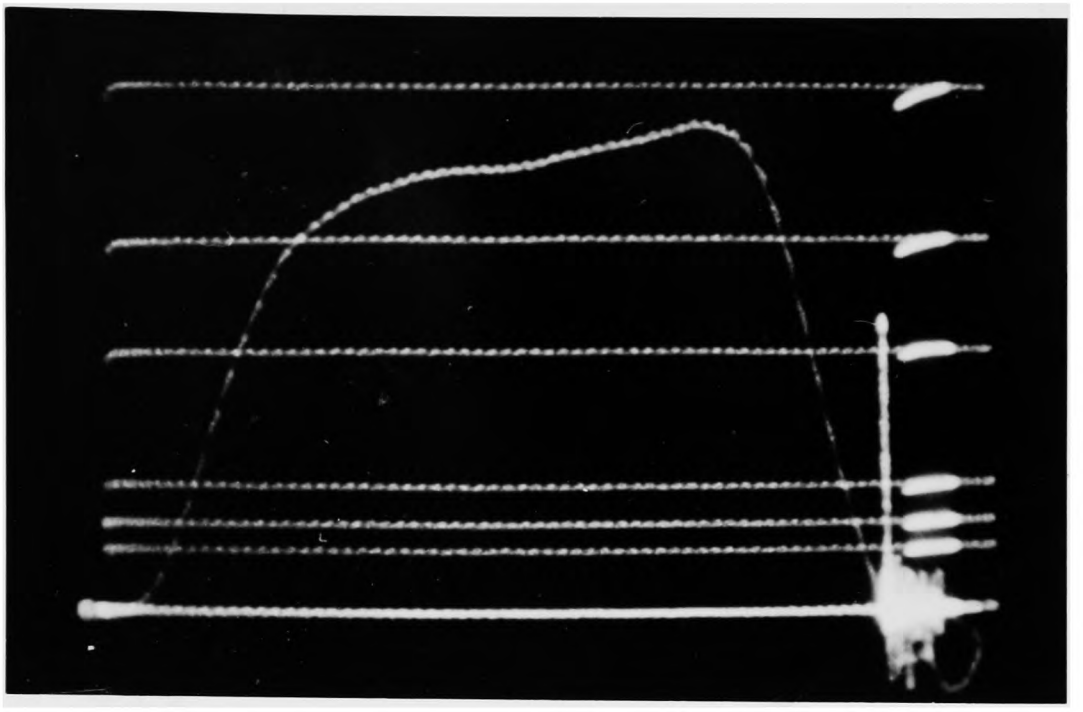
39(a)



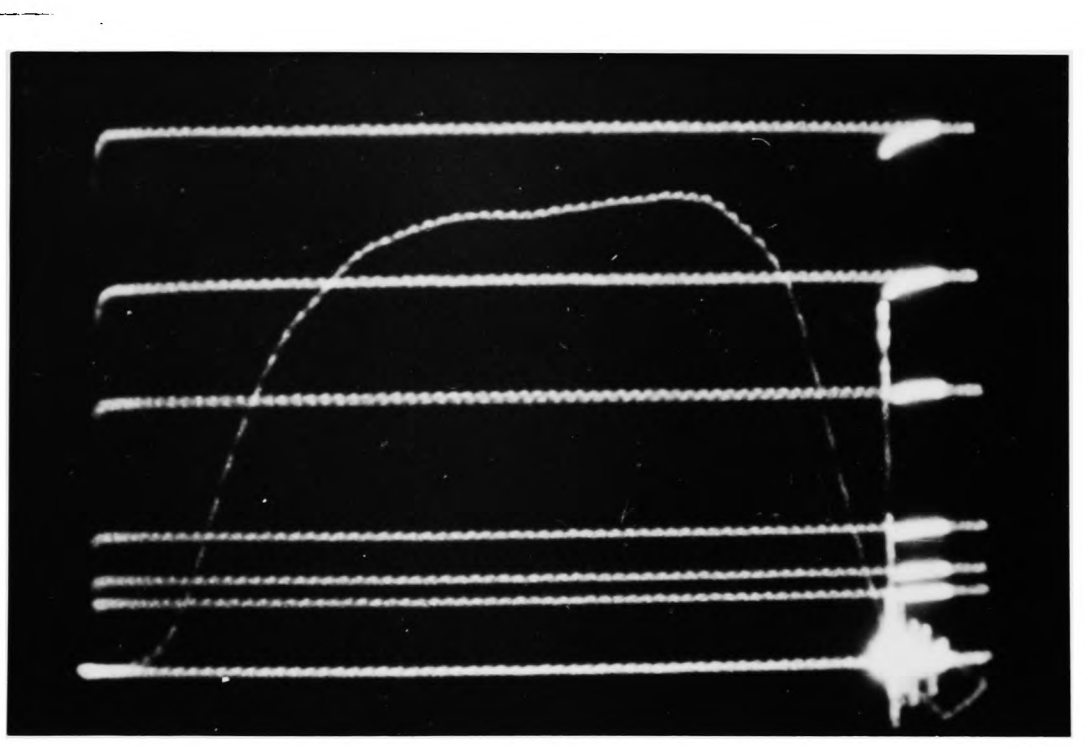
39(b)

FIGURE 39 Records obtained at impact velocities of 308 in./sec. and 340 in./sec.

(a) and (b) Weighbar records at 308 in./sec. Rg = 369Ω S = 1·94.



39(c)

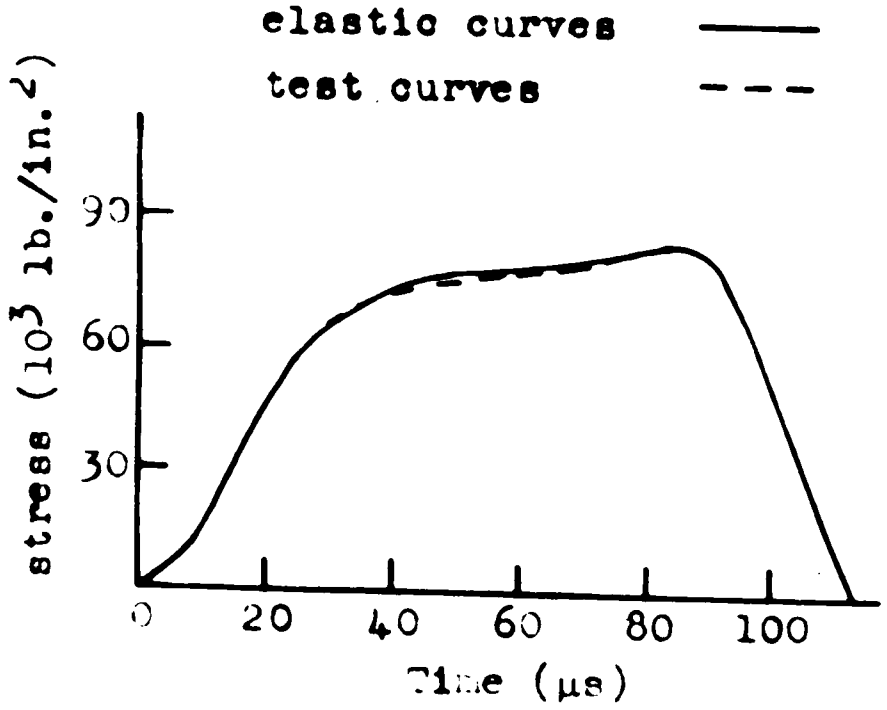


39(d)

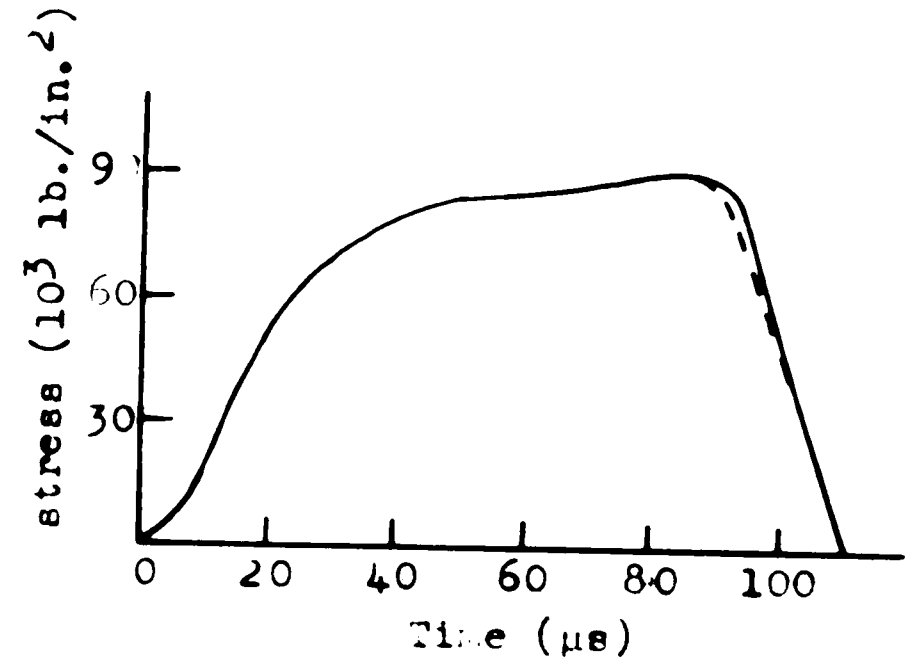
FIGURE 39 (continued)

(c) Elastic record at 340 in./sec.
Rg ≒ 369Ω S = 1•94.

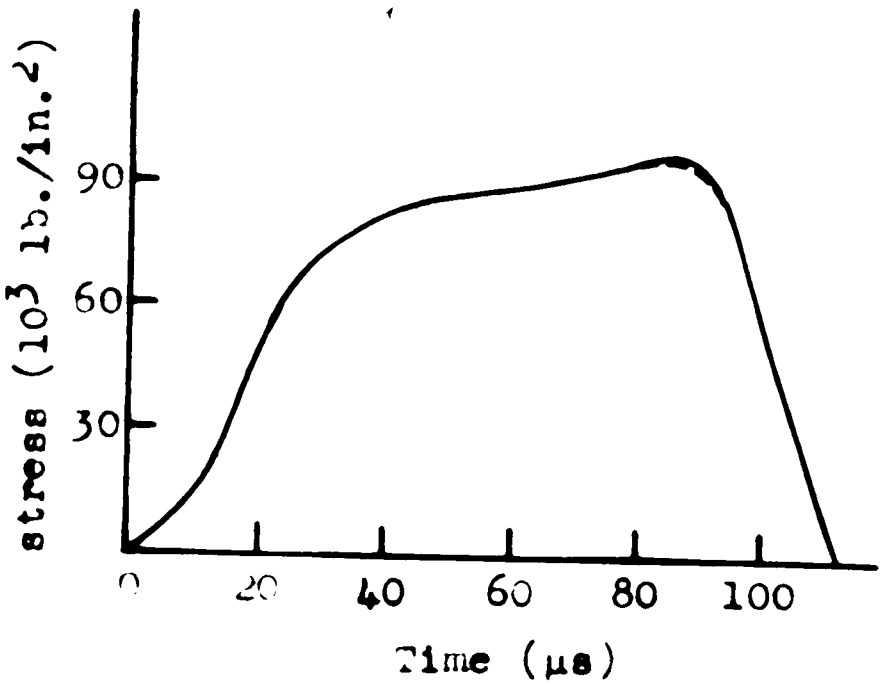
(d) Weighbar record at 340 in./sec.
Rg ≒ 369Ω S = 1•94.



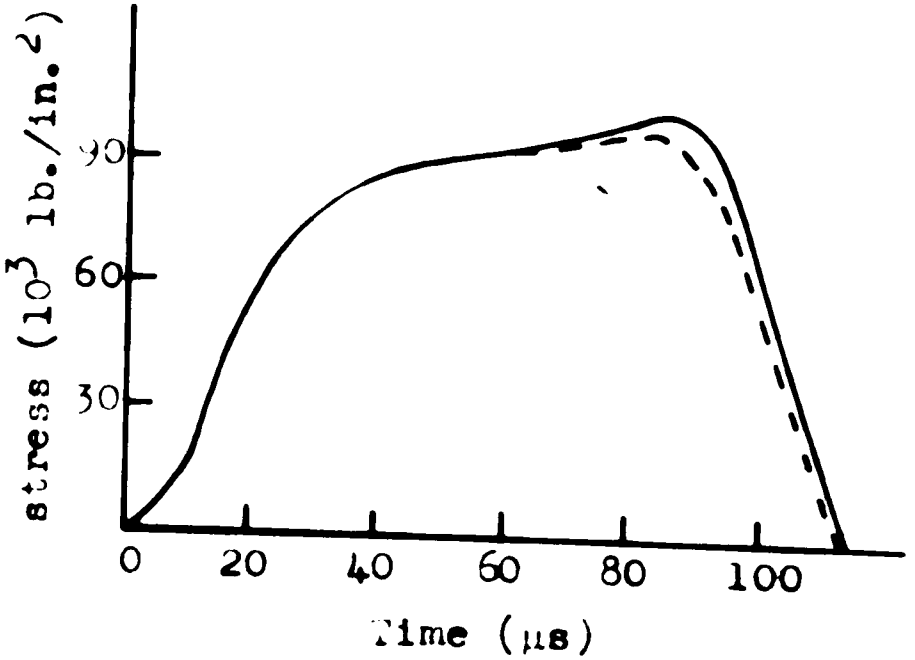
Impact velocity = 277 in./sec.



Impact velocity = 243 in./sec.

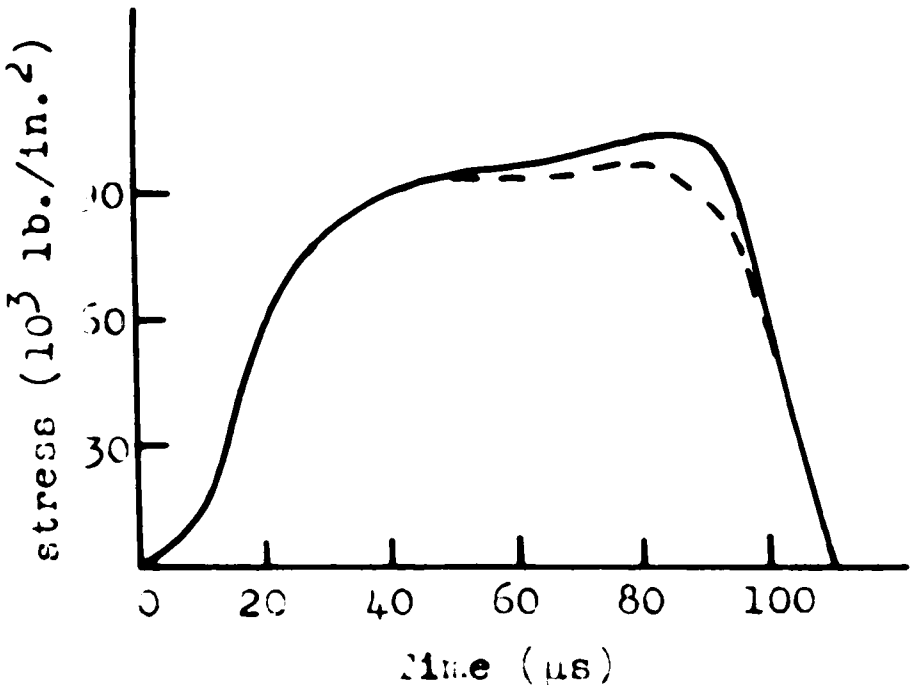


Impact velocity = 308 in./sec.

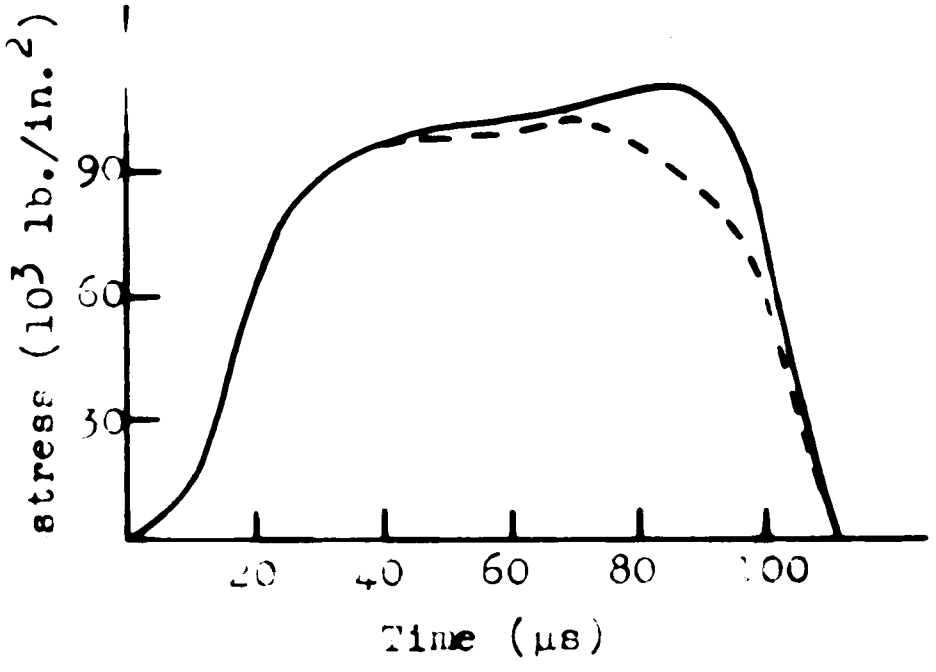


Impact velocity = 326 in./sec.

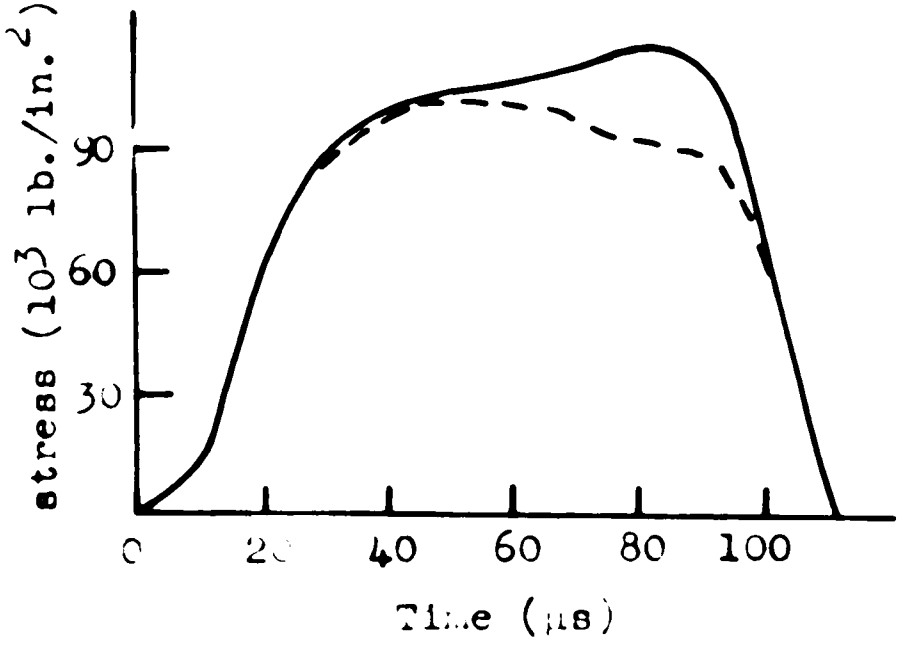
FIGURE 40 Elastic and test stress-time curves obtained at various impact velocities.



Impact velocity = 340 in./sec.



Impact velocity = 352 in./sec.



Impact velocity = 365 in./sec.

FIGURE 40 (continued) Elastic and test stress-time curves obtained at various impact velocities.

326 in./sec., is reached there is very little difference between the elastic curve and that obtained with a test specimen. It thus appears that no appreciable plastic deformation occurred in the tests corresponding to impact velocities of below 326 in./sec. This was also indicated by micrometer measurements of the specimens dimensions before and after impact.

Figure 41 shows the static stress-strain curves obtained immediately after impacting. The strain co-ordinate represents total (permanent dynamic plus static) strain. It is seen that the upper static yield stress is reduced by pulsing without yielding, however, the lowest value of the upper yield stress does not occur until the steel has been dynamically strained approximately 1%. It is also to be observed that an upper yield point persists even after considerable dynamic strain has taken place.

(11) Effect of impacting at a low temperature.

To investigate the effect of increasing the magnitude and duration of the impact stress, a specimen was impacted twice at a temperature of -84°C and a velocity of 303 in./sec. The resultant permanent strain was found to be 4·2%, 2·6% from the first impact and 1·6% from the second. By varying the impact velocity, it was found that

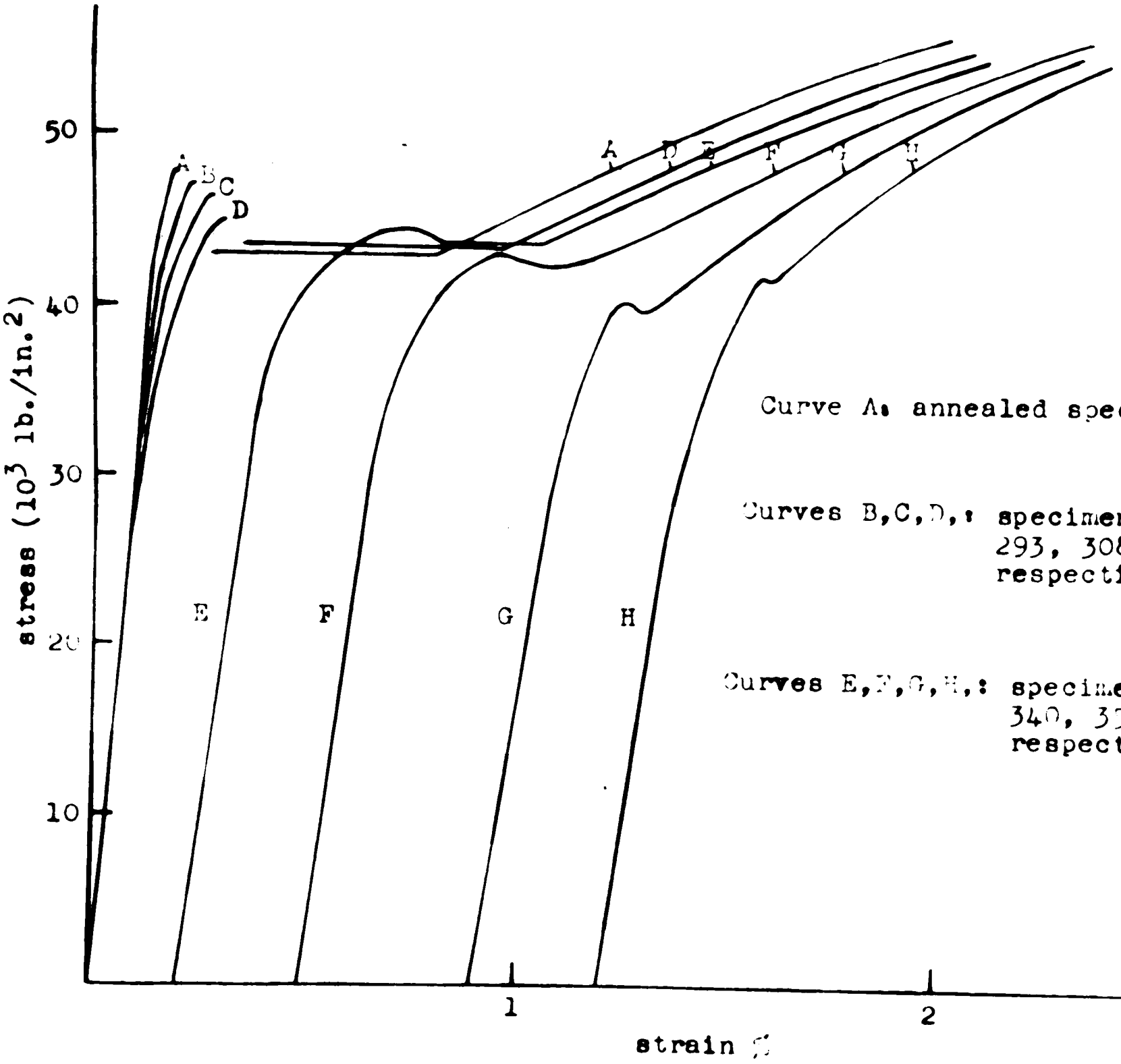


FIGURE 41 Static stress-strain curves obtained after dynamic impact.

a specimen impacted at 450 in./sec., and room tempera-ture sustained the same permanent strain of 4·2 . Analysis of the strain gauge records for these tests showed that the stresses applied to the specimen deformed at -84°C were some 3 % higher than those applied to the specimen deformed at room temperature (see section 2-3). The stress at which the metal yielded in the room temperature impact was 108,000 lb./in. whereas the yield stress at -84°C was 151,000 lb./in. In addition at the low temperature the total duration of the stress was doubled.

The two specimens were tested statically within a few minutes of the impacts tests, and Figure 42 shows the stress-strain curves obtained. It is seen that there is little difference between the curves for the two impacted steels. These tests were repeated and the static stress-strain curves obtained were in each case found to agree with those shown in Figure 42 to within 2 .

From the above tests, the conclusion may be drawn that the shape of the static stress-strain curves obtained after impact is dependent mainly on the amount of dynamic deformation and not the temperature at which the steel was impacted.

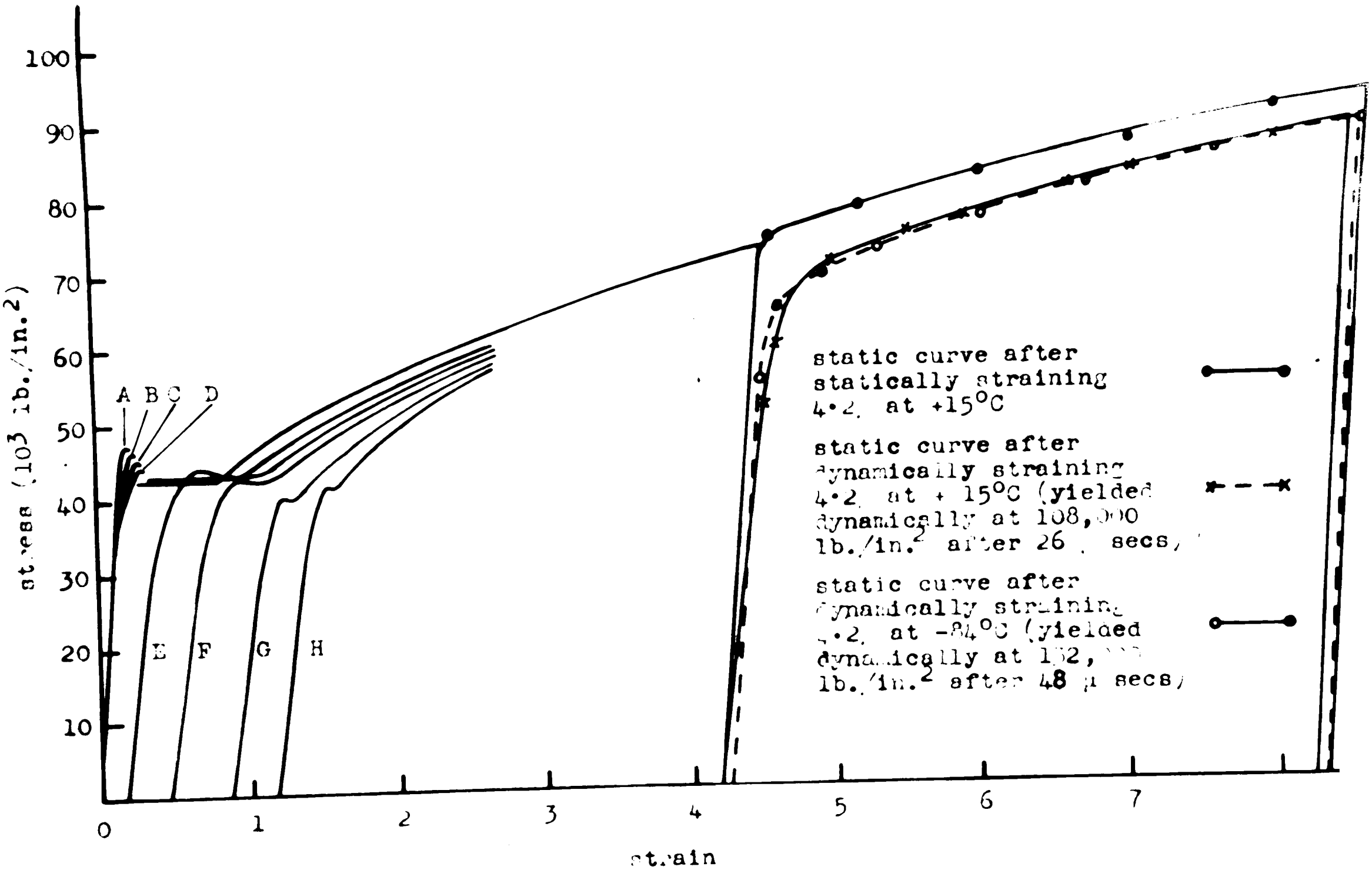


FIGURE 42 Static stress-strain curves showing the softening effect of a previous dynamic test.

(111) Micrographic examination.

Several specimens were prepared for micrographic examination before undergoing tests similar to those described above. For those specimens which were impacted at room temperature, examination before static retest showed that in only one case could the fine slip be resolved. This specimen was that strained 4·2% with an impact velocity of 450 in./sec.

It was thought that subsequent static deformation of the above specimens would occur on these planes in which slip had already occurred in the prior dynamic impact. Hence it was expected that the slip observed after static retest would be fairly fine. A comparison of Figure 43, which shows the slip observed in a specimen dynamically strained 1·2% followed by static deformation of 2·8%, with Figure 16(b) confirms that the slip after static retest is much finer than that observed in a specimen strained statically the same amount. It was also found that if a specimen sustains a dynamic stress in the region of stresses just insufficient to cause yield, then the slip observed after static deformation is also slightly finer than after static deformation alone.

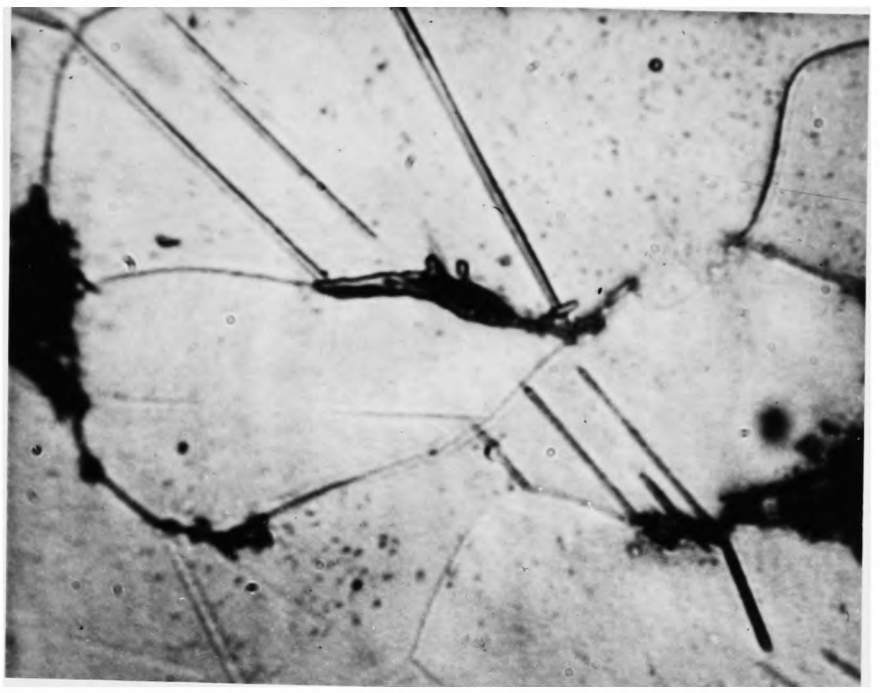
As expected from the results described in section 2-3, twins were observed after impacting a specimen at -84°C at



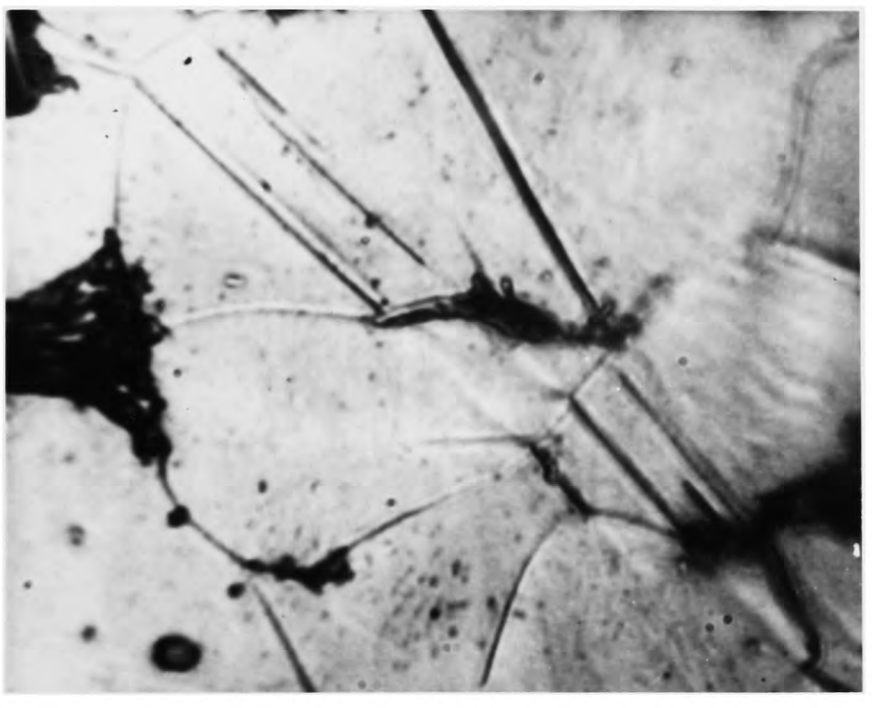
FIGURE 43 Micrograph taken after 4.5 strain — 1·2 dynamic plus 2·8 static (×1400)

an impact velocity of 503 in./sec. Micrographs were taken at several positions on the prepared surface where twinning was evident. After subsequent impact, at the same impact velocity of 503 in./sec., and specimen temperature of $-84^{o}C$, micrographs were again taken at these positions. By comparisons of the micrographs taken before and after the second low temperature impact, it was observed that although many more twins were found in the second impact, they formed in crystals in which there were no initial twins. Also it was noticed that several of the twins formed during the first impact did not completely traverse the crystal. It was thus expected that on impacting again these twins would lengthen. However, this appeared not to occur, the effect of the second impact was to widen the twins rather than lengthen them. Figures 44(a) shows a micrograph taken after the first impact and Figure 44(b) one taken after the second impact. Some of the phenomena mentioned above are evident.

Upon statically retesting a specimen subjected to the two impacts mentioned above, it was found that the twins not only widened but deformed somewhat due to subsequent slip. Figures 45(a) and 45(b) show twins deformed by subsequent static deformation. It is of interest to notice that although the twins have distorted and widened consid-



44(a)



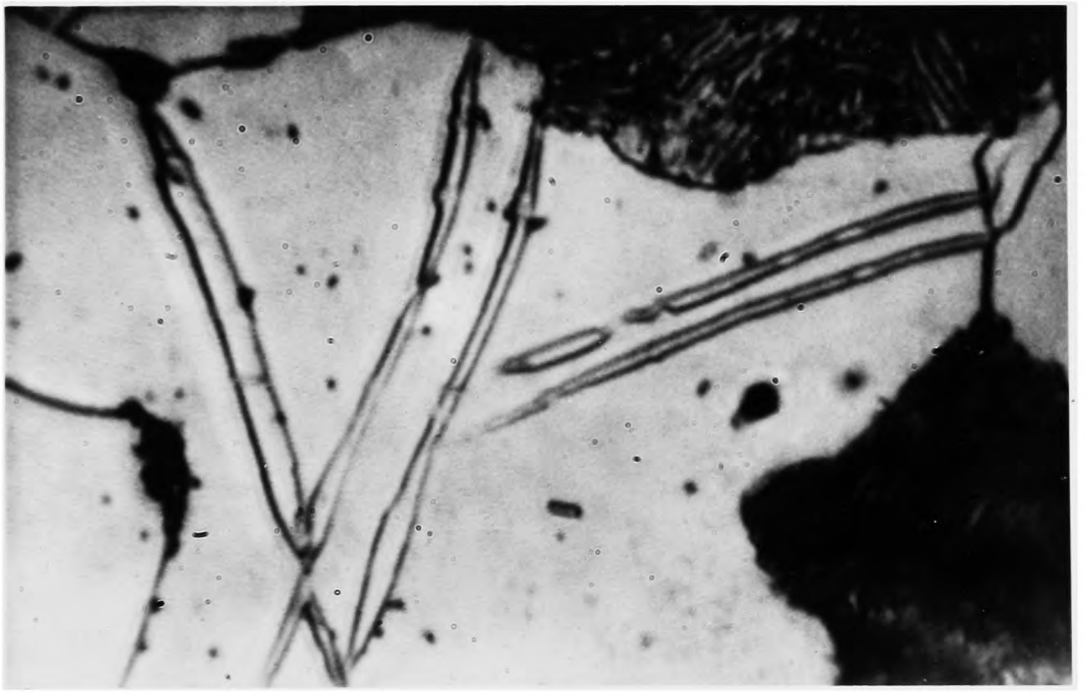
44(b)

FIGURE 44 Micrographs obtained after impacts at 503 in./sec. and -84°C.

(a) After the first impact (2·6% strain)
(b) After the second impact (4·2 strain)
} ×1400



45(a)



45(b)

FIGURE 45 Micrographs obtained after 8·2 strain — 4·2 dynamic at -84°C plus 4 static at +15°C. Magnification = ×2800

N. B. Specimen prepared after test.

erably the ends appear to be anchored throughout.

(3) Discussion

(1) It has been suggested by Campbell (13) that yielding occurs when the density of released dislocations reaches a critical value. With certain assumptions (see section 1-4) it is shown that the density of released dislocations at time t is approximately proportional to $\int_0^t (\sigma)^{\alpha_m} dt$ (equation 10), where σ is the applied stress at time t and α_m is a constant at any given temperature.

From previous dynamic tests by Campbell and Duby (44) on steel of the same composition and heat treatment as that used in the present investigation, it was determined that at room temperature α_{RT} was approximately 15. This value was therefore used in evaluating the integral (equation 10).

Stress-time curves for the top face of the specimens were derived from the strain gauge records in the manner described in section 1-5. Figure 46 shows the elastic and weighbar stress-time curves for an impact velocity of 365 in./sec., (curves A and B), it also shows the derived stress-time curve for the upper face of the specimen. (curve C). The integral (10) was evaluated graphically up to the maximum of this curve, which was taken as giving τ,

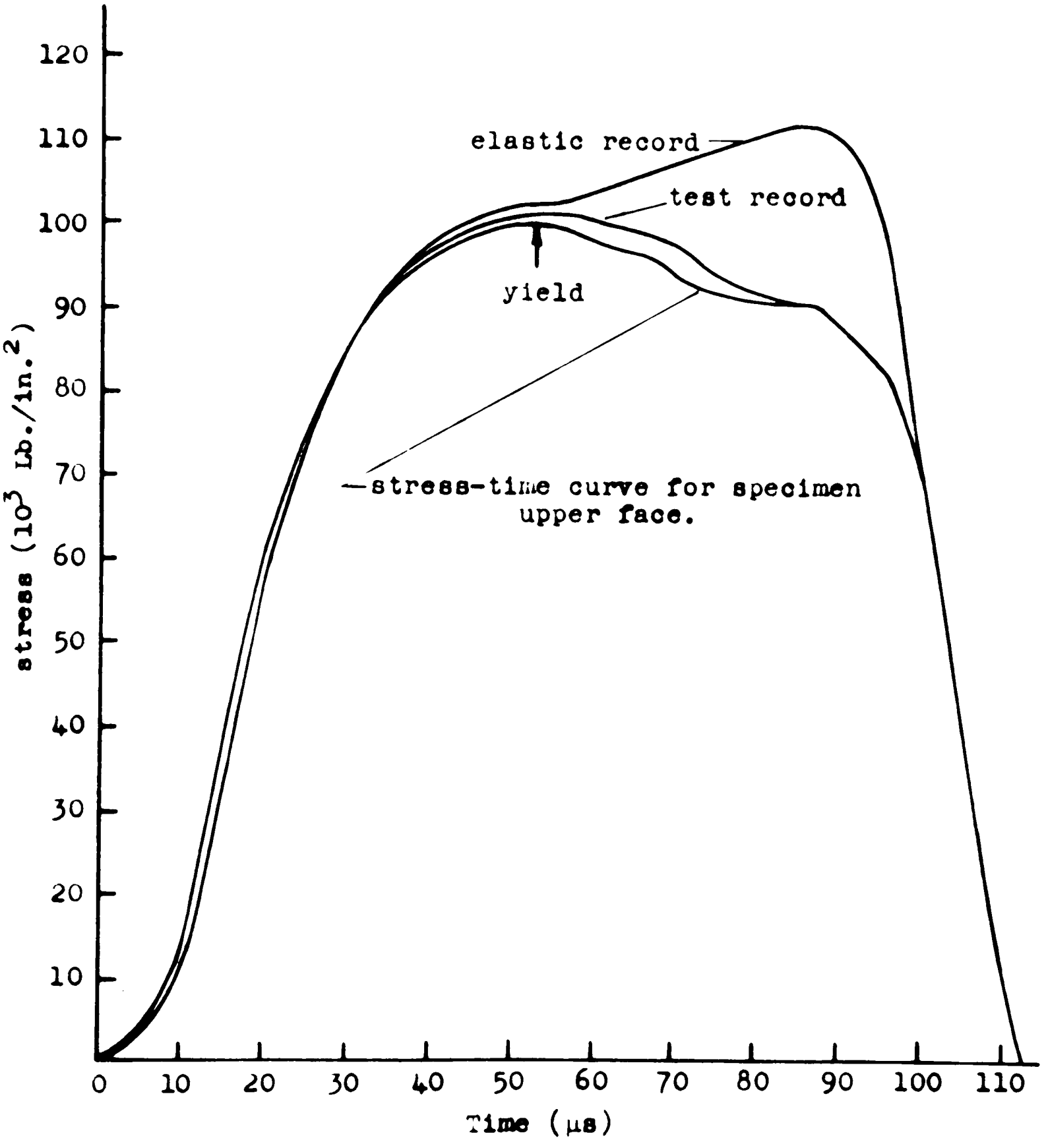


FIGURE 46 Elastic record, test record, and stress-time curve for the specimen upper face (impact velocity = 365 in./sec.

the time at which yielding began. Figure 47 shows the curves of σ^{13} obtained for seven different impact velocities. At the three lowest velocities there was no measurable permanent deformation of the specimen, and the integrals were evaluated for the complete duration of loading, τ_o.

Table III gives the results pertaining to tests in which yielding occurred. The variation in the values of the integral from the average of 16·1 is ±10%, this is within the experimental accuracy attainable, since the value of the integral is very sensitive to errors in the stress measurement. Values of the integral could also have been obtained from the room temperature records used in deriving the dynamic stress-strain curves, however, it was thought best to deal solely with those tests described above. In fact, as will be seen later, (section 2-6) the value of 16·1 is very near the average value found for all the room temperature tests performed in this investigation. Also the fact that the integral is approximately constant over the whole range of impact velocities confirms the value of 13 taken for α_{RT}.

The reduction in upper yield stress due to pulsing i.e. to dynamic loading insufficient to cause yield, may reasonably be postulated to depend on the ratio of the number of dislocations released to the number required to cause

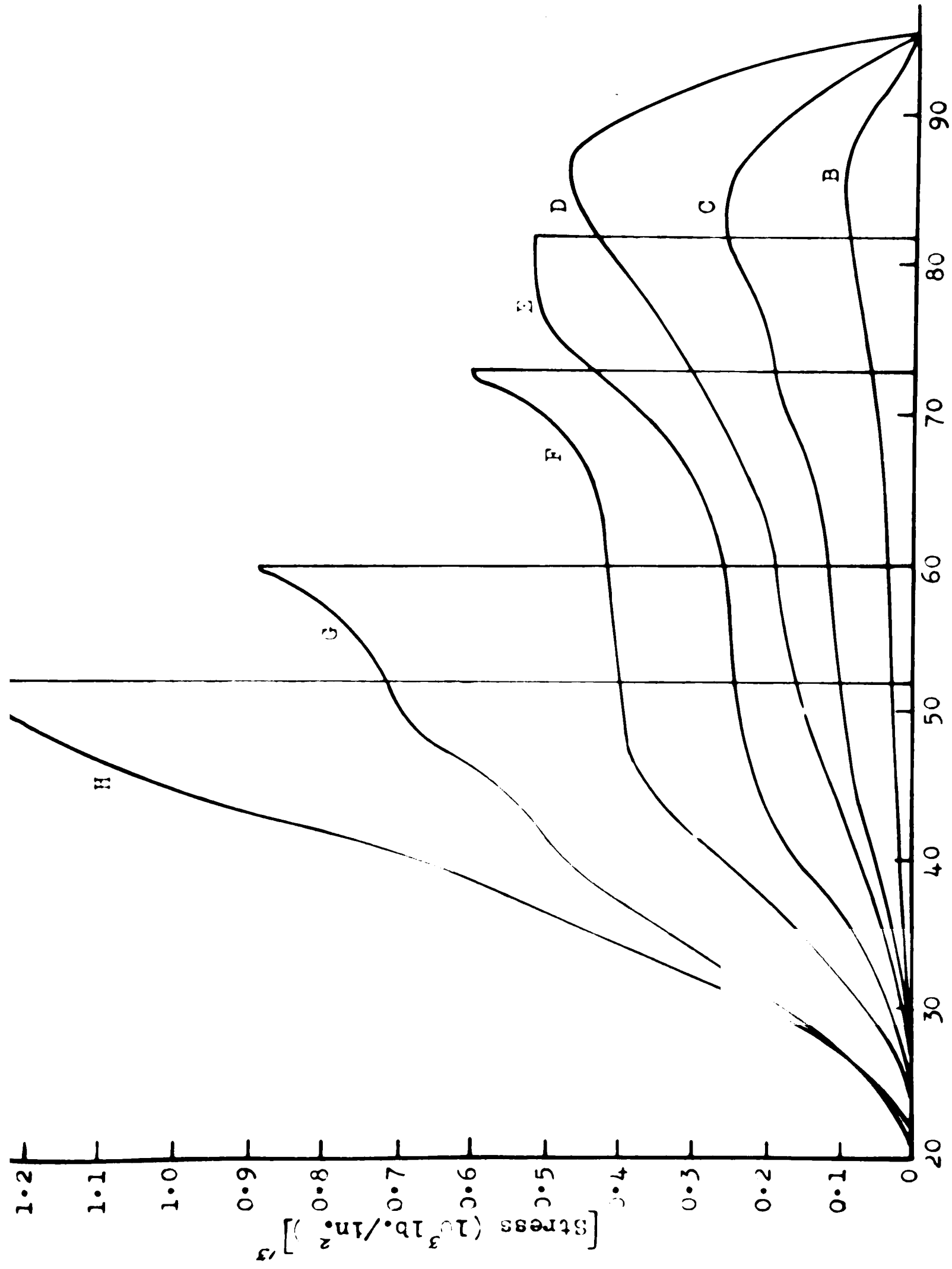


FIGURE 47 Curves of (stress)$^{1/3}$ against time, for dynamic tests.

TABLE III

Delay-time results at +15°C.

Impact velocity in./sec.	Time to yield microsec.	Yield stress 10^3 lb./in^2	$\int_0^t \left(\frac{\sigma}{105\,16/in^2}\right)^{13} dt$ microsec.	Permanent axial deformation
326	82	95	14·1	0·2
340	73	96	15·1	0·5
352	60	99	17·7	0·9
365	52	102	1[illegible]·3	1·2
		Average	16·1	

TABLE IV

The effect of various stress pulses on the subsequent static upper yield stress.

	Impact velocity in./sec.	$\int_0^t \left(\frac{\sigma}{105\,16/in^2}\right)^{13} dt$ microsec.	[illegible]	r
First series of tests	Not pulsed	-	-	0·107
	277	2·8	0·17	[illegible]·087
	293	8·3	0·51	0·067
	308	14·4	0·89	0·036
Second series of tests	Not pulsed	-	-	[illegible]·095
	277	2·4	0·15	0·085
	293	7·3	0·45	[illegible]·068
	308	13·8	[illegible]·86	0·023

yield. This ratio is given by

$$R = \frac{\int_0^{\tau_o} \sigma^{13}\, dt}{\int_0^{\tau} \sigma^{13}\, dt} \qquad (39)$$

where the integral in the numerator refers to a test in which yield does not occur, and that in the denominator to tests in which yield does occur. Table IV shows results obtained from tests in which yield did not occur. The values of R were calculated by taking for the denominator the mean value of the integrals given in Table III. As a check on the values obtained, the pulsing tests were repeated. The results of the repeat tests are also given in Table IV and are in good agreement with the earlier results.

It was decided to use, as a measure of the reduction in the static upper yield stress caused by pulsing, the ratio

$$r = (\sigma_{YU} - \sigma_{YL})/\sigma_{YL} \qquad (40)$$

where σ_{YU}, σ_{YL} are the static upper and lower yield stresses respectively.

Figure 48 shows the values of R plotted against those of r, for the two series of pulsed specimens. It is seen

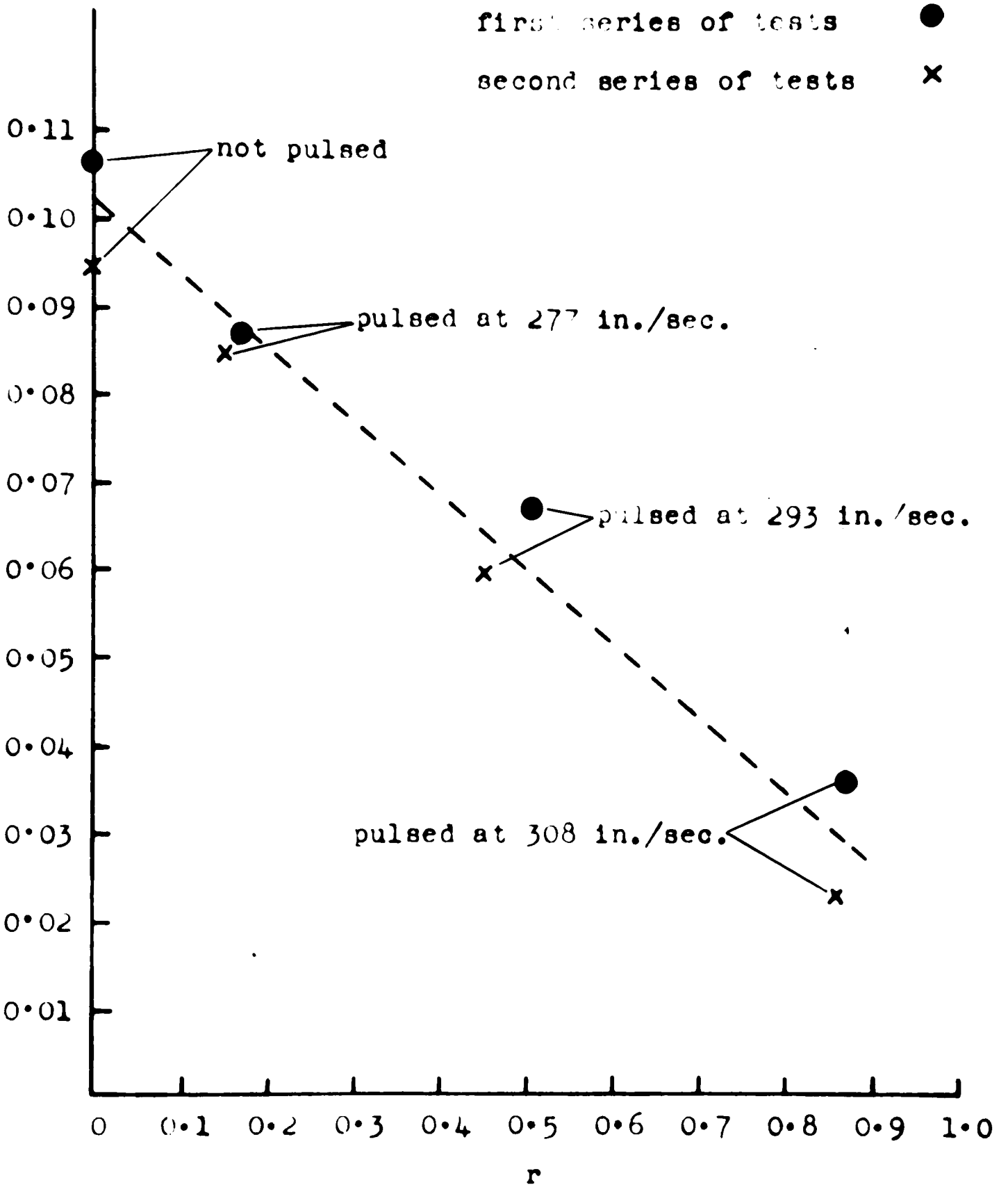


FIGURE 48 Reduction of static upper yield stress caused by pulsing.

that there is a reasonable correlation between the two quantities, it is, however, difficult to obtain either ratio accurately, and the straight line drawn in Figure 43 only serves to indicate the general trend of the relationship.

(11) From Figure 41 is seen that the steel is in a softer state after dynamic deformation than after a corresponding amount of static straining. This agrees with earlier results of Campbell and Eaby (19) who suggested that the effect is caused by the large number of free dislocations that the specimen must contain after dynamic straining. Since dynamic deformation occurs by fine slip, those dislocations are more uniformly distributed than would be the case in a specimen strained an equal amount statically, and hence the back stress on each source due to dislocations piled up against obstacles or grain boundaries is lower. On reloading statically, further slip can occur on planes on which dynamic slip has occurred, thus the steel is softer than when reloaded after static deformation. That further slip does tend to take place on planes on which dynamic slip has occurred is shown by the relative fineness of the slip observed after static retest (Figure 43).

The static reloading curves of Figure 41 show that the hardness of the dynamically deformed steel is very little affected by the temperature at which it is deformed, provided that the total amount of deformation is the same. According to the yielding criterion discussed above, the number of dislocations freed before yielding occurs is independent of the magnitude of the stress pulse causing yield. Assuming that it is also independent of temperature, the number of free dislocations at yield is the same in any dynamic test. Assuming also that the disturbances at yield are of the same order, then two specimens which have been deformed dynamically to the same permanent strain may therefore be expected to contain similar numbers of dislocations similarly distributed, irrespective of the temperature of testing. The two specimens should therefore give similar stress-strain curves when reloaded statically at room temperature.

Figure 40 also shows that the static upper yield stress is a minimum when the steel has been strained about 1% dynamically. After greater amounts of dynamic strain, the yield stress increases again, this is presumably caused by dislocations piling up against obstacles such as grain boundaries and sessile dislocations, and thus causing increasingly high back stresses to act on the sources.

It is also to be noted that even after more then 1% dynamic deformation the steel still exhibited a perceptible drop of stress at yield, though the lower yield strain was greatly reduced. The perceptible drop in stress at yield may possibly be explained as follows. During static reloading some dislocations become relocked. Thus, provided the additional stress required to free these dislocations from their atmospheres is significant compared to the stress required to move the free dislocations, there will be a perceptible drop in stress at yield. However, at a certain stage when a specimen has been initially strained past the dynamic lower yield strain, the additional stress required to free the few dislocations that relock during static re-test will be insignificant. Hence in such a case the drop in stress at yield will be too small to be observed.

(iii) Figures 45(a) and 45(b) shows that subsequent static deformation of a specimen containing twins caused the twins to widen considerably. It may thus be concluded that the stress required to widen twins is considerably less than that required for their formation.

2-5. DYNAMIC PROPERTIES OF THE STEEL AFTER DYNAMIC COMPRESSION.

(1) General

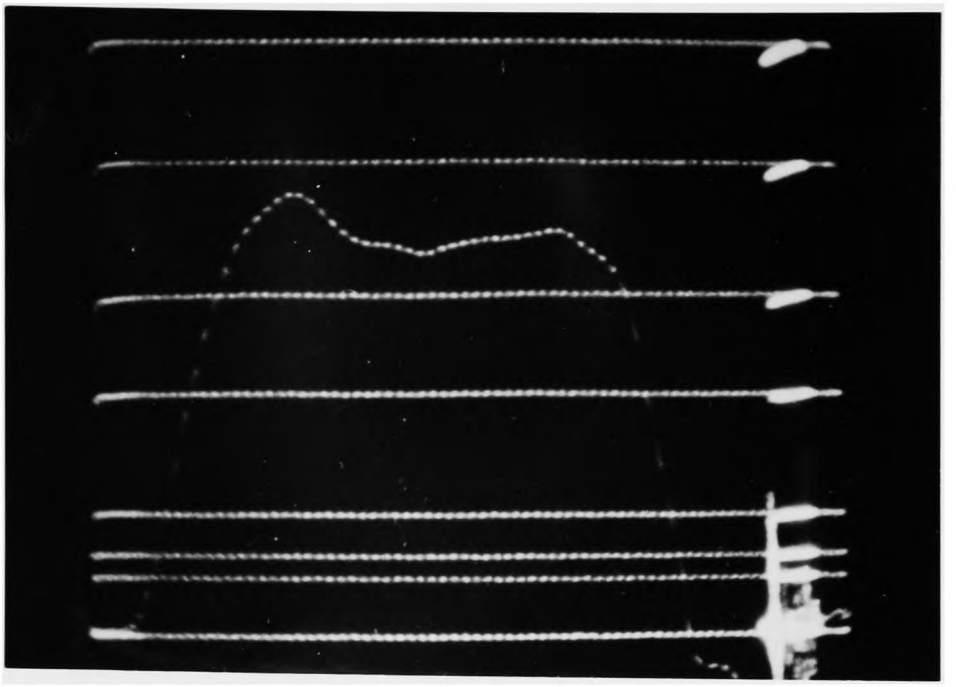
Section 2-4 was concerned with the static properties of the steel after dynamic compression. In practice, however, the subsequent loading of steel treated in this manner is often dynamic rather than static. For instance when rolled sheet steel is pressed the load is suddenly applied and of short duration. The present set of tests was undertaken to find the dynamic properties of the steel after dynamic compression.

The steel specimens were loaded by compressive stresses of the same order and durations as those applied to the steel before static retest (section 2-4). As was found in the previous section the specimens yielded in some of these tests but in others no appreciable permanent deformation occurred. The specimens were retested dynamically within 8 to 13 minutes of the first impact in order to minimise ageing effects. The results permit a comparison to be made between the dynamic and static properties of the steel after dynamic compression.

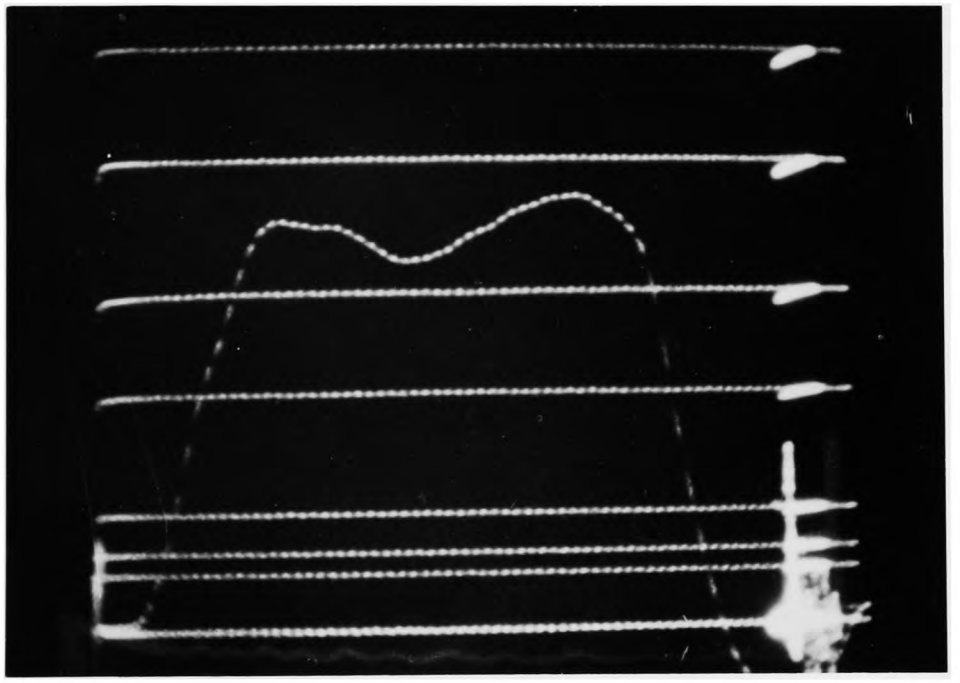
(2) Experimental Results

A series of room temperature impacts was carried out on the test specimen and on a high-tensile steel specimen, at impact velocities ranging from 277 in./sec., to 352 in./sec. Within 8 to 13 minutes of the first impacts the specimens were again impacted this time at a velocity of 430 in./sec. This rather large impact velocity was chosen for the second impact as it gives well defined upper yield points (see Figures 18(c), and hence enables the effect of the previous impact to be easily observed.

Three typical weighbar records with calibration lines, all for an impact velocity of 430 in./sec., are shown in Figures 18(c), 49(a) and 49(b). Figure 18(c) is the record obtained with a specimen that has not been previously dynamically compressed. Figures 49(a) and 49(b) are records obtained for specimens that have been subjected to an initial dynamic compression. The specimen corresponding to Figure 49(a) had been pulsed at an impact velocity of 293 in./sec., and that corresponding to Figure 49(b) had been dynamically strained 0·9 at an impact velocity of 352 in./sec. By means of the calibration curves the records were converted to stress-time curves which are shown in Figure 50. This Figure shows the stress-time curves obtained for each specimen at both impact velocities. The elastic



49(a)

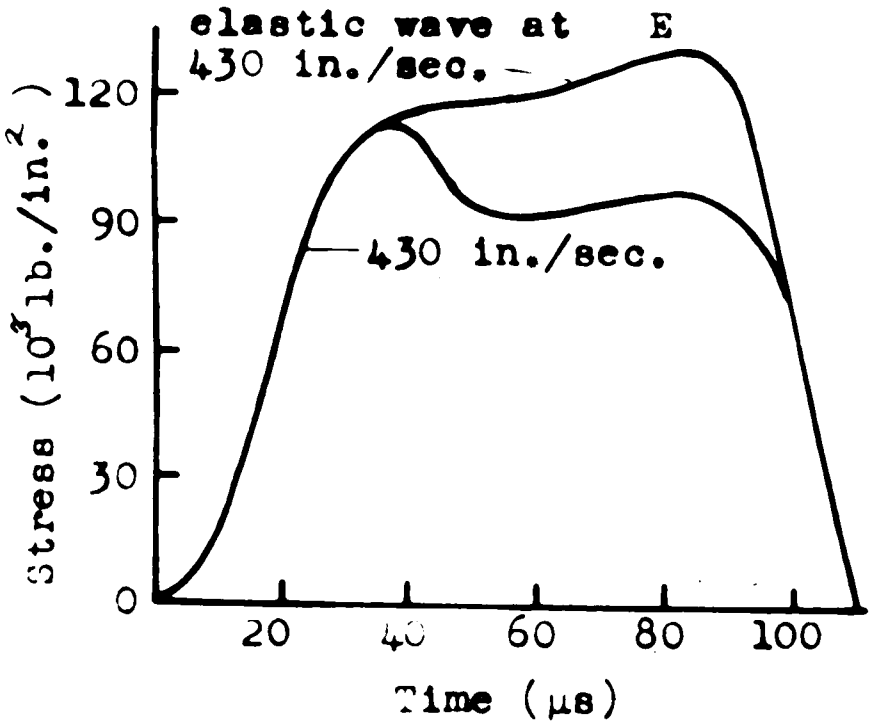


49(b)

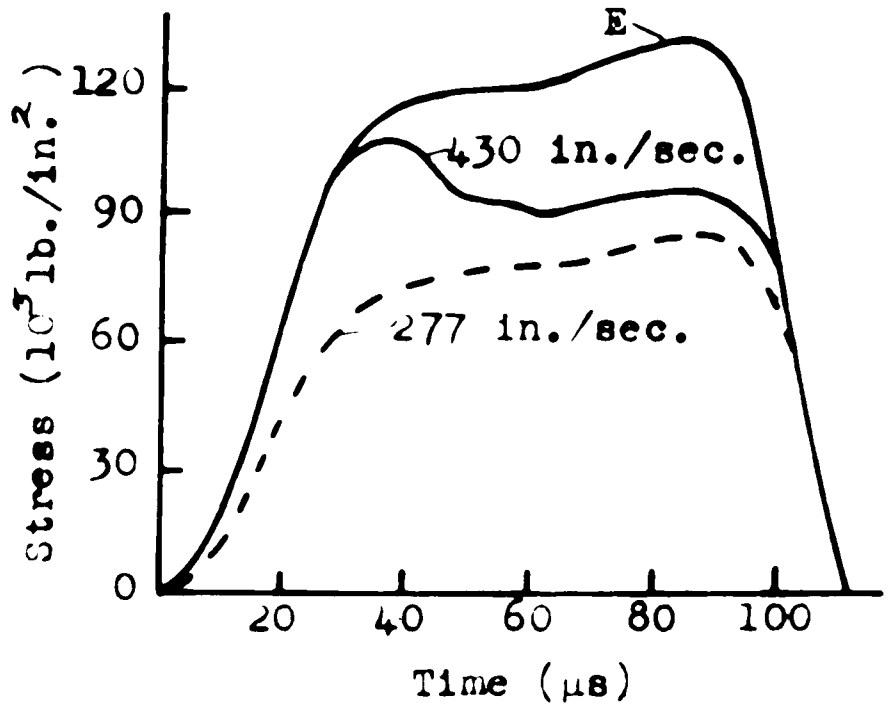
FIGURE 49 Records obtained for an impact velocity of 430 in./sec.

(a) Specimen first pulsed at 293 in./sec. Rg ≐ 376Ω S = 1·94.

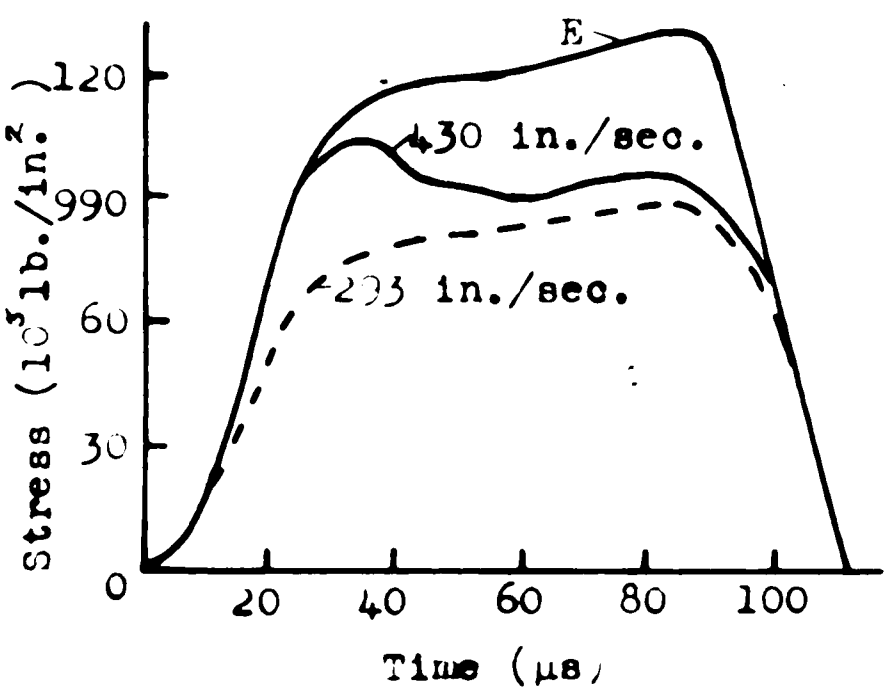
(b) Specimen first strained 0·9 dynamically Rg ≐ 376Ω S = 1·94.



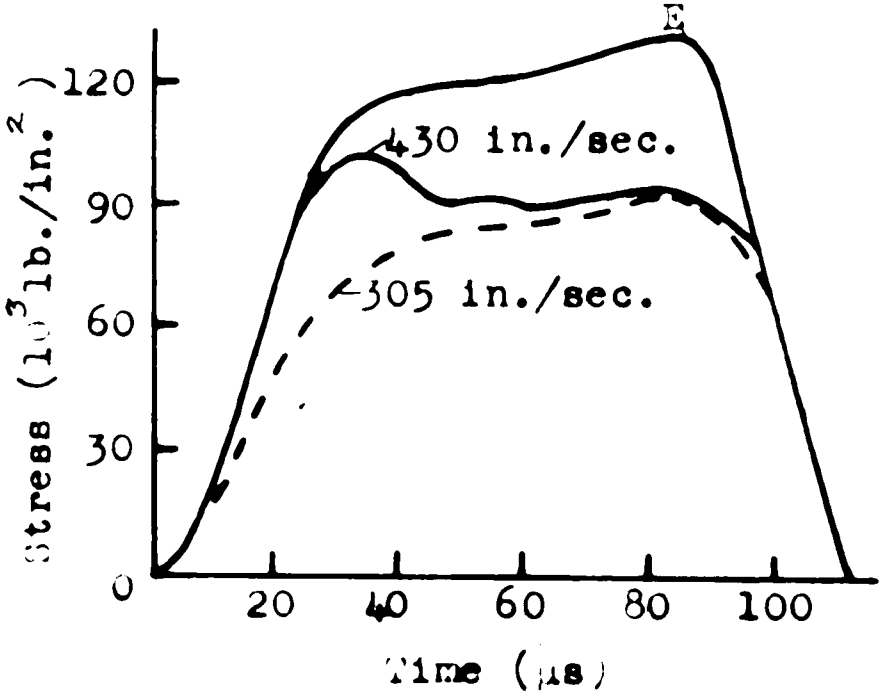
Not pulsed, impact velocity = 430 in./sec.



Pulsed at 277 in./sec. followed by impact at 430 in./sec.

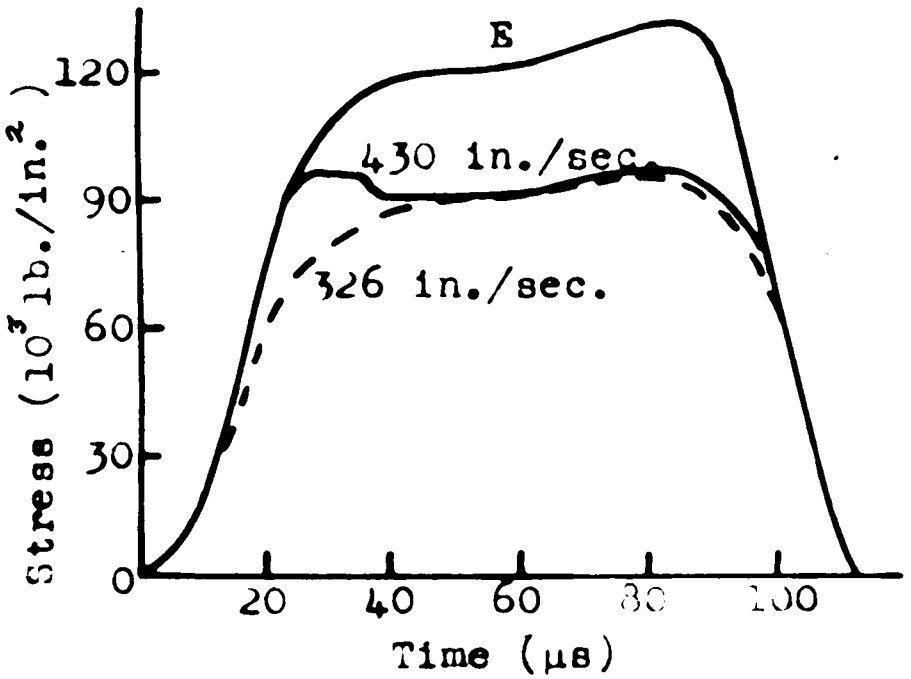


Pulsed at 293 in./sec. followed by impact at 430 in./sec.

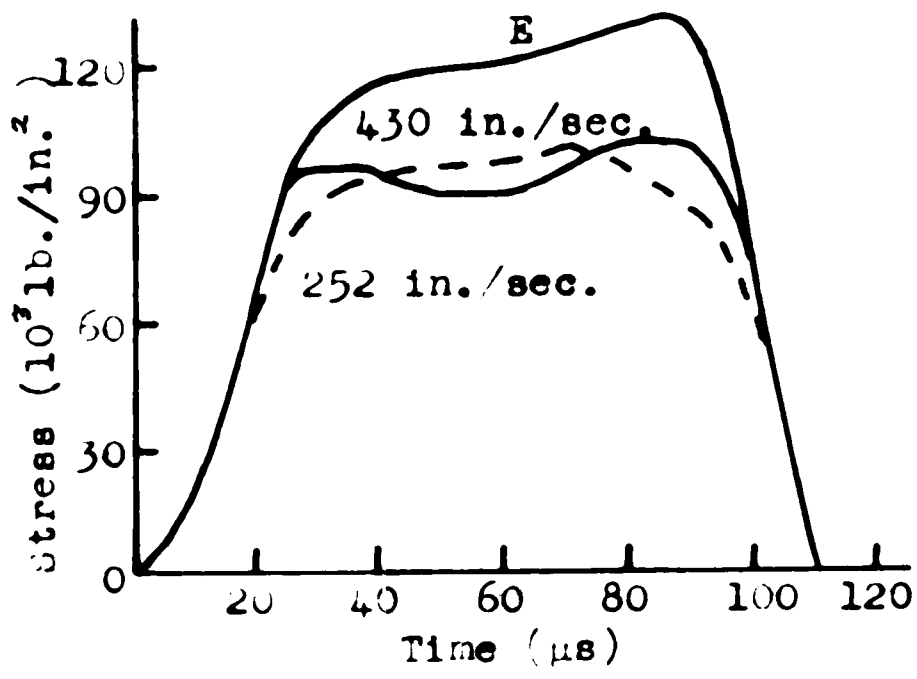


Pulsed at 305 in./sec. followed by impact at 430 in./sec.

FIGURE 50 Elastic and test stress-time curves obtained at various impact velocities.

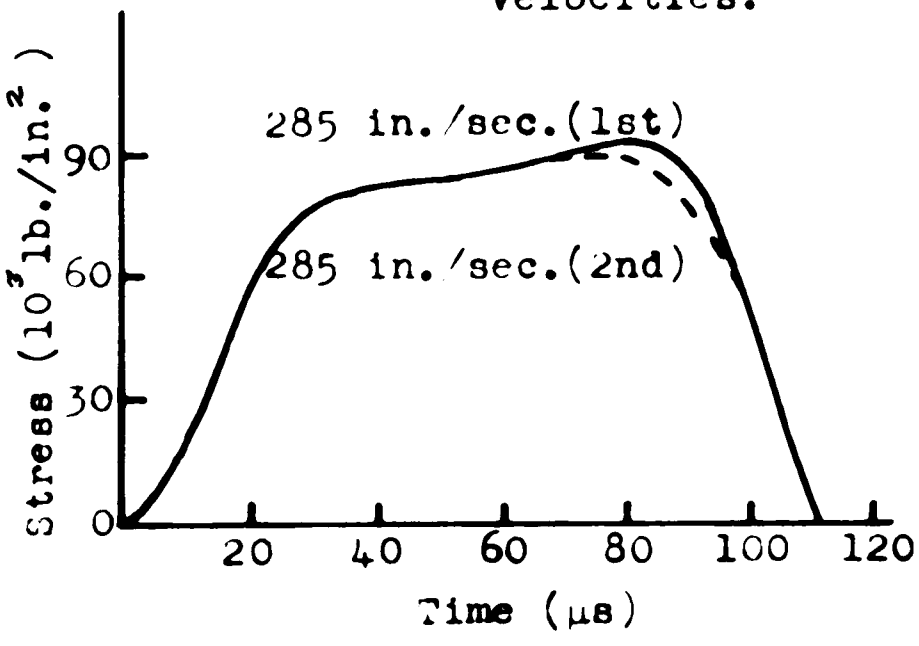


First impact at 326 in./sec.
Second impact at 430 in./sec.



First impact at 352 in./sec.
Second impact at 430 in./sec.

FIGURE 50 Elastic and test stress-time curves obtained at various impact velocities.
(continued)



Pulsed at 285 in./sec. followed by impact at 285 in./sec.

FIGURE 54 Test stress-time curves obtained by impacting a specimen twice at 301 in./sec.

stress-time curves for the first impacts are not shown in this Figure, however, except for the impact velocity of 305 in./sec., they are the same as those shown in Figure 39. Until an impact velocity of 326 in./sec., is reached there is very little difference between the elastic curve and that obtained with a test specimen. As in section 2-4 it was assumed that those specimens impacted at a velocity less than 326 in./sec., had not yielded.

Stress-time curves for the top face of the specimen were derived, by the usual method, for all impacts. The derived stress-time curves for the second impact are shown in Figures 51 and 52. Figure 51 shows the stress-time curves for those specimens that had previously been impacted at velocities up to 326 in./sec., and Figure 52 shows the derived stress-time curve for the specimen previously impacted at a velocity of 352 in./sec. It is seen that the dynamic upper yield stress is reduced by pulsing without yielding, however, the lowest value of the upper yield stress does not occur until the steel had been dynamically strained approximately 0·2 . It is also to be observed that at this strain the upper yield point has almost been removed, as indeed it has after 0·9% initial dynamic strain. In Figure 51, for clarity, only the front portion of the derived stress-time curves are plotted. In fact, once the

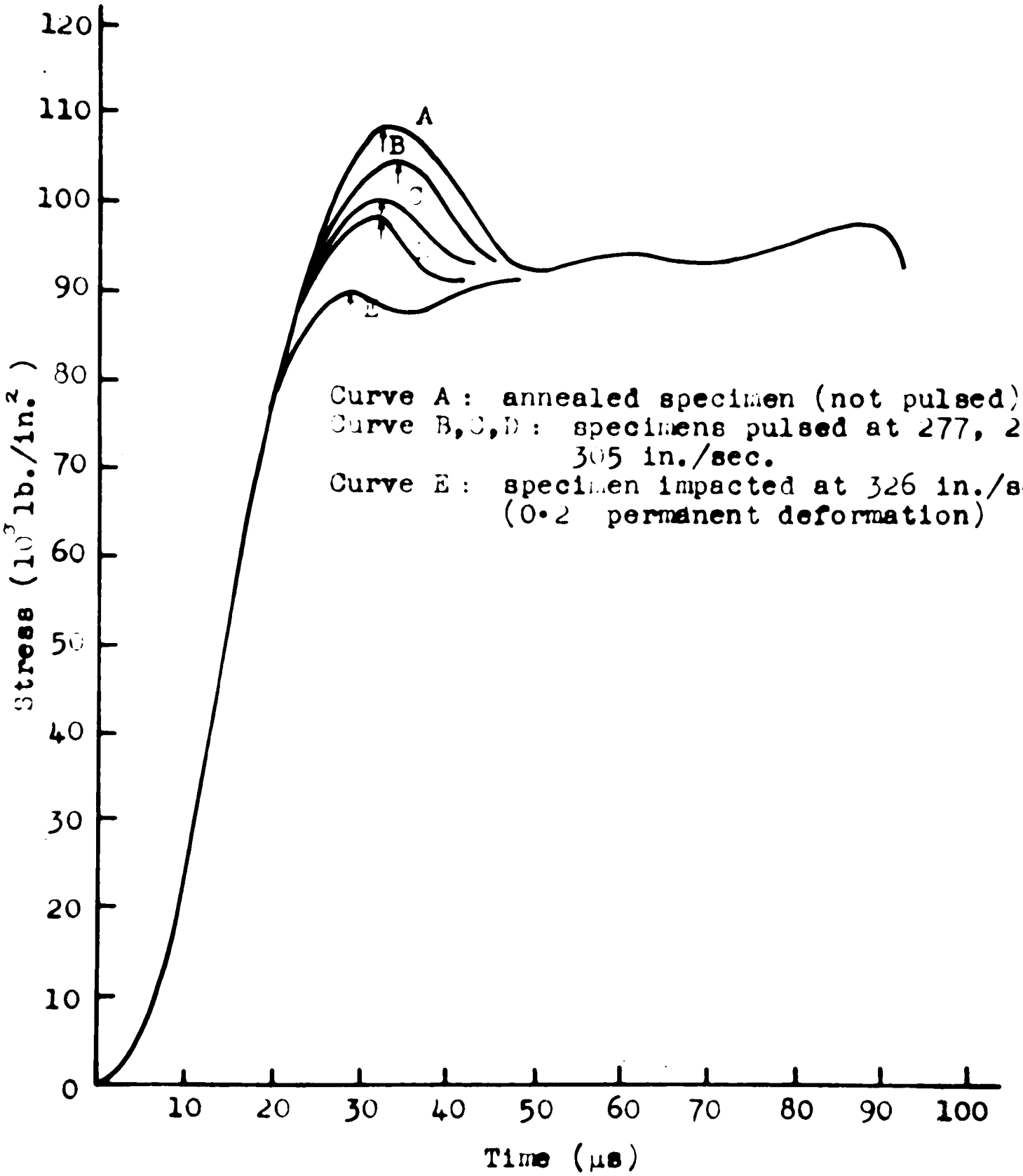


FIGURE 51 Derived stress-time curves for the specimen upper face (second impact).

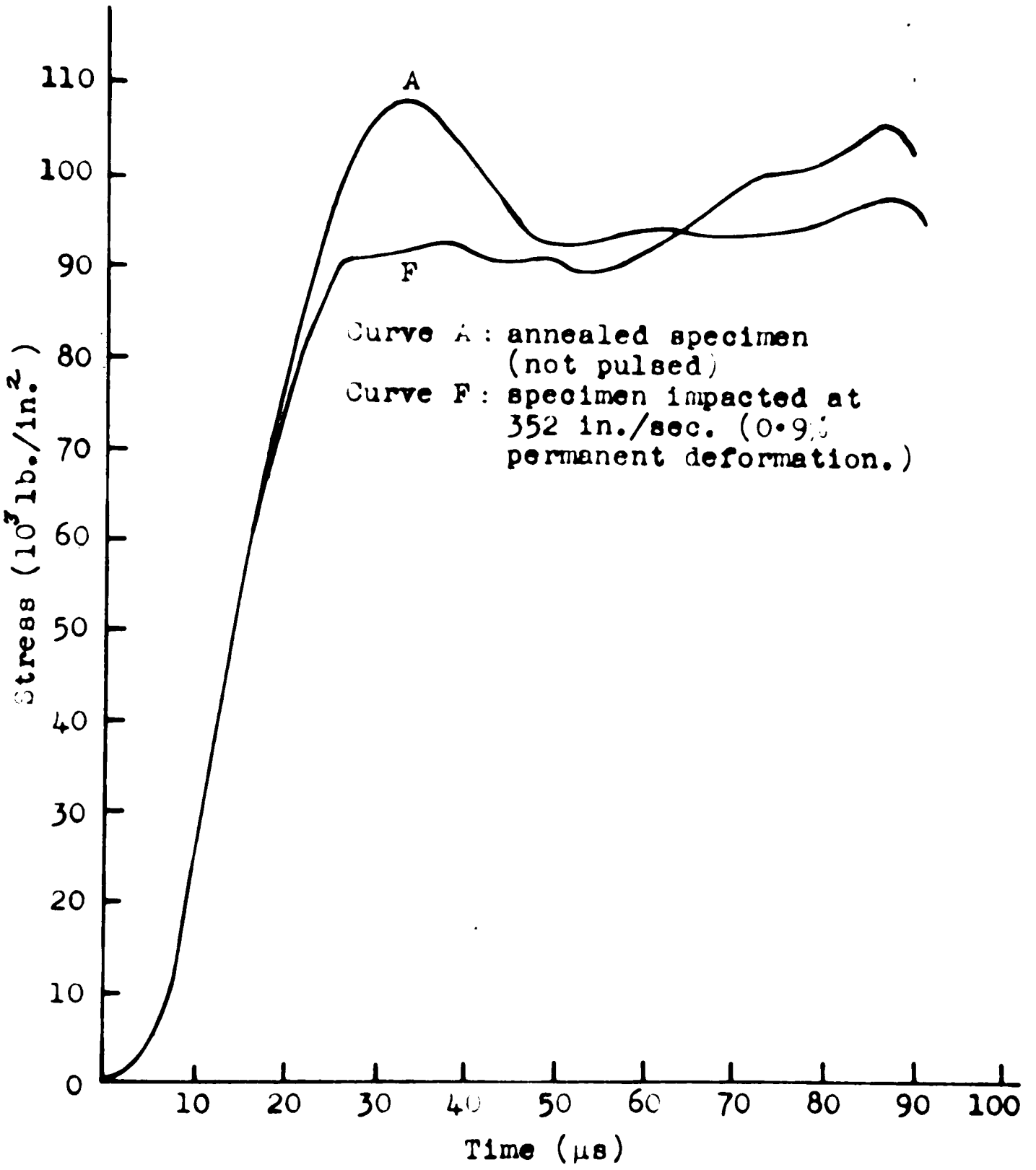


FIGURE 52 Derived stress-time curves for the specimen upper face (second impact).

lower yield stress has been reached the stress-time curves for those specimens that had previously been pulsed were found to agree very closely.

(3) Discussion

(i) The effect of 'pulsing' the steel, i.e. subjecting it to a rapidly applied stress of insufficient magnitude and duration to cause yielding, is seen to reduce the upper yield stress obtained during subsequent dynamic loading. This dynamic behaviour subsequent to pulsing can be attributed to the freeing of a number of dislocations during the application of the stress pulse. In section 1-4 it was seen that Campbell's (13) criterion for yield, i.e. that a critical number of dislocations must be freed before yield will occur, required the value of $\int_0^\tau (\sigma)^{13}\,dt$ to be a constant for all tests in which the specimen yielded. That the value of the integral is indeed approximately constant was shown in section 2-4 in which the value of the integral was found to be $16{\cdot}1 \pm 10\%$. This value of 16·1 was obtained for specimens yielded in single impacts, whether or not the value of the integral would be constant in the case of the specimen requiring two impacts to yield was not known. Several investigators (36, 14, 27) had concluded that

provided the ageing period between pulses is small, a specimen yields when the cumulative time at a constant stress is approximately equal to the normal delay time at that stress. Hence from this conclusion it would appear that the total number of dislocations requiring to be freed before yield occurs, and hence the value of the integral, (equation 10), will be constant irrespective of the number of stress pulses required to cause yield. However, from Vreeland, Wood, and Clark's (36) investigations of the anelastic macrostrain that occurs before yield, it would seem that the greater the numbers of stress pulses sustained before yield commences the greater will be the value of the integral. This conclusion is drawn from the fact that the above researchers found that under conditions of rapid loading an anelastic microstrain of 30 x 10^{-6}/sec., precedes the yield strain, of which 50% is recovered immediately after pulsing. Hence assuming that the microstrain is due to those dislocations which have been freed before yield commences it would appear that if 50% return to their original position on unloading, the first stress pulse would only be 50% effective and hence the total value of the integral for two impacts should be greater than 1·1. To investigate this it was decided to ascertain the total value of $\int_0^\tau (\sigma)^3 \, dt$ for the present

set of repeated impacts.

Figure 53 shows the curves of $(\tau)^{13}$ for those specimens which did not yield in the first impact. For each specimen the integral was evaluated graphically for the total time up to yield. The values of the integral obtained are seen to be 14·3, 16·6, 16·0 and 16·9, these values corresponding to a specimen not pulsed and to specimens pulsed at impact velocities of 277 in./sec., 293 in./sec., and 305 in./sec., respectively. The value of 14·3 for a specimen not pulsed compares favourably with the average value of 16·1 found for the integral in section 2-4. For the three specimens that were pulsed prior to deformation at an impact velocity of 430 in./sec., the average value of the integral is 16·5. It thus appears that the number of dislocations that relock after the first pulse must be very small. This result agrees with those researchers who found that the cumulative time to yield at a constant stress is approximately equal to the normal delay time at that stress, however, it appears not to be consistent with Wreeland, Wood and Clarke's microstrain measurements. It was decided to check the value of 16·5 obtained for the integral by impacting a specimen twice at the same impact velocity. To prevent yield occurring in the first impact a reasonably low impact velocity was

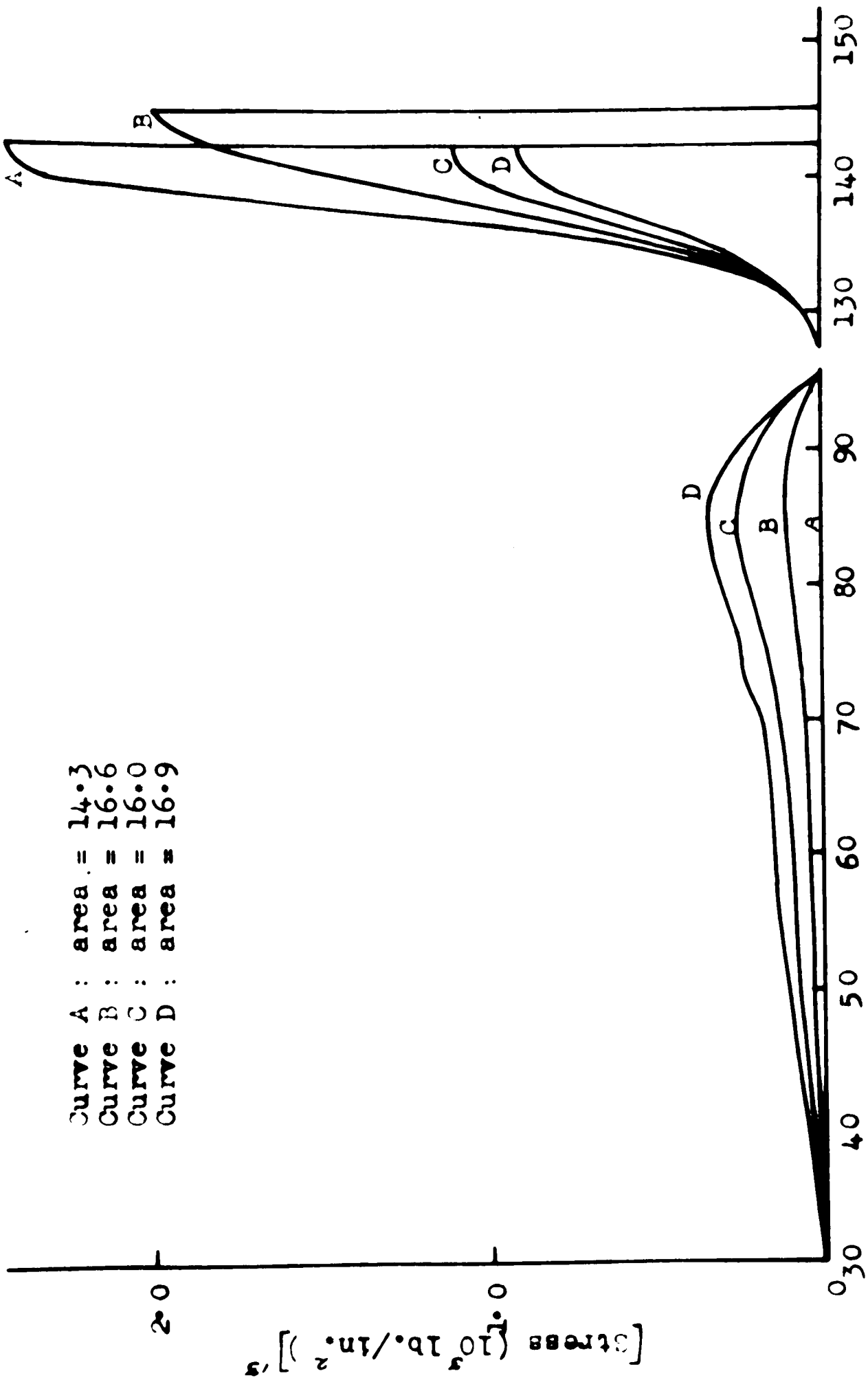


FIGURE 53 Curves of (stress)$^{-3}$ against time for various impact velocities.

chosen. The velocity chosen was 285 in./sec., this velocity was of magnitude such that, although yield did not occur in the first impact, it was large enough to yield the specimen on the second impact. Figure 54 shows the stress-time curves for the specimen upper face, the elastic wave is not shown as it differs by less than 1% from the stress-time curve obtained for the first impact. It is seen that yield occurred in the second impact at a stress of 90,000 lb./in.^{2} after a total time of 188 microseconds. The curves of $(\text{stress})^{13}$-time were again integrated graphically, and the value of the integral was found to be 17.2, 11.6 from the first stress-pulse and 6.6 from the second. This value of 17.2 is in close agreement with the value of 16.9 found for the integral in the previous tests, and confirms the earlier conclusion that the number of dislocations that relock after the first pulse must be very small.

(11) It is of interest to compare the dynamic and the static properties of the steel after it has been subjected to dynamic compression. It has been shown in the present section and section 2-4 that pulsing the steel reduces the upper yield stress obtained during both static and dynamic reloading. As a measure of the reduction in the static and dynamic upper yield stresses two ratios may be used

i.e.

$$r = (\sigma_{YU} - \sigma_{YL})/\sigma_{YL}$$

and

$$r^1 = (\sigma_{DU} - \sigma_{DL})/\sigma_{DL} \qquad (41)$$

where σ_{YU}, σ_{YL} are the static upper and lower yield stresses, and σ_{DU}, σ_{DL} are the dynamic upper and lower yield stresses respectively. The values of r and r^1 may be used to obtain an estimate of the effect of a particular stress pulse on the subsequent static and dynamic properties of the steel. In section 2-4 it was shown that for a specimen that had not been pulsed, r was equal to 0·102 (average of the values in Table V). It was also shown that the effect of pulsing at a velocity of say 293 in./sec., reduced the value of r to 0·063, i.e. r was reduced by 38 . From Figure 52 it is seen that the value of r^1 for a specimen not pulsed is 0·18, and for a specimen pulsed at the above velocity of 293 in./sec., r^1 is 0·90, i.e. r^1 has been reduced by 50 . Thus the effect of the pulsing treatment appears to be greater on the subsequent dynamic upper yield stress than on the subsequent static upper yield stress. Also comparing Figures 40 and 52 it is seen that whereas in the static retest after 0·2 permanent dynamic deformation there is still a very perceptible drop of stress at yield, in the dynamic retest

after the same dynamic deformation the upper yield stress has been very nearly eliminated. The smaller reduction of the static upper yield stress due to pulsing and the existence of a perceptible drop of stress at yield, in a static retest, even after considerable dynamic deformation, may possibly be explained by the fact that during the static retests carbon atoms can diffuse and relock the free dislocations. In the dynamic retests there is insufficient time for any significant relocking to occur, and hence the effect of either pulsing or dynamically deforming will be greater on the subsequent dynamic yield point than on the subsequent static yield point.

2-6. A COMPARISON OF THE DELAY-TIME RESULTS WITH A DELAY-TIME THEORY.

(1) General

In this section all the experimental delay-time results are compared with the delay-time theory as outlined in section 1-4. This theory postulates that at any temperature, yield occurs when the density of released dislocations reaches a critical value. It has been shown that this occurs when the integral $\int_0^\tau (\dot{\gamma})^{13} dt$, (equation 10) reaches a value c_T, c_T being a constant at a constant temperature. Using the above theory Campbell and Ruby (44) found a room temperature value of $\alpha_{RT} = 12{\cdot}5$ for steel of the same composition and heat treatment as that used in the present research, however, they suggested that a somewhat larger value of $\alpha_{RT} = 13$ might be more accurate. Hence in section 2-4 and 2-5 a value of $\alpha_{RT} = 13$ was used and was found to give a reasonably constant value of the integral. From this room temperature value of α_T, its value at any other test temperature may be found, as it is inversely proportional to the absolute temperature of the test. Thus the values of α_T at the other test temperatures, i.e. $-41^{\circ}C$, $-84^{\circ}C$, $-121^{\circ}C$, are 16, 19·5 and 24·3 respectively. Using these values of α_T, the value of c_T at any test

temperature may be found (equation 10). If the theory is in agreement with the test results then the values of these integrals c_n should not only be approximately constant at a constant test temperature, but also be related to the room temperature value c_{RT} by equation (13)

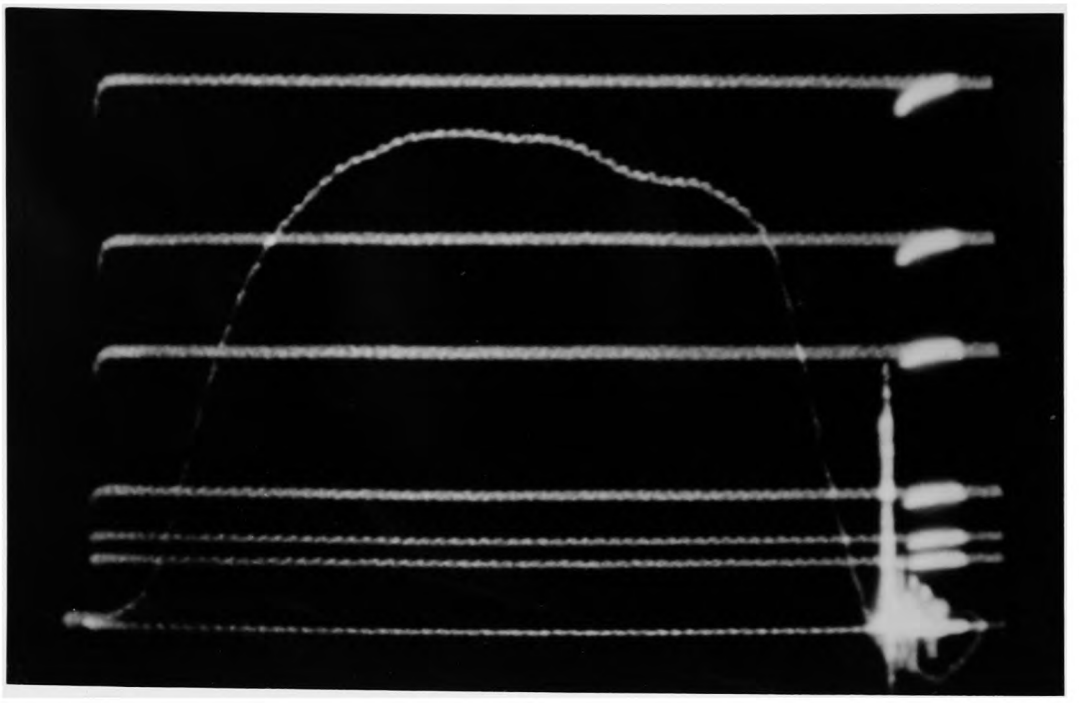
i.e.

$$\frac{c_T}{c_{RT}} = c_0^{\alpha_T - \alpha_{RT}}$$

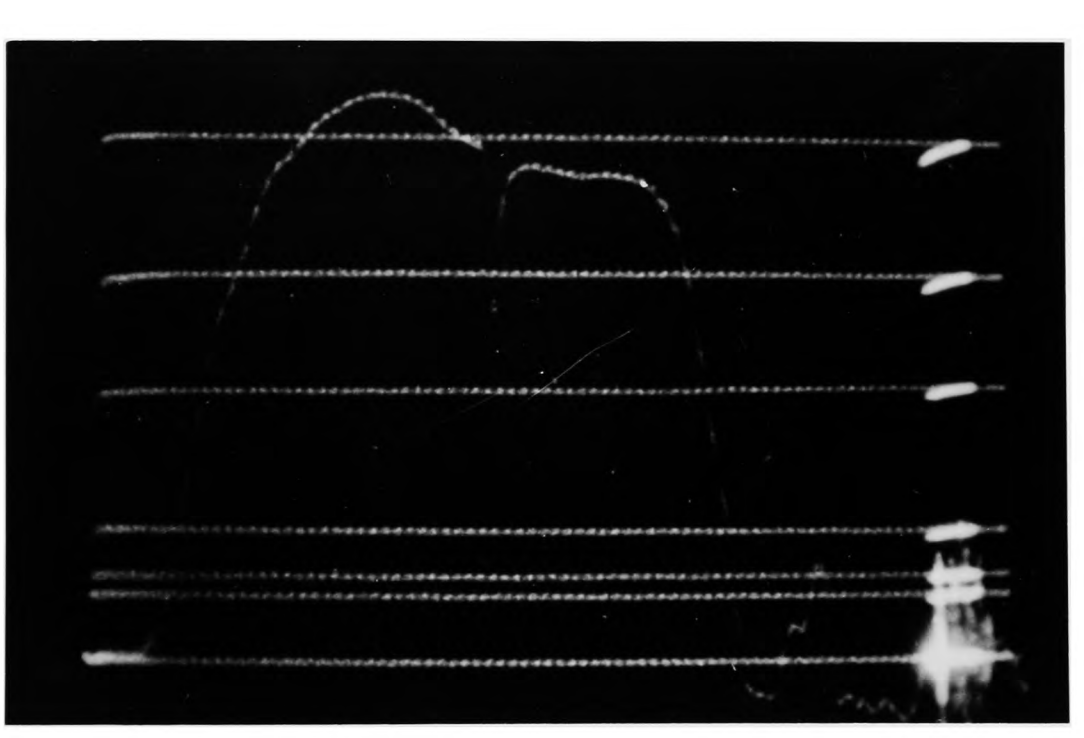
where α_{RT} is the value of α_T at room temperature, α_T is the value at a temperature T (absolute), and c_0 is the upper yield stress at absolute zero.

(2) Experimental Results

To obtain the stress at yield and the time to yield only the elastic and weighbar records were required. Many weighbar records corresponding to various impact velocities and temperatures of test have been shown in earlier sections (see Figures 18(c), 24(b), 29(b), 35(a), 35(b), 39(a), 39(b), 39(d), 49(a), 49(b). Two further records with calibration lines are shown in Figures 55(a) and 55(b). Figure 55(a) is a record obtained at room temperature for an impact velocity of 345 in./sec., and Figure 55(b) is a record obtained at -41°C for an impact velocity of 430 in./sec.



55(a)



55(b)

FIGURE 55 Weighbar records at +15°C and -41°C.

(a) For an impact velocity of 365 in./sec.
Rg ≒ 369Ω S = 1·94.

(b) For an impact velocity of 430 in./sec.
Rg ≒ 369Ω S = 1·94.

Each record and its corresponding elastic wave was analysed to obtain the stress-time curve for the specimen upper face. From this stress-time curve the stress at yield and the time to yield were found. As in section 2-4 and 2-5, curves of $(\text{stress})^{\alpha_T}$ were plotted and integrated up to the time at which yield occurred, thus giving values of σ_T. Table V gives the details of all the room temperature dynamic tests. For a given impact velocity columns 2, 3 and 4 give values of the yield stress, delay time and integral σ_{RT} respectively. The values of σ_{RT} shown in column 4 are reasonably constant over the whole range of impact velocities, this confirms the value of 13 taken for α_{RT}. Also the average value of the integral is 16.4 which is not very different from the values of 16.1 and 16.5 found in sections 2-4 and 2-5 for limited number of impacts. The results corresponding to the tests described in section 2-4 are included in Table V.

Using the average value of σ_y and σ_{RT} at each particular impact velocity, the equivalent time to yield at a stress σ_y in a constant strain rate test was found. Consider the specimen impacted at a velocity of 365 in./sec. Figure 46 shows the derived stress-time curve for the specimen upper face, and Figure 47 shows the curve of $(\text{stress})^{13}$ plotted against time. The specimen yielded after 52 micro-

TABLE V

Yield stress, delay-time results at +15°C.

Impact velocity in./sec.	Delay-time μ secs	Yield stress 10^3 lb./in^2.	c_{RT} μ secs	Equivalent time to yield μ secs
326	82	95	14·1	
	78	94	12·0	
Average	80	94·5	13·0	382
340	73	96	15·1	
	69	97	16·1	
Average	71	96·5	15·6	347
352	60	99	17·7	
	60	98	17·2	
Average	60	98·5	17·5	299
365	52	102	17·3	236
430	32	109	14·3	
	34	109	20·5	
	34	108	17·1	
Average	33	108·5	17·3	84
470	30	111	15·0	
	26	110	17·4	
	30	108	13·9	
Average	29	110	15·4	63
503	28	115	19·9	
	28	111	15·0	
	26	112	18·3	
Average	27	113	17·7	42
		Average	16·4	

seconds at a stress of 102,000 lb./in. and the value of the integral α_T is 17.3. Hence if yield were to occur at 102,000 lb./in. in a constant strain-rate test the time taken to yield would be given by equation 11 as $\frac{17.3 \times 14 \times 10^{-6}}{(1.02)} = 236$ microseconds. It is thus seen that the time to yield, at 102,000 lb./in^2 in a constant strain-rate test is considerably greater than the time actually taken to yield. Column 5 in Table V shows the equivalent delay times for constant strain-rate tests. It is seen that for all impact velocities the time to yield in a constant strain-rate test is greater than the actual time taken to yield. This difference is due to the fact that the stress waves used in this research approximate more to constant stress tests than to constant strain-rate tests.

Table VI, VII, and VIII give results similar to those shown in Table V, for test temperatures of -41°C, -84°C and -121°C respectively. To calculate the values of the integral and the equivalent delay time, the values of α_T used were 16 at -41°C, 19·5 at -84°C and 24·3 at -121°C. In Table VIII only one result is shown. This is because at this very low temperature it became extremely difficult to obtain smooth weighbar records (see section 1-6). The weighbar record corresponding to the test results

TABLE VI

Yield stress, delay-time results at $-41^{\circ}C$

Impact velocity in./sec.	Yield stress 10^3 lb./in^2.	Delay-time μ secs	σ_{-41} μ secs	Equivalent delay-time at constant strain μ secs
430	119	45	164	
	114	45	126	
	119	45	160	
Average	117	45	150	257
Theoretical	120	46		
470	121	39	212	
	122	39	224	
	121	39	212	
Average	121	39	219	116
Theoretical	125	36		
503	129	30	180	
	126	32	250	
Average	128	31	216	71
Theoretical	129	30		
Average 193				

TABLE VII

Yield stress, delay-time results at -84°C.

Impact velocity	Yield stress	Delay-time	σ_{-84}	Equivalent delay-time at constant strain rate
in./sec.	10^3 lb./in.^{2}	μ secs	μ secs	μ secs
470	132	49	2540	
	130	50	2760	
	130	50	2470	
Average	131	49	2600	295
Theoretical	134	51		
503	135	38	2530	
	136	40	3040	
	131	40	2140	
Average	133	39	2500	188
Theoretical	140	40		
Average 2550				

TABLE VIII

Yield stress, delay-time results at -121°C.

Impact velocity	Yield stress	Delay-time	σ_{-121}	Equivalent delay-time at constant strain rate
in./sec.	10^3 lb./in.^{2}	μ secs	μ secs	μ secs
503	140	60	150,000	2430
Theoretical	147	65		

in Table VIII is that shown in Figure 35(a), it can be seen from this Figure that the record is an exceptionally good one, and hence the results tabulated in Table VIII can be expected to be as accurate as those obtained at higher temperatures.

From the above Tables it is seen that the average values of the integral e_T are 16·4, 193, 2550, and 150,000 at test temperatures of 15°C, -41°C, -84°C and -121°C respectively. The delay-time theory under consideration requires the value of the integral e_T to be related to the room temperature value e_{RT} by the relationship — $\frac{e_T}{e_{RT}} = \sigma_o^{\alpha_T - \alpha_{RT}}$ (equation (13). It was seen in section 2-2 that σ_o, the upper yield stress at absolute zero, appears to lie between the limits of 220,000 lb./in.^{2} and 240,000 lb./in.^{2} Hence taking the average of these two values i.e. 230,000 lb./in.^{2}, and using e_{RT} = 16·4, the theoretical values of e_T at -41°C, -84°C and -121°C are 201, 3690 and 199,000 respectively. The actual values of e_T at the low test temperatures are thus less than the theoretical values, however, as the integrals are very sensitive to changes in stress these differences correspond only to small differences in the yield stress and delay time.

It is of interest to calculate, from the theory, the

yield stress and delay-time corresponding to a given impact velocity and temperature, and to compare these results with the experimental values. This can be done provided the shape of the elastic wave, at the impact velocity concerned, is known. The elastic stresses are raised to the required power (α_2) and plotted against time, the yield stress and delay-time are obtained by finding the point on the curve at which the integral of the curve reaches the theoretical value of α_1. The theoretical results obtained in this manner are shown in Tables VI, VII and VIII for all impact velocities. It is seen that at -121°C, for an impact velocity of 503 in./sec., the theoretical yield stress is 147,000 lb./in.^{2} and the delay-time 65 microseconds. These values compare very favourably with the observed yield stress of 146,000 lb./in.^{2} and delay-time of 60 microseconds. Also at -84°C, at an impact velocity of 503 in./sec., the theoretical values of yield stress and delay-time were found to be 140,000 lb./in.^{2} and 40 microseconds respectively, whereas the observed values were 134,000 lb./in.^{2} and 40 microseconds. Similarly at -41°C, for an impact velocity of 430 in./sec., the theoretical values of the yield stress and delay-time are 120,000 lb./in.^{2} and 46 microseconds, and the measured values are 117,000 and 43 microseconds. From these and other results

shown in Tables VI, VII and VIII it is seen that the theory predicts the experimental results to a high degree of accuracy.

The yield stress and equivalent delay-time results tabulated in Tables V, VI, VII, and VIII are shown plotted in Figure 56 on a log log scale. The theoretical relationships at each temperature, as given by equation (11), are shown plotted as straight lines. Also plotted on the graph are two points representing room-temperature results obtained by Dickson (45) on steel of the same composition and heat treatment as that used in the present investigation. It is seen that his experimental results are also in good agreement with the delay-time theory. The lines representing the theory have been terminated at a delay-time of approximately 0·1 second. This has been done in order to emphasise the fact that at delay-times longer than 0·1 sec., carbon atoms may begin relocking the freed dislocations(42, 43, 44,) and hence the theory becomes invalid.

(3) Discussion

(i) It is of interest to compare the value of the

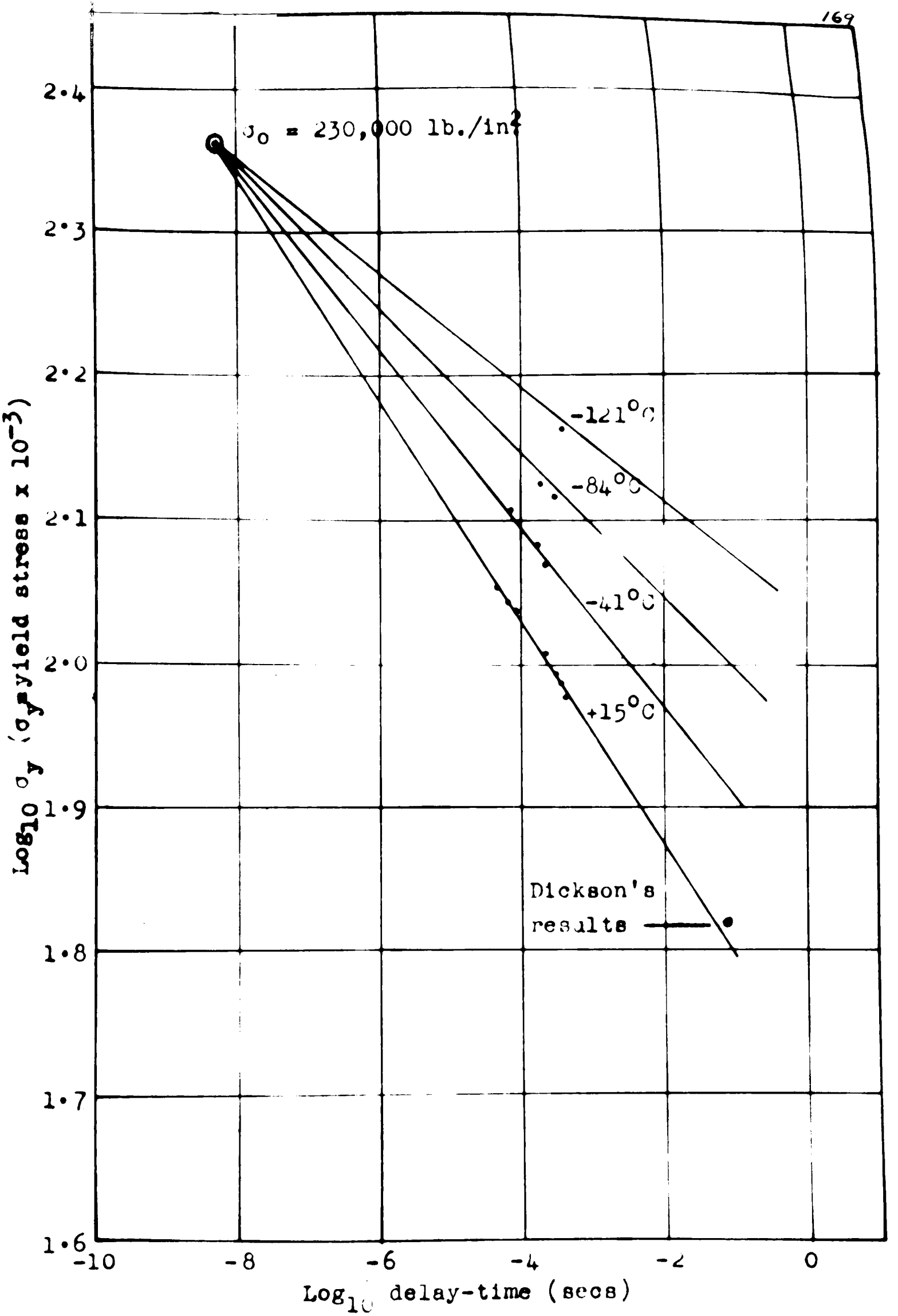


FIGURE 56 Yield stress against time to yield, referred to constant strain-rate conditions.

σ_{RT} obtained by Campbell and Duby (44), with the value of 16·4 given in Table V. The average value of the integral found by the above researchers was 30·5, nearly twice the value obtained in this investigation. The discrepancy between the two results corresponds to a difference of about 5% in the stress measurement. A possible cause of systematic error in this measurement is variation in the value of the gauge factor. In the earlier investigation gauges of length 0·64 inch were used. The manufacturers state that the actual gauge factor should not differ by more than 2 , from the quoted value, for either type of gauge. It seems therefore that the observed discrepancy is somewhat greater than can be accounted for by errors in the gauge factors used. Another possible cause of systematic error is the change in specimen diameter. In the earlier tests the diameter was $\frac{1}{2}$ inch compared with $\frac{1}{8}$ inch used in the present tests. The smaller specimens might be expected to give lower yield stresses for two reasons. (a) a given eccentricity of loading would cause a greater non uniformity of stress across the section, and (b) the effect of transverse stresses due to the radial acceleration of the specimen material would be less. In addition to the factors already discussed, it is possible that the specimens used

in the two investigations differed slightly in composition or structure.

(ii) It was observed in section 2-3 that twins were only formed in those specimens that were impacted at -84°C and -121°C. Several investigators (24, 31) have suggested that the upper yield stress is reduced when twins are formed at a lower stress. Hence it is reasonable to suppose that for those tests in which twins were formed the actual value of the integral c_f will be lower than the theoretical value. Table VII and VIII show that this is so, however, the differences between the actual and theoretical values of c_{-84} and c_{-121} is small. Thus it appears that the effect of twinning on the actual value of the integrals c_{-84} and c_{-121} is slight, and the main differences between the actual and theoretical values of the integrals is probably due to inevitable shortcomings of the theory. That the twins only affect the values of c_{-84} and c_{-121} very slightly seems reasonable, as comparatively few twins were formed at both -84°C and -121°C.

(iii) Equation 11 shows that small changes in the value of σ_o, the upper yield stress at absolute zero, will give fairly large changes in the theoretical values

of σ_T. From Figure 15 it is seen that σ_0 could lie between 227,000 lb./in.^{2} and 240,000 lb./in.^{2}. If these extreme values of σ_0 had been used to calculate the theoretical values of σ_T, the present theoretical values i.e. 291 at -41°C, 3690 at -84°C and 199,000 at -121°C would have been altered by approximately ±13 , ±28 and ±50% respectively. Hence an assumed value of σ_0 = 240,000 lb./in.^{2} would have given still greater discrepancies between the theoretical and actual values of the integral, whereas a value of σ_0 = 220,000 lb./in.^{2} would make the theoretical value of σ_{-121} too small and not significantly alter the values of σ_{-84} and σ_{-41}. It thus appears that the chosen value of σ_0, i.e. 230,000 lb./in.^{2}, is in the vicinity of the value that gives the best agreement between the theoretical and actual values of the integral σ_T. It is also to be noted that a fairly large change in the values of the integral only shifts the lines in Figure 56 by a very small amount.

(iv) It is of interest to compare the delay-time theory with Clark and Wood's (22) results obtained in constant stress tests on 0·17% carbon steel. Their results for five different temperatures are shown in Figure 57. The theoretical relationships found by taking α_T = 13

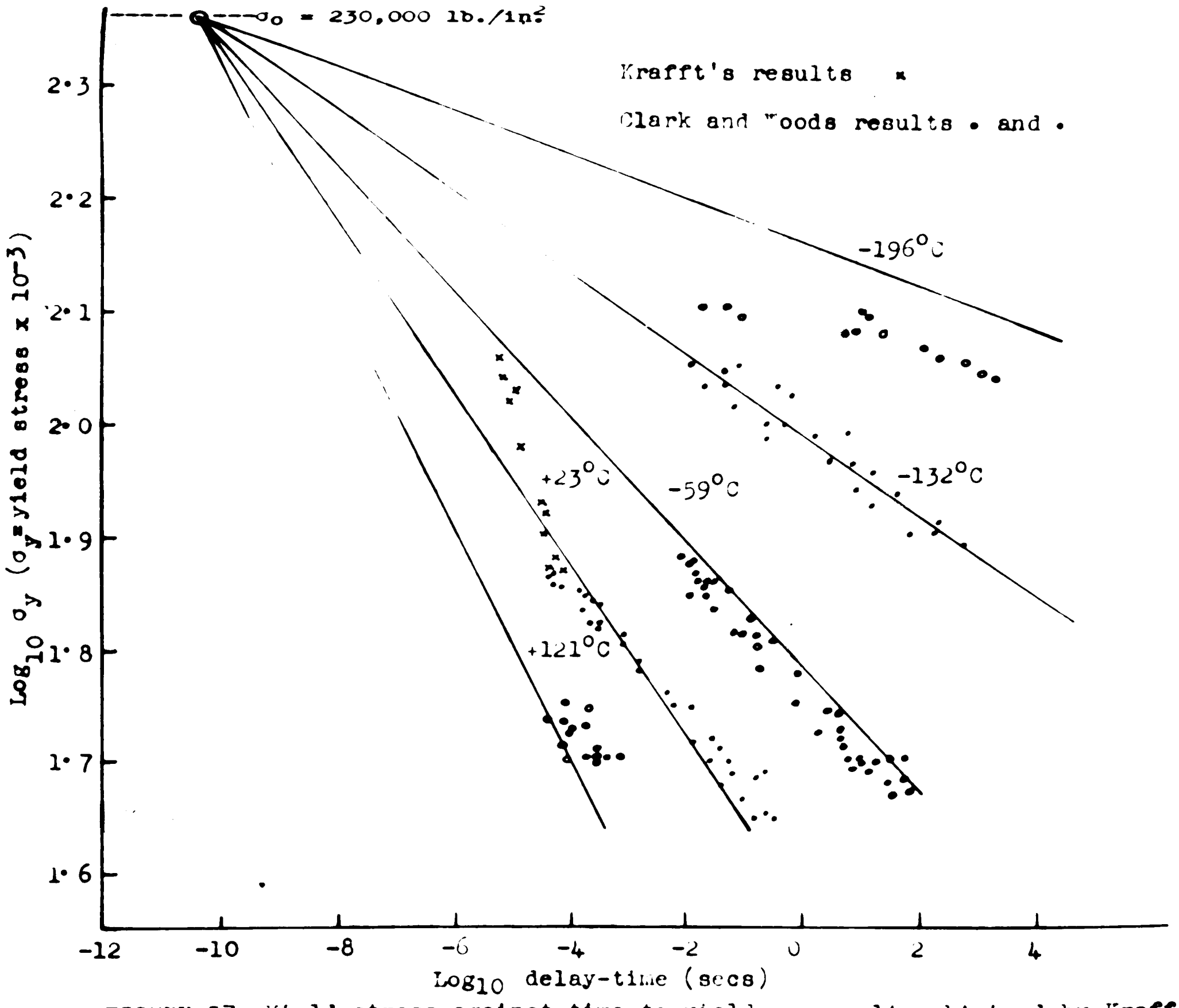


FIGURE 57 Yield stress against time to yield - results obtained by Krafft (27), Clark and Wood (22) in constant stress tests.

and σ_o = 230,000 lb./in^2 are also shown in the Figure. The room-temperature line was drawn to fit the experimental results and the above values α_{RT} and σ_o then enabled the theoretical relationships at the other temperatures to be found. It is seen that the theory again predicts the experimental results fairly well, and that at the lowest test temperature the discrepancy between the actual and theoretical results is greatest. Also plotted in Figure 57 are Krafft's (27) room temperature results obtained on the same steel. It is seen that his results obtained for very short delay-time show a considerable difference from the theory. This is probably due to the fact that these very short delay times are comparable to the rise time of his stress waves, and hence the delay times given are not really appropriate to constant stress tests.

2-7. TWINNING

(1) Experimental Results

The specimens tested as described in sections 2-2, 2-3, 2-4, 2-5, and 2-6, were all examined for twins. It was found that twinning was not initiated in any of the static tests nor in any of the room temperature dynamic tests. Twins were found only in specimens impacted as follows.

(a) at -41°C at an impact velocity of 503 in./sec.

(b) at -84°C at impact velocities of 470 in./sec., and 503 in./sec.

(c) at -121°C at an impact velocity of 503 in./sec.

Hence, from the values of the upper yield stresses given in Tables V, VI, VII and VIII, the stresses at which twinning is initiated at the test temperatures are limited as follows.

(a) at $+15^{\circ}$C, the stress at which twins form must be above 113,000 lb./in^2.

(b) at -41°C, the stress at which twins form must be between 121,000 lb./in^2 and 128,000 lb./in^2.

(c) at -84°C the stress at which twins form must lie below 131,000 lb./in^2.

(d) at -121°C, the stress at which twins form

must lie below 146,000 lb./in^2.

These limitations are such that if a critical stress for twin formation, independent of temperature and strain rate does exist, then this stress must lie in the range 121,000 lb./in^2. to 128,000 lb./in^2. However, it appeared possible that the stress for twinning varies with the test temperature, and that only at -41°C is this stress in the range 121,000 lb./in^2 to 128,000 lb./in^2. Hence it was decided to determine as accurately as possible the stress at which twinning is initiated at a temperature much lower than -41°C. The temperature chosen was -121°C. The first test at this temperature was at an impact velocity of 430 in./sec. The specimen showed no sign of having yielded during impact, and the weighbar record obtained differed only very slightly from the elastic record corresponding to the same impact velocity (Figure 18(a)). Examination of this specimen after impact revealed the formation of fairly fine twins near the upper face of the specimen. As the maximum stress sustained by this specimen during impact was 132,000 lb./in^2, it appears that the stress at which twins form at -121°C is less than 132,000 lb./in^2.

The second and third tests were at impact velocities of 360 in./sec., and 375 in./sec., the maximum stresses sustained by the specimens being 120,000 lb./in^2 and

126,000 lb./in.^{2} respectively. In neither of these tests were twins formed, hence it follows that at -121°C twins are initiated at some stress between 126,000 lb./in.^{2} and 132,000 lb./in.^{2}. This stress range for the initiating of twinning at -121°C differs little from the stress range found at -41°C, i.e. 121,000 lb./in.^{2} to 128,000 lb./in.^{2}. Thus there seems to be some evidence that the stress for the formation of twins is approximately constant and only slightly dependent on temperature and strain rate. An excellent check of this conclusion would be to determine the stress at which twins are formed at room temperature. Unfortunately, in all the tests performed at +15°C, yield occurred at stresses too low to initiate twinning. It is hoped that further work in tension on the same steel will give an indication of the magnitude of stresses required for twinning at room temperature.

(2) Discussion

(a) The results appear to indicate that if the stress required to initiate twinning varies with temperature then it does not vary a great deal. Cottrell and Bilby (50) have suggested a dislocation mechanism for twinning, hence it is reasonable to suppose that thermal fluctuations will

help in starting the mechanism. Thus one would expect the stress at which twinning is initiated to become higher as the temperature is lowered. The experimental results obtained have not disproved this possibility, but, the difference in twinning stresses obtained at various temperatures are smaller than was at first expected. It is thought that this is due to the activation energy required to initiate twinning being comparatively large.

2-8. CONCLUSIONS

(1) The variation in the static upper yield stress with temperature is only in reasonable agreement with Cottrell and Bilby's yield theory. The main discrepancy between the experimental and theoretical values of the upper yield stress is considered to be due to the effect of the pearlite. Also, extrapolation of the curve relating upper yield stress to temperature indicates that σ_o, the yield stress at absolute zero, lies in the range of stresses 220,000 lb./in^2. to 240,000 lb./in^2.

(2) The lower the test temperature the finer the slip by which the metal deforms during a static test.

(3) At the test temperatures considered Campbell's delay-time theory is in fairly good agreement with the observed delay-time results. Also, at a particular test temperature the dynamic stress-strain relation depends on the rate of deformation.

(4) Dynamic deformation occurs primarily by fine slip, however, at the lower test temperatures some twinning is initiated.

(5) The stress at which twinning is initiated appears to be fairly independent of temperature and strain rate. It is thought that, for the steel tested, twinning occurs at stresses in the range 121,000 lb./in^2 to 128,000 lb./in^2.

(6) The stress required to widen twins is much less than that required to initiate them.

(7) The effect of 'pulsing' steel i.e. subjecting it to a rapidly applied stress of insufficient magnitude and duration to cause yielding is to reduce the upper yield stress obtained during static reloading. It has been found that the reduction in the drop of stress at yield varies approximately linearly with the number of dislocations released in the pulsing test, though it does not appear to be possible to eliminate the drop altogether.

(8) The effect of deforming a medium carbon steel dynamically is to render it softer for subsequent static deformation of the same type. In particular the static upper yield stress is reduced to a minimum after about 1 permanent dynamic strain. However, a perceptible drop of stress during static yielding exists even after about 1·2 permanent dynamic strain.

(9) The static stress-strain curve obtained after impacting is little affected by lowering the temperature of testing provided that the magnitude and duration of the impact stress are increased so as to obtain the same permanent strain.

(10) The effect of pulsing steel is to reduce the dynamic upper yield stress as obtained during dynamic reloading. The effect of a stress pulse of given magnitude on the subsequent dynamic upper yield stress is greater than the effect of an identical stress pulse on the subsequent static upper yield stress.

(11) The effect of dynamically deforming steel is to remove the drop of stress at yield in a subsequent impact test. This appears to be true even if the amount of dynamic deformation that has been caused by the first impact is very small.

(12) Campbell's criterion for yielding, i.e. that a critical number of dislocations must be freed before yield will occur, appears to be reasonably valid whether or not the dislocations are freed in a single impact or in several impacts provided no significant strain ageing occurs between impacts.

APPENDIX I

AN ANALYSIS OF THE LOW TEMPERATURE STRAIN GAUGE.

(1) The gauge is shown diagrammatically in Figure 58. It is required to find the strain s at points A, B, C and D caused by a relative movement $\frac{\Delta}{2}$ of the plunger faces. As the specimens are $\frac{1}{2}$ inch long this movement corresponds to a specimen strain Δ.

The following assumptions are made

(a) The flats EG and FI are rigid and move with the plunger-faces. Hence no rotation occurs at points E, F, G and I.

(b) The deflections are small and changes from the initial radius of the rings (1") are negligible.

Consider the ring shown in Figure 58. When a relative movement $\frac{\Delta}{2}$ occurs between the plunger faces, let the vertical force at points E and F be H, and the fixed-end moments at these points be M_E . From the theory of arch analysis (52) the relative movement $\frac{\Delta}{2}$ is then given by

$$\frac{\Delta}{2} = \int_F^E \frac{M}{EI} y\,ds \qquad (42)$$

where M is the moment at any point P of co-ordinates x and y, E is the elastic modulus, I is the moment of inertia of the ring section and ds represents a small element of length of the ring. Also as there is no change of slope between E and F then

$$\int_F^E \frac{M}{EI}\,ds = 0 \qquad (43)$$

i.e.
$$\int_F^E M\,ds = 0 \qquad (44)$$

Now at any point P the moment M is given by

$$M = My - M_E \qquad (45)$$

Hence by substituting this value of M in equation (44) we obtain

$$M_E = M\frac{\int_F^E y\,ds}{\int_F^E ds} \qquad (46)$$

and from (42)

$$\frac{\Delta EI}{2} = \int_F^E My^2\,ds - M_E\int_F^E y\,ds$$

$$= H \left[\int_F^E y^2 ds - \frac{\left(\int_F^E y ds \right)^2}{\int_F^E ds} \right] \qquad (47)$$

$$= H K$$

where K is defined as the term in the brackets.

$$\text{thus} \qquad H = \frac{M_E I}{2K} \qquad (48)$$

From these values of M_E and H, (equations 46 and 48) the strain at the points A, B, C and D may now be calculated.

At points A, B C and D the surface strain s is given by

$$s = \frac{P_A}{E} \qquad (49)$$

where P_A is the stress at the points under consideration.

Also as $\frac{M_A}{I} = \frac{P_A}{d/2}$ then s is given by

$$s = \frac{M_A \, d}{EI \, 2} \qquad (50)$$

where d is the thickness of the rings.

and from equation (45).

$$M_A = Hy_A - M_E$$

$$= \frac{\Delta EI}{2K}\left(y_A - \frac{\int_F^E y\,ds}{\int_F^E ds} \right)$$

$$= \Delta EI\,\frac{K^1}{2K} \qquad (51)$$

where K^1 is given by the terms in the bracket.

Hence substituting this value of M_A in equation (50) the strain at points A, B, C and D is given by

$$s = \frac{3}{4}\,\frac{K^1}{K} \qquad (52)$$

For a ring of dimensions shown in Figure 58 the values of K^1 and K were found to be 0·913 inches and 2·848 in^3 respectively, hence equation (53) gives the strain at points A, B, C and D as

$$s = 0{\cdot}0075\,\Delta \qquad (53)$$

where s is measured in inches. The strain s therefore varies linearly with the specimen strain Δ.

(11) Consider the strain-measuring circuit shown in Figure 6. The change ΔR in the variable resistance R which is required to balance the bridge after a change in gauge

resistance R_g, is given by

$$\frac{\Delta R}{R} = \frac{2(R_1 + R)}{R_1} \frac{\Delta R_g}{R_g} \tag{54}$$

Hence as $$\varepsilon = \frac{1}{S} \frac{\Delta R_g}{R_g}$$

where $S = 1.94$ is the gauge factor,

then $$\varepsilon = 1.852 \times 10^{-2} \frac{\Delta R}{R},$$

and from equation (53)

$$\Delta = 1.235 \frac{\Delta R}{R} \tag{55}$$

This equation is shown plotted in Figure 12.

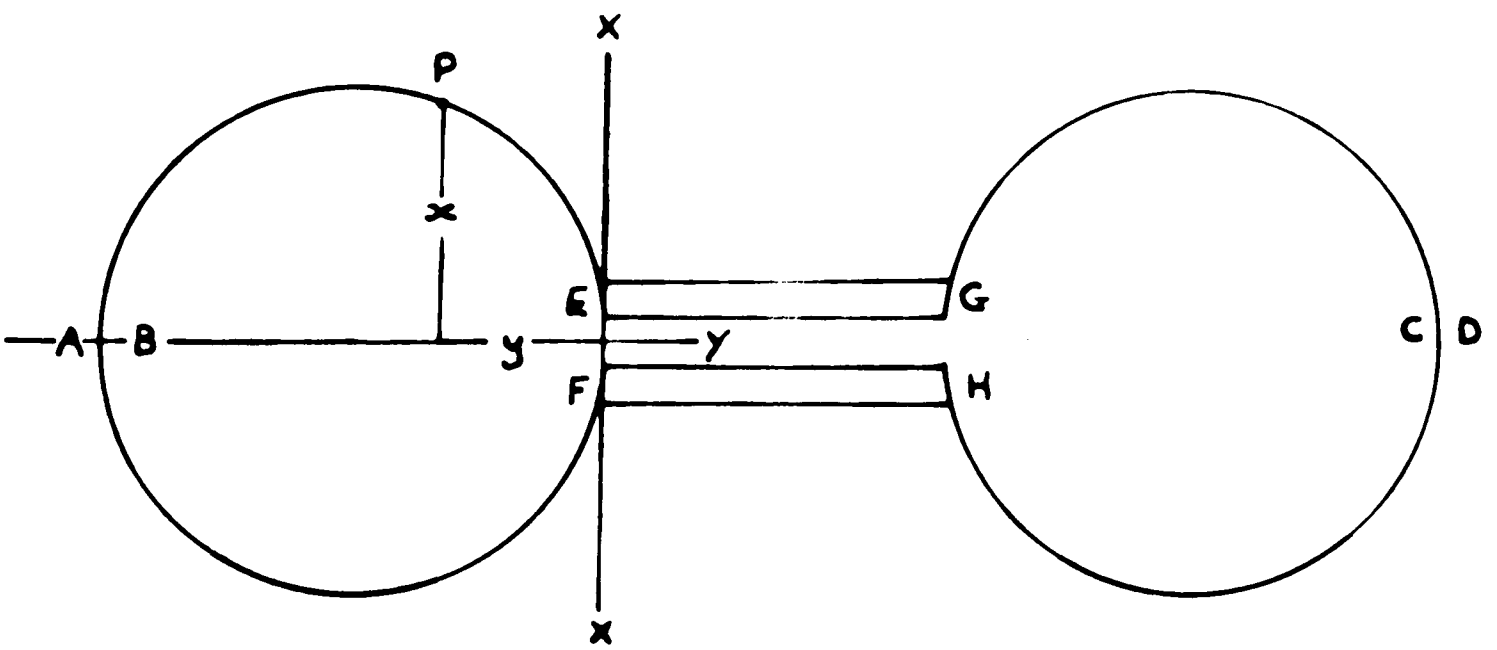


FIGURE 58 Diagramatic representation of the low temperature strain gauge.

APPENDIX II

THE RISE IN TEMPERATURE OF A SPECIMEN DURING DYNAMIC DEFORMATION.

Consider a specimen impacted at room temperature at a velocity of 503 in./sec. The total work done during such an impact is proportional to the area under the dynamic stress-strain curve. (curve A in Figure 22) From graphical integration it is found that this work done is equal to 232 ft.lbs. i.e. 0·0166 C.H.U. Taylor and Quinney (52) found that approximately 90% of the work done in dynamic torsion tests is converted into heat energy. Hence in the above test a reasonable assumption is that 90% of the work done is also converted into heat energy. To find the rise in temperature of the specimen, due to such a heat addition, the density and specific heat of the steel need to be known. The density ρ was known to be 490 lbs/ft^3 and the specific heat S was assumed to be 0·117. Hence the temperature rise of the specimen ΔT, ignoring conduction to the weighbar and anvil bar, is given by

$$\Delta T = \frac{Q}{S\rho V_s} = \frac{0{\cdot}0166 \times 1728}{490 \times {\cdot}117 \times {\cdot}065} = 8^{\circ}C$$

where V_s represents the volume of the specimen in cu.ins. This increase in temperature during the test corresponds to an increase in absolute temperature of 2·7°. In all the other tests represented by the stress-strain curves in Figures 22, 28, 33, 38 the percentage rise in temperature is less than 2·7°, hence it is considered that the effect of rise in temperature on the dynamic stress-strain curves is small.

REFERENCES

1) Howe, J. Trans. Roy. Inst., xiv, 393, 1894

2) Hadfield, R.A. Jour. Iron Steel Inst., 67, 147, 1905

3) De Haas, W.J., Hadfield, R.A. Proc. Roy. Soc., A 232, 297, 1933

4) Lindemann, F.A., Lindemann, C.A. Festschrift, v. Nernst, 264, 1912

5) Fahrenhorst, W., Schmid, E. Zeitschrift fur Physik, 64, 845, 1930

6) Eldin, A.N., Collins, R.C. Jour. App. Phys., 22, 1296, 1951

7) McAdams, D.J., Mebs, R.W. Am. Soc. Test. Mat., 43, 543, 1943

8) Cottrell, A.H., Churchman, A.T. Nature, 167 943, 1951

9) Paxton, H.W., Cottrell, A.H. Acta Metal. 1, 475, 1953

10) Hopkinson, B. Proc. Roy. Soc., A 74, 498, 1905

11) Mason, W. Jour. Mech. Eng., 128, 409, 1934

12) Morrison, J.L.M. The Engineer, 158, 183, 1934

13) Campbell, J.D. Acta Metal, 1, 706, 1953

14) Vreeland, T., Wood, D.S., Clark, D.S. Trans. Am. Soc. Metals, 45, 620, 1953

15) Ginns, W.W. Jour. Inst. Metals, 61, 61 1937

16) Taylor, G.I. Inst. Civil Eng., 26, 486, 1946

17) Thiffen, A.J. Proc. Roy. Soc., A 194, 300 1948

18) Taylor, G.I. Proc.Roy.Soc., A 194, 1948

19) Campbell, J.D., Duby, J. Proc.Roy.Soc. A 235, 24, 1956

20) Zener, C., Holloman, J.H. Jour.App.Phys., 15, 22, 1943

21) Clark, D.S., Wood, D.S. Trans.Am.Soc.Metals, 43, 571, 1951

22) Clark, D.S., Wood, D.S. Am.Soc.Test Mat. 49, 717, 1949

23) Clark, D.S., Wood, D.S. Trans.Am.Soc.Metals 44, 726, 1952

24) Baron, E.G. U.K.A.E. Metallurgy Rept., 22, 1954

25) Cottrell, A.H., Bilby, B.A. Phys.Soc., 62, 49, 1949

26) Krafft, J.M., Sullivan, A.M., Tipper, C.F. Proc.Roy.Soc., A 221, 114, 1954

27) Krafft, J.M. Trans.Am.Soc.Metals, 1955

28) Campbell, J.D., Duby, J., Puttick, K.E. Phil. Mag. 1957

29) Clark, D.S., Craig, G.B. Prog.Metal Phys. 3, 115, 1952

30) Geil, G.W., Carwile, N. Jour.Metals, 5, 213, 1953

31) Carrington, W.E., Gayler, M.L.V. Proc.Roy.Soc. A 194, 323, 1948

32) King, H. Nature, 169, 543, 1952

33) Warnock, F.W., Pope, J.A. Inst. Mech.Eng., 157, 1947

34) Harris, W.B., White, M.P. Jour.App.Mech., 21, 194, 1954

35) Duby, J. Doctor's Dissertation, 1957

36) Vreeland, T., Wood, W.G., Clark, D.S. Acta Metallurgica, 1, 415, 1953

37) Docherty, J.G., Thorne, F.V. Engineering, 132, 295, 1931

37a) Johnson, J.E., Clark, D.S., Wood, W.E. 4th Tech.Rept.Contract N.Onr.—24418, office of Naval Research, 1951

38) Kolsky, H. Stress Waves in Solids, O.U.P. 1953

39) Koster, W. Zeitschrift fur Metal, 39, 1, 1948

40) Scott, N.R. 'Temperature. Its measurement and control in Science and Industry', Reinhold.Pub.Corp., 206, 1941

41) Yokobori, T. Jour.App.Phys., 25, 593, 1954

42) Gibson, J. Inst.Mech.Eng., 1B, 536, 1953

43) Fisher, J.C. Trans.Am.Soc.Met., 47, 451 1955

44) Campbell, J.D., Ruby, J. Conference on the properties of materials at high rates of strain. Inst.Mech.Eng., 1957

45) Dickson, A.G. Private communication. Mech. Eng.Dept., Bristol Univ., 1955

46) Frank, F.C., Read, W.T. Physics Review, 79, 722, 1950

47) Mott, N.F. Phil.Mag., 43, 1151, 1952

48) Eshelby, J.D., Frank, F.C., Nabarro, F.R.N., Phil.Mag., 42, 351, 1951

49) Davies, R.M. Proc.Roy.Soc. A 197, 416, 1949

50) Cottrell, A.H., Bilby, B.A. Phil.Mag., 42, 573, 1951

51) Morley, A. 'Theory of Structures', Longmann's Press, 542, 1948

52) Taylor, G.I., Quinney, H. Proc.Roy.Soc., 143, 307, 1934